

Inaugural dissertation
for
obtaining the doctoral degree
of the
Combined Faculty of Mathematics, Engineering and Natural Sciences
of the
Ruprecht - Karls - University
Heidelberg

Presented by

M.Sc. Yu-Chan Chih

Born in: Taipei, Taiwan (R.O.C.)

Oral examination: 12th of December 2024

Development of MHC-dependent immunotherapy for gliomas

Referees: Prof. Dr. Michael Platten
Prof. Dr. Oliver Fackler

Acknowledgements

“It takes a village to raise a child,” and it certainly takes another village to raise a graduate student. First, I want to thank the founder of the village, Michael Platten, and one of the village managers, Lukas Bunse, for providing almost unlimited resources, scientific inputs, and the freedom to pursue research of my interest with great independence. I understand that we are in a rare and privileged position, and I am extremely grateful to be part of this well-equipped village. Next, I want to thank my TAC members, Moritz Mall and Lucas Schirmer, for your mindful support and advice throughout my doctoral journey. I am also deeply grateful to Oliver Fackler and Pei-Chi Wei for taking the time to evaluate this work and form my examination committee.

Second, I would like to thank my students, Philipp Koopmann, Amelie Dietsch, Kuralay Aman, Andreas Dobbelstein, Manuel Wagner, and Vahid Khaki Bakhtiarvand, who have trained my temper and patience, reminded me of the pure passion for research, and made me realize that transferring knowledge is just as important. Watching you grow from a slight burden to tremendous help is one of the best feelings in the world.

Third, I want to thank: Michael Kilian, for showing me work-life balance isn't a thing—just have a drink and have them both; Alexandros Kourtesakis, from a neighboring village, for your support as a friend and a colleague; Tamara Boschert, for showing me the good sides of Germans; Ankita Sati, for reminding me life is about more than just work; and Dennis Agardy, for your Alman-Humor and mouse surgery companionship.

Fourth, I would like to thank all the villagers (lab mates) and collaborators who have contributed to this work practically, spiritually, and insightfully, and who have helped mentally. Special thanks to Angela Wang, who has brought support all the way from home to Europe, and to Melisa Wartusch for your boundless and immeasurable positive energy that brightened my life again.

Finally, I thank my former village, my family, who raised me to be a resilient and self-developing individual, for your open-mindedness and unconditional backing in sickness and in health, and for your encouragement urging me to go and see the world.

I have met so many great people along the way who made me a better person each time, and I am so glad all these encounters happened. For those I could not mention in detail here, thank you!

Zusammenfassung

Glioblastome (GB) sind die häufigste und aggressivste Art von Hirntumoren, für die es nur begrenzt wirksame Behandlungsmöglichkeiten gibt. Trotz bedeutender Fortschritte in der Immuntherapie haben GB-Patienten bisher nicht wesentlich davon profitiert. Dies ist auf krankheitsspezifische Merkmale wie den Schutz durch die Blut-Hirn-Schranke, ein immunsuppressives Tumormikromilieu und eine relativ niedrige Mutationslast zurückzuführen. Die Therapie mit TCR-transgenen T (TCR-T) Zellen, die in der Behandlung solider Tumoren vielversprechende klinische Ergebnisse gezeigt hat, stellt eine potenzielle Umgehung dieser Barrieren dar, da sie eine sichere und zielgerichtete Reaktion auf das GB-spezifische Peptidom ermöglicht. In dieser Arbeit wurde das GB-assoziierte Antigen (GAA) PTPRZ1 umfassend in Hirntumoren charakterisiert. Dabei konnte gezeigt werden, dass es ausschließlich in Krebszellen exprimiert und auf MHC Klasse I (MHCI) präsentiert wird. Unter Verwendung von Patientenmaterial aus der GAPVAC-101-Impftherapiestudie wurde ein PTPRZ1-reaktiver TCR identifiziert, der sich sowohl in in-vitro- als auch in in-vivo-Modellen als wirksam bei der Kontrolle von GB-Tumoren erwies. Dies geschah auf antigenspezifischer und HLA-restringierter Weise, ohne Hinweise auf unspezifische Reaktivität. Interessanterweise wurden GB-Stammzellen und bestimmte Subtypen von GB-Zellen aufgrund ihrer Assoziation mit PTPRZ1 bevorzugt angegriffen. Diese Ergebnisse führten zur Planung einer Phase-I-klinischen-Studie (INVENT4GB), in der die TCR-T-Zelltherapie gegen GB getestet werden soll. Um das Potenzial der TCR-T-Zelltherapie für GB weiter auszubauen, wurden zusätzliche GAAs ausgewählt und ihre immunogenen Epitope vorhergesagt. Für die Entdeckung dieser TCRs wurden HLA-humanisierte A2.DR1-Mäuse mit immunogenen Peptiden immunisiert. Antigen-reaktive CD4⁺ T-Zellen wurden *in vitro* isoliert und expandiert, und eine reaktive TCR wurde im Anschluss kloniert und validiert. Gleichzeitig wurden auch antigen-reaktive CD8⁺ T-Zellen isoliert und mit einem optimierten Expansionsprotokoll *in vitro* expandiert, wobei die reaktiven TCRs in laufenden Versuchen noch validiert werden. Darüber hinaus wurde die Expression von MHC Klasse II (MHCII) in Tumoren mit der Wirksamkeit von Immuntherapien in Verbindung gebracht, wobei die Rolle in GB noch nicht vollständig geklärt ist. Durch Immunfärbung und transkriptomische Analysen konnte die MHCII-Expression in Gliomen bestätigt werden. Zelllinien, die MHCII-exprimierende und MHCII-defiziente Gliome nachbilden, wurden im Rahmen dieser

Studie etabliert. Im Einklang mit den humanen Daten konnte gezeigt werden, dass in murinen MHCII⁺ Gliommodellen mehr Immunzellen rekrutiert wurden und T-Zellen einen erschöpften Phänotyp erreichten. Allerdings konnte die in menschlichen Patienten beobachtete Assoziation mit einer schlechten Prognose, in den präklinischen Mausmodellen nicht bestätigt werden. Weitere Studien sind erforderlich, um die Rolle von MHCII in Gliomen im Allgemeinen und in Bezug auf die Effektivität von Immuntherapien zu untersuchen.

Abstract

Glioblastoma (GB) is the most common and aggressive brain tumor with limited effective treatments available. Despite significant advances in cancer immunotherapy, GB patients have not benefited substantially due to disease characteristics, including protection from the blood-brain barrier, an immunosuppressive tumor microenvironment, and a relatively low mutation burden. TCR-transgenic T (TCR-T) cell therapy, which has shown promising clinical results in treating solid tumors, presents a potential circumvention as it allows safe and ubiquitous targeting of GB-derived peptidome. Here, a GB-associated antigen (GAA), PTPRZ1, was well-characterized in brain tumors, exclusively expressed in cancer cells and abundantly presented on MHC class I (MHCI). Using patient material from the GAPVAC-101 vaccine therapy trial, a PTPRZ1-reactive TCR was retrieved and demonstrated to be potent in controlling GB *in vitro* and *in vivo* in an antigen-specific and HLA-restricted manner without evidence of off-target reactivity. Intriguingly, GB stem cells and distinct subsets of GB cells were preferentially targeted due to their association with PTPRZ1 expression. These results prompted a first-in-human TCR-T cell therapy phase I clinical trial against GB, INVENT4GB. To further expand the horizon of TCR-T cell therapy for GB, additional GAAs were shortlisted with their immunogenic epitopes predicted. For TCR discovery, their immunogenic peptides were employed to immunize the HLA-humanized mouse A2.DR1, resulting in corresponding immunogenicity. Antigen-reactive CD4⁺ T cells were isolated and expanded *in vitro*, and a reactive TCR was cloned and authenticated. Concurrently, antigen-reactive CD8⁺ T cells were isolated and expanded *in vitro* using an optimized expansion protocol, yet the truly reactive TCRs await validation. Furthermore, tumoral MHC class II (MHCII) expression has previously been linked to immunotherapy efficacy though its role remained poorly understood in GB. Through immunostaining and transcriptomic analysis, glioma MHCII expression was confirmed. Cell lines recapitulating MHCII-proficient and MHCII-deficient gliomas were established. In alignment with human data, MHCII⁺ gliomas in mice recruited more immune cells and promoted T cell exhaustion, but the association with poor prognosis observed in human patients could not be modeled. Further research is required to elucidate glioma MHCII role with validated immunotherapy models.

List of publications related to this work

List of publications not related to this work

Tu, W.-L., Chih, Y.-C., Shih, Y.-T., Yu, Y.-R., You, L.-R., and Chen, C.-M. (2022). Context-specific roles of diphthamide deficiency in hepatocellular carcinogenesis. *J Pathol* 258, 149-163.

Bunse, L., Bunse, T., Krämer, C., Chih, Y.-C., and Platten, M. (2022). Clinical and Translational Advances in Glioma Immunotherapy. *Neurotherapeutics* 19.

Kilian, M., Sheinin, R., Tan, C.L., Friedrich, M., Krämer, C., Kaminitz, A., Sanghvi, K., Lindner, K., Chih, Y.-C., Cichon, F., *et al.* (2023). MHC class II-restricted antigen presentation is required to prevent dysfunction of cytotoxic T cells by blood-borne myeloids in brain tumors. *Cancer Cell* 41.

Krämer, C., Kilian, M., Chih, Y.-C., Kourtesakis, A., Hoffmann, D.C., Boschert, T., Koopmann, P., Sanghvi, K., De Roia, A., Jung, S., *et al.* (2024). NLGN4X TCR transgenic T cells to treat gliomas. *Neuro-Oncology* 26.

Contents

Acknowledgements	I
Zusammenfassung	III
Abstract	V
List of publications related to this work	VI
List of publications not related to this work	VI
List of Abbreviations	XI
List of figures	XIII
List of tables	XV
1 Introduction	1
1.1 Immunotherapy for cancers	1
1.1.1 CAR-T cell therapy	1
1.1.2 TIL and TCR-T cell therapy	2
1.2 Immunotherapy for brain tumors	4
1.3 Brain tumor-derived antigens	6
1.3.1 GB-associated antigen and GB stem cell marker: PTPRZ1	8
1.4 Cancer-reactive TCR discovery	10
1.5 Tumoral MHCII expression and therapy efficacy	12
1.6 Objectives of the study	14
2 Results	15
2.1 Targeting glioblastoma stem cells with a vaccine-induced patient-derived HLA-A*02-restricted TCR specific to the cancer-associated antigen PTPRZ1	15
2.1.1 <i>PTPRZ1</i> is exclusively overexpressed in glioma cells and associated with tumor purity and poor prognosis	15
2.1.2 <i>PTPRZ1</i> is abundantly expressed at protein levels and dominantly presented on MHC I	20
2.1.3 <i>PTPRZ1</i> is associated with distinct cellular states and GB stem cells	22

2.1.4 A vaccine-induced T cell receptor binds to intracellularly processed and presented PTPRZ1 ¹⁸¹⁴⁻¹⁸²² without evidence of off-target reactivity	24
2.1.5 PTPRZ1 ¹⁸¹⁴⁻¹⁸²² TCR acts antigen-specifically and facilitates orchestration of antigen-reactive CD4 ⁺ and CD8 ⁺ primary T cells.....	29
2.1.6 PTPRZ1 ¹⁸¹⁴⁻¹⁸²² TCR-T cells are efficacious in controlling experimental flank and brain tumors.....	34
2.1.7 PTPRZ1 ¹⁸¹⁴⁻¹⁸²² TCR targets all examined patient-derived HLA-A*02 ⁺ GB spheroid cell lines, especially the stem-like slow-cycling cell	39
2.1.8 PTPRZ1 ¹⁸¹⁴⁻¹⁸²² TCR-T cells partly control tumors in patient-derived xenograft model in combinatorial therapy.....	42
2.1.9 PTPRZ1 ¹⁸¹⁴⁻¹⁸²² TCR-T cells impact GB cellular state distribution and target GB stemness in individual patient tumor organoids	44
2.2 Developing TCRs against glioblastoma-associated antigens	47
2.2.1 Glioblastoma-associated antigen selection and immunogenic epitope prediction	47
2.2.2 GAA-reactive CD4 ⁺ T cell identification and expansion.....	52
2.2.3 GAA-reactive CD8 ⁺ T cell identification and expansion.....	54
2.2.4 <i>In vitro</i> vaccination expanding antigen-reactive T cells from healthy donors	56
2.3 Glioma MHCII expression and its effects on immunotherapy	58
2.3.1 A subset of gliomas express MHCII.....	58
2.3.2 Glioma MHCII expression is associated with poor prognosis and immune infiltration	60
2.3.3 Glioma MHCII is functional	62
2.3.4 Glioma MHCII does not promote disease progression but attracts immune cells	64
2.3.5 Glioma MHCII induces immune checkpoint molecules intrinsically and extrinsically and expands but exhausts reactive T cells	67
2.3.6 Glioma MHCII does not impact immunotherapy efficacy.....	71

3	Discussion	73
3.1	Phase I clinical trial with the discovered PTPRZ1 ¹⁸¹⁴⁻¹⁸²² TCR and further discovery of PTPRZ1-reactive receptors.....	73
3.2	Routes for adoptive cell transfer for brain tumors	76
3.3	Cell therapy with further equipped cell products or other effector cells.....	77
3.4	Antigen-reactive TCR discovery platforms	79
3.5	Models for brain tumor immunotherapy.....	80
3.6	Conclusion.....	82
4.	Materials and Methods.....	83
4.1	Models.....	83
4.1.1	Animals	83
4.1.2	Individual-patient tumor organoid (IPTO).....	83
4.2	Cell culture	84
4.2.1	Cell lines	84
4.2.2	CD4 ⁺ antigen-specific T cell expansion	85
4.2.3	CD8 ⁺ antigen-specific T cell expansion	86
4.2.4	Dendritic cell generation	86
4.2.5	Electroporation of Jurkat cells	87
4.2.6	Transduction of primary human T cells.....	87
4.2.7	Adoptive cell transfer on IPTO	88
4.2.8	<i>In vitro</i> vaccination with healthy donor PBMCs	88
4.2.9	Knockout cell line generation.....	89
4.3	Animal handling.....	90
4.3.1	Subcutaneous tumor inoculation	90
4.3.2	Intracranial tumor inoculation	90
4.3.3	Intravenous adoptive cell transfer.....	90

4.3.4 Intracerebroventricular adoptive cell transfer	91
4.3.5 Organ harvest and murine brain tumor processing	91
4.3.6 Immune checkpoint blockade treatment (ICB)	92
4.3.7 Vaccination and vaccine therapy	92
4.3.8 Magnetic resonance imaging.....	92
4.4 Antibody-based assays	93
4.4.1 Immunofluorescence	93
4.4.2 Flow cytometry and fluorescence-activated cell sorting (FACS)	94
4.4.3 Enzyme-linked immunosorbent spot (ELISpot)	94
4.4.4 T2 presentation assay	95
4.4.5 Antibodies and fluorescence labeling kits.....	95
4.5 Molecular assays.....	97
4.5.1 Untargeted ligandomics.....	97
4.5.2 LDH release.....	98
4.5.3 RNAscope™	98
4.5.4 RNA isolation	99
4.5.5 Reverse transcription.....	99
4.5.6 qPCR	100
4.6 Computational analysis	100
4.6.1 TCGA and publicly available dataset analysis	100
4.6.2 Single-cell RNA-seq and analysis	100
4.6.3 ARDitox off-target prediction.....	101
4.6.4 Immunogenic epitope prediction.....	101
4.6.5 Statistical analysis and figures	101
5. References	102

List of Abbreviations

AC-like	Astrocyte-like
ACT	Adoptive cell transfer
AI	Artificial intelligence
APC	Antigen-presenting cell
BBB	Blood-brain barrier
CAR	Chimeric antigen receptor
CAR-T cell	CAR-transgenic T cell
CSF	Cerebral spinal fluid
DC	Dendritic cell
DEG	Differentially expressed gene
FACS	Fluorescence-activated cell sorting
FBS	Fetal bovine serum
FCC	Fast-cycling cell
FDA	Food and Drug Administration
Flu	Influenza
GAA	GB-associated antigen
GB	Glioblastoma
GSA	GB-specific antigen
GSEA	Gene set enrichment analysis
GvHD	Graft-versus-host disease
HEV	High endothelial venule
HLA	Human leukocyte antigen
HLAI	HLA class I
i.cv.	Intracerebroventricular
i.t.	Intratumoral
i.v.	Intravenous
ICB	Immune checkpoint blockade
INVENT4GB	Intraventricular T cell receptor transgenic T cell therapy to treat glioblastoma
iPSC	Induced pluripotent stem cell
IPTO	Individual patient tumor organoid
KO	Knock out
LGG	Low-grade glioma
MACS	Magnetic-activated cell sorting
MES-like	Mesenchymal-like
MHC	Major histocompatibility complex
MHCII	MHC class II
NPC-like	Neural-progenitor like
OE	Overexpress
OPC-like	Oligodendrocyte-progenitor-like
P/S	Penicillin/Streptomycin

PBMC	Peripheral blood mononuclear cell
PDX	Patient-derived xenograft
PTPRZ1	Protein tyrosine phosphatase receptor type Z1
s.c.	Subcutaneous
S/MAR	Non-viral, non-integrating episomal scaffold matrix attachment region
sc	Single-cell
SCC	Slow-cycling cell
scFv	single-chain variable fragment
scRNA-seq	Single-cell RNA sequencing
scRTCR-seq	Single-cell TCR sequencing
TAA	Tumor-associated antigen
TCGA	The Cancer Genome Atlas
TCR	T cell receptor
TCR-T cell	TCR-transgenic T cell
Tfh	T follicular helper
Th1	T-helper 1
Th17	T-helper 17
Th2	T-helper 2
TIL	Tumor-infiltrating lymphocyte
TME	Tumor microenvironment
TMG	Tandem minigene
Treg	Regulatory T cell
TSA	Tumor-specific antigen
TTA	Tumor-testis antigen
WT	Wild-type

List of figures

Figure 1: Immunotherapy against cancers	3
Figure 2: Mutation burden association with immunotherapy response and current advances in glioma immunotherapy	5
Figure 3: Known PTPRZ1 molecular interactions and downstream signaling	9
Figure 4: Outcomes of MHCII interaction through extracellular and intracellular signaling.....	13
Figure 5: <i>PTPRZ1</i> expression and its association with tumor purity and prognosis in gliomas.....	16
Figure 6: <i>PTPRZ1</i> expression at single-cell resolution in published and self-generated scRNA-seq datasets	18
Figure 7: Protein expression of PTPRZ1 and its presentation on MHCI in GB	21
Figure 8: Correlation of <i>PTPRZ1</i> expression with GB cellular states and stemness	23
Figure 9: Identification of PTPRZ1-reactive TCR.....	25
Figure 10: Tandem minigene cell line establishment and assessment of TCR recognition against intracellularly processed antigen	26
Figure 11: PTPRZ1 ¹⁸¹⁴⁻¹⁸²² TCR off-target reactivity evaluation	28
Figure 12: Characterization of TCR-engineered primary human T cell product	30
Figure 13: Activation of CD8 ⁺ TCR-T cells and cytotoxicity upon antigen recognition	31
Figure 14: Activation of CD4 ⁺ TCR-T cells and effects of additional irradiation on tumor cells.....	32
Figure 15: Detailing the role of CD4 ⁺ T cells carrying the CD8-restricted TCR	33
Figure 16: Intravenous ACT of PTPRZ1 ¹⁸¹⁴⁻¹⁸²² TCR-T cells in a flank tumor model	34
Figure 17: Intravenous and intracerebroventricular delivery of PTPRZ1 ¹⁸¹⁴⁻¹⁸²² TCR-T cells in an experimental brain tumor model	36
Figure 18: Profiling transferred T cells and investigating recurrence mechanism	38

Figure 19: Preferential killing of stem-like slow-cycling cells by PTPRZ1 ¹⁸¹⁴⁻¹⁸²² TCR-T cells.....	40
Figure 20: HLA-A*02-dependency of PTPRZ1 ¹⁸¹⁴⁻¹⁸²² TCR and its coverage.....	41
Figure 21: Patient-derived xenograft models treated with PTPRZ1 ¹⁸¹⁴⁻¹⁸²² TCR-T cells	43
Figure 22: Preferential targeting GB subsets by the PTPRZ1 ¹⁸¹⁴⁻¹⁸²² TCR-T cell.....	45
Figure 23: Candidate GAA selection and characterization in brain tumors	48
Figure 24: Immunogenic epitope prediction and auto-reactivity and peptide binding validation.....	50
Figure 25: Identification and isolation of GAA-reactive CD4 ⁺ T cell in A2.DR1 mice	53
Figure 26: Identification and isolation of GAA-reactive CD8 ⁺ T cell with A2.DR1 mice	55
Figure 27: <i>In vitro</i> vaccination.....	56
Figure 28: Glioma MHCII expression at protein and transcript levels.....	59
Figure 29: Clinical and molecular impacts of glioma MHCII expression in LGG	61
Figure 30: Generation of MHCII ⁻ and MHCII ⁺ murine glioma cell lines with GL261..	63
Figure 31: Glioma MHCII expression impacts in <i>in vivo</i> mouse models.....	65
Figure 32: Immune microenvironment alteration in I-A-expressing gliomas.....	66
Figure 33: Glioma MHCII expression functional effects on tumor cells	67
Figure 34: Glioma MHCII expression functional effects on CD4 ⁺ T cells.....	68
Figure 35: Glioma MHCII expression functional effects on CD8 ⁺ T cells.....	69
Figure 36: MHCII intracellular signaling-directed cell death	70
Figure 37: Glioma MHCII expression effects on immunotherapy efficacy	72

List of tables

Table 1: Antigens encoded in TMG	27
Table 2: ARDitox predicted off-target safety score and presentation score	28
Table 3: Shortlisted NetMHCpan-4.1-predicted immunogenic epitopes of GAAs for HLA-A*0201	51
Table 4: Shortlisted NetMHCIIpan-4.0-predicted immunogenic epitopes of GAAs for HLA-DRB1*0101	51
Table 5: Frequency of MHCII expression in gliomas	59

1 Introduction

1.1 Immunotherapy for cancers

Modern technology and medicine have enabled a constant increase in life expectancy, yet they have also led to a moderately growing incidence rate of cancer (Garmany et al., 2021; Shelton et al., 2024). Despite advances in the biomedical field, cancer remains the second leading cause of death (Poorolajal, 2020). Traditional standard of care includes surgical resection followed by radio- and/or chemotherapy to eradicate potential circulating tumor cells or micrometastases (Kaur et al., 2023). However, these treatments are not specific to cancers and can result in significant adverse effects; moreover, the malignant disease often becomes resistant to these treatments and recurs. Therefore, different modalities of therapies have been exploited to combat the cancer crisis over the last decades, including immunotherapy, which can be designed to be cancer-specific and has demonstrated remarkable success (Kaur et al., 2023). Nevertheless, one of the main hallmarks of cancer is its ability to evade immune surveillance (Hanahan, 2022).

Immunotherapy can be summarized into five categories: cancer vaccines, cytokine therapies, immune checkpoint blockade (ICB), oncolytic virus therapies, and adoptive cell transfer (ACT) (**Figure. 1A**) (Zhang and Zhang, 2020). The first three assist and enhance endogenous pre-existing anti-tumor immunity, while oncolytic viruses directly act on tumor cells, and ACT employs expanded tumor-reactive T cells or engineered T cells. ICB prevents the co-inhibitory signal between T cells and antigen-presenting cells (APCs) or tumor cells, allowing the full unleashing of T cell effector function and tumor control, and is approved by the FDA to treat many cancers such as melanoma, lung cancer, and lymphoma (Xiao et al., 2020; Yadav et al., 2022). On the other hand, ACT has greatly counteracted blood cancers with more than a 50% clinical response rate, leading to long-term survival, but it is still under extensive exploration to treat solid tumors (Cappell and Kochenderfer, 2023; Marco et al., 2023).

1.1.1 CAR-T cell therapy

One mode of ACT equips T cells with chimeric antigen receptors (CARs) to facilitate recognition and lysis of target tumor cell by binding to cell surface antigen. CAR is constructed with a single-chain variable fragment (scFv) derived from a monoclonal

antibody incorporated with co-stimulatory domains from CD3, CD28, or CD137 (**Figure. 1B**) (Drougkas et al., 2022). Several CAR-transgenic T (CAR-T) cell therapies are FDA-approved to treat hematologic cancers, such as refractory B-cell lymphoma, B-cell acute lymphoblastic leukemia, and refractory multiple myeloma (Wang and Wang, 2023). However, CAR-T cell therapy against solid tumors has not shown promising results in the clinic unless synthetically improved (Choi et al., 2024; Marco et al., 2023). CAR-T cell therapy trials and their target antigens are further discussed in **1.3 Brain tumor-derived antigens**. The challenges, including limited cancer-specific cell surface antigens and marginal clinical benefits of CAR-T cell therapy, urge the development of combinatorial treatments and other modalities of cell therapy.

1.1.2 TIL and TCR-T cell therapy

Tumor infiltrating lymphocytes (TILs) consist of a higher frequency of tumor-reactive T cells; hence, another mode of ACT, TIL therapy, involves expanding TILs with high-dose IL-2 and reinfusing the cells back to patients, using spontaneously tumor-reactive T cells to combat malignancy. TIL therapy is extensively conducted in melanoma cases as the tumor is relatively more immunologically hot (Monberg et al., 2023), making it easy to retrieve TILs. Several trials have attempted this therapy on melanoma patients with 40-50% response rates. Eventually in 2024, the first TIL therapy received FDA approval for the treatment of unresectable/metastatic melanomas (NatBiotech, 2024). TIL therapy is also investigated for non-melanoma cancers in phase I and II trials but the response rates have not been as promising (Creelan et al., 2021; Stevanović et al., 2019). Depending on the tumor microenvironment (TME) and due to chronic antigen exposure, cancer-reactive TILs are often too exhausted or dysfunctional to be expanded or to exert effector functions. Therefore, yet another mode of ACT engineers T cells with cancer-reactive T cell receptors (TCRs) discovered in TILs or immunized individuals (see **1.4 Cancer-reactive TCR discovery**).

TCRs engage through the major histocompatibility complex (MHC), which differs from individual to individual, they can essentially target any antigen as long as it is processed and presented on MHC, unlike CARs, whose antigens are restricted to cell membrane proteins (**Figure. 1C**) (Rosenberg and Restifo, 2015). The nature of antigen recognition by TCRs conceivably broadens the range of targetable antigens. Besides hematologic cancers, TCR-transgenic T (TCR-T) cell therapy is extensively explored for solid tumors. Hitherto, more than 15 phase I and over nine phase II trials

are currently underway (Baulu et al., 2023), and encouraging results have been reported from the trials with objective response rates ranging from 10% to 60%. Recently, a TCR-based T cell engager therapy, Tebentafusp, which is composed of a TCR specific to human leukocyte antigen (HLA)-A*02:01-gp100 to bind to tumor cell and an antibody arm binding to CD3 to activate close-proximity T cells, was FDA-approved due to its substantial overall survival benefit in treating unresectable metastatic uveal melanoma (Mullard, 2022; Nathan et al., 2021). The first approved CAR-based T cell engager and CAR-T cell therapy were in 2014 and 2017 respectively, starting with hematologic malignancies (Mitra et al., 2023; Viardot and Bargou, 2018). Only very recently, in July 2024, did the FDA grant accelerated approval to a TCR-T cell therapy against synovial sarcoma (Harrison, 2024). A long road and significant efforts still lie ahead to fully realize the potential of TCR-T cell therapy in the clinic for solid tumors, particularly brain cancers.

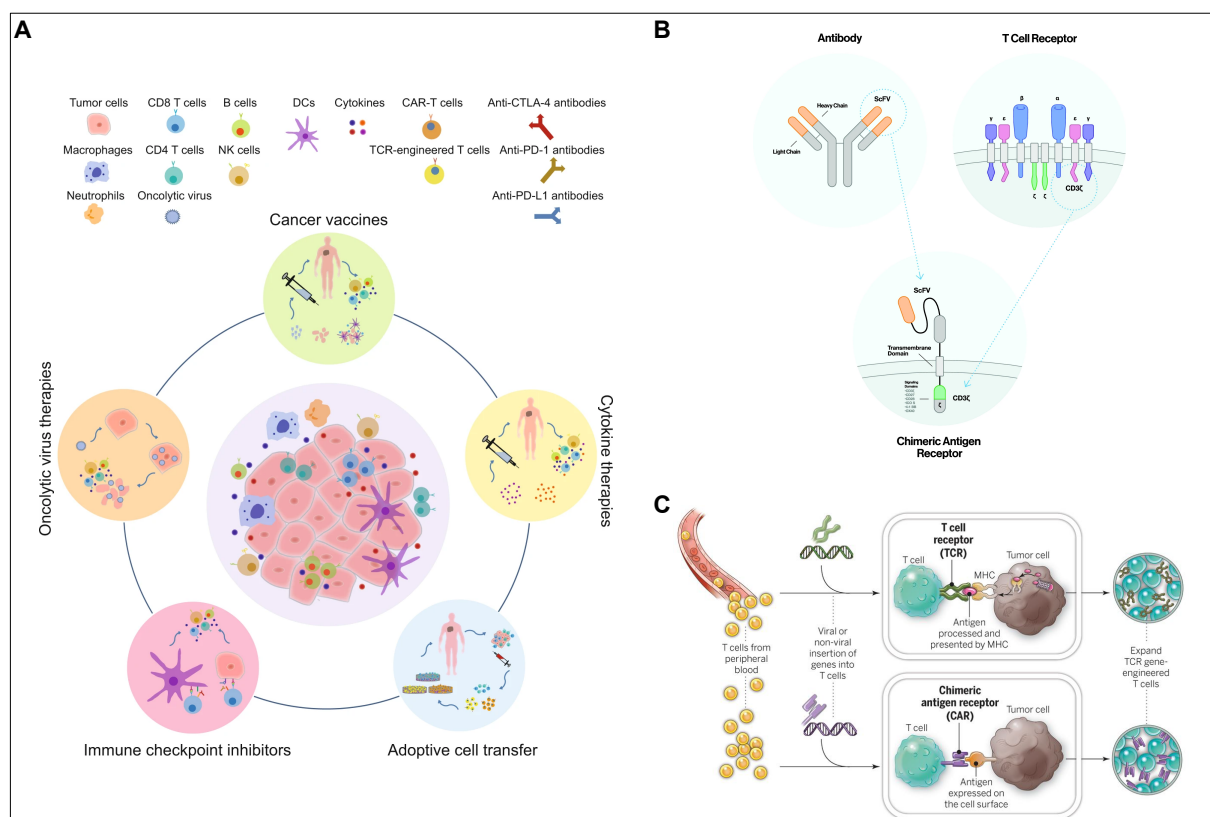


Figure 1: Immunotherapy against cancers

A. Different modalities of immunotherapies to treat cancers. Adapted from Zhang and Zhang (2020). **B.** Chimeric antigen receptor (CAR) structure, consisting of an scFV derived from a monoclonal antibody and co-stimulatory domains from TCR signaling. Adapted from Drougkas et al. (2022). **C.** Generation of CAR-T and TCR-T cells and the mechanism of antigen presentation for TCR recognition. Adapted from Rosenberg and Restifo (2015).

1.2 Immunotherapy for brain tumors

Apart from the high mortality rate and the expected 15-month median survival, glioblastoma (GB), the most common malignant tumor of the central nervous system and, unlike other solid tumors, is characterized by immune-privileged compartmentalization by the blood-brain barrier (BBB), an immunosuppressive TME, and a relatively low mutation burden (Bausart et al., 2022; Tian et al., 2015). The existence of tight junction-forming BBB limits the delivery of most large-molecule therapeutics and cells from the periphery unless further engineered (Kim et al., 2020; Ulapane et al., 2019). Moreover, immunotherapy efficacy is associated with tumor mutation burden; a previous study revealed that GB is one of the least responsive entities to ICB (**Figure. 2A**) (Yarchoan et al., 2017). Together, these features make GB a tough malignancy for immunotherapy application, as reflected by several immunotherapy trials that have been conducted.

The IMA950 and GAPVAC-101 trials vaccinated newly diagnosed GB patients with warehouses of peptides covering tumor-associated antigens (TAAs) or TAAs (APVAC1) and patient-individual tumor-specific antigens (TSAs, APVAC2) respectively (**Figure. 2B**) (Bunse et al., 2022; Hilf et al., 2018; Migliorini et al., 2019). The vaccines elicited immunogenicity with mild-to-moderate adverse effects, but some patients showed radiographic responses. Meanwhile, CAR-T cell therapy was also utilized to treat GB, targeting cell surface TAAs or TSAs, yet only limited efficacy was observed even in combination with ICB (Bagley et al., 2024a; Bunse et al., 2022; Wang and Wang, 2022). CAR-T cell therapy for GB is limited by subclonal and scarce transmembrane TAAs and TSAs, including IL13R α 2, HER2, B7-H3, and EGFRvIII (see **1.3 Brain tumor-derived antigens**); furthermore, a recent study demonstrated that CAR-T cell therapy efficacy is influenced by target altered glycosylation (Heard et al., 2022), and such aberrant post-translation modification is often reported in cancers with GB being no exception (Rosa-Fernandes et al., 2022; Tokumura et al., 2024). On the other hand, GB rarely alters MHC expression or the antigen presentation pathway (Dhatchinamoorthy et al., 2021), and thereby, TCR-T cell therapy may serve a better strategy to combat the disease.

Previously, several glioma-reactive TCRs have been developed. An HLA-A*02-restricted TCR targeting a GB-associated antigen (GAA), NLGN4X, was retrieved and

examined in an experimental glioma mouse model, showing preclinical therapeutic efficacy (Krämer et al., 2024). In addition, over 30 MHC class II (MHCII)-restricted TCRs specific to H3K27M, a TSA of a distinct subtype of diffuse midline glioma, were characterized (Boschert et al., 2024). Both studies involved isolation of reactive T cells from patients who were immunized and experienced favorable clinical responses. Similarly, upon vaccination, a TCR restricted to HLA-DRA*0101 HLA-DRB1*0101 against CICR215W, a subclonal TSA of oligodendroglioma, was identified using a humanized mouse strain, A2.DR1 (see **4 Materials and Methods**), and interestingly, such MHCII-restricted TCR-engineered T cells could hinder tumor growth in an experimental glioma mouse model although they did not mediate direct target killing (Kilian et al., 2022). As evidenced above, glioma-reactive TCRs could be elicited and retrieved; thus, the selection of antigens and immunogenic epitopes is of importance to cover as many patients as possible.

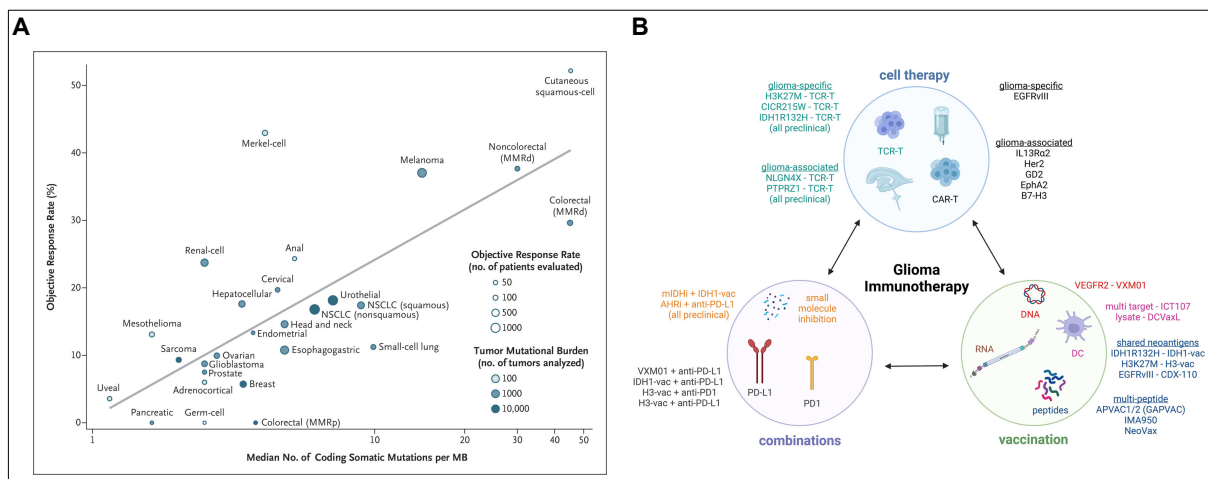


Figure 2: Mutation burden association with immunotherapy response and current advances in glioma immunotherapy

A. Various cancer entities and their mutation burden correlation to ICB response. Adapted from Yarchoan et al. (2017). **B.** Different immunotherapy modalities applied to gliomas and example cases listed for each modality. Adapted from Bunse et al. (2022).

1.3 Brain tumor-derived antigens

Cancers originate from and are featured with a series of mutation events, resulting in potentially targetable TSAs. The most frequent somatic mutations occur in genes involved in DNA repair/maintenance, cell cycle regulation, and signaling pathways (Mendiratta et al., 2021). Unlike other solid tumors, where the majority of patients carry loss-of-function TP53 mutation or gain-of-function proto-oncogene mutations (Hu et al., 2021; Yang et al., 2019), GB is not characterized by distinct shared mutations but rather by altered signaling pathways, including PI3K, MAPK, p53, and pRB pathways (Ah-Pine et al., 2023). This presents challenges for the application of TCR-T or CAR-T cell therapies. Nonetheless, several relatively common neoantigens have been investigated for their targetability and treatment efficacy in preclinical and clinical brain tumor studies in cell therapy context.

IDH1 mutations occur in over 70% of glioma patients with IDH1R132H being the most frequent variant (Yan et al., 2009). The mutant protein possesses the enzymatic function to produce the oncometabolite *R*-2-hydroxyglutarate, which suppresses myeloid and lymphocyte functions in the TME (Bunse et al., 2018; Friedrich et al., 2021). A peptide vaccine covering the mutant IDH1 is able to elicit CD4⁺ T cell response and control experimental tumors (Platten et al., 2021; Schumacher et al., 2014). In addition, multiple IDH1R132H-reactive TCRs from the vaccinated patients upon *in vitro* mutant peptide-mediated expansion were identified (Lindner, 2023). Further investigation is required to determine if the identified CD4 TCRs can be used to generate TCR-T cell products to control immunosuppressed IDH1R132H-glioma and whether the vaccine also induces reactive cytotoxic CD8⁺ T cells.

Besides TCRs discovered for the aforementioned neoantigens H3K27M and CICR215W (Boschert et al., 2024; Kilian et al., 2022), targeting EGFRvIII, a GB-specific antigen (GSA) generated by alternative splicing and found in approximately 20% of GB patients, is being explored with CAR-T cell therapy (Bunse et al., 2022). However, recent studies revealed that intravenous (i.v.) delivery of EGFRvIII-CAR T cells, alone or in combination with ICB, did not benefit newly diagnosed or recurrent EGFRvIII⁺ GB patients (Bagley et al., 2024a; O'Rourke et al., 2017). Interestingly, using intracerebroventricular (i.cv.) delivery of CARv3-TEAM-E T cells, EGFRvIII-CAR T cells engineered to secrete wild-type (WT) EGFR-binding T cell engagers, to treat

GB exhibited rapid and dramatic radiographic response in all three patients (Choi et al., 2024). To be taken cautiously, although over half of GB patients carry WT EGFR amplification or upregulation, some adult normal tissues also express WT EGFR at moderate level, including intestine (Suzuki et al., 2010), which could lead to on-target off-tumor targeting of CARv3-TEAM-E T cells as shown in one patient whose cause of death was attributed to gastrointestinal perforation after the treatment in spite of local administration of the cell product (Choi et al., 2024).

Apart from TSAs, targeting TAAs is also heavily researched on and should be further explored for GB treatment as it does not harbor as many mutations as other cancers (**Figure. 2A**). Nonetheless, one crucial caveat is that some TAAs are adequately expressed in adult normal tissues, similar to the example of WT EGFR, although greatly upregulated in tumors. CAR-T cell therapies have been developed to target cell surface GAAs, HER2, B7-H3, and IL13R α 2 (Bunse et al., 2022). While these GAAs are overexpressed in more than half of GB patients, they are often intra-tumorally heterogeneously expressed and are also present in some adult normal tissues (Jarboe et al., 2007; Liu et al., 2004; Nehama et al., 2019; TheHumanProteinAtlas, 2024). GB patients treated with CAR-T cells for these GAAs experienced minor adverse effects and limited therapeutic benefits, with some patients showing antigen loss upon the treatment (Ahmed et al., 2017; Brown et al., 2015). Notably, a recent trial employed a bivalent CAR-T cell product targeting both EGFR and IL13R α 2 to treat recurrent GB and showed early radiographic response in all six patients accompanied by, however, early onset of neurotoxicity that had to be controlled with high-dose immunosuppressants (Bagley et al., 2024b).

As constrained by CAR-antigen recognition mechanism, cell surface GSA and GAAs were emphasized. Nevertheless, with advances in TCR-T therapy, other GAAs were investigated for their targetability using cancer vaccines and TCR-T cells as they are not restricted by target expression location in the presence of antigen presentation machinery. An MHC class I (MHCI) ligandomic analysis was conducted to discover GAAs presented on GB tumors, and NLGN4X, a postsynaptic adhesion molecule, was found to be overexpressed and abundantly presented on MHCI (Dutoit et al., 2012; Dutoit et al., 2018). The IMA950 and GAPVAC-101 trials vaccinated GB patients with the identified HLA-A*02 NLGN4X peptide along with other candidate GAAs and/or GSAs (Hilf et al., 2018; Migliorini et al., 2019). A subsequent study multimer-sorted an

NLGN4X-reactive TCR and demonstrated its potential in controlling GB with an experimental murine GB model (Krämer et al., 2024). Another GAA, protein tyrosine phosphatase receptor type Z1 (PTPRZ1), and its presented peptides were also identified abundantly in the ligandomic analysis (Dutoit et al., 2012).

1.3.1 GB-associated antigen and GB stem cell marker: PTPRZ1

PTPRZ1 is involved in central nervous system development, including axon guidance and outgrowth (Eill et al., 2020; Johnson and Vactor, 2003). Binding to its ligands, PTN and MK, leads to oligomerization and inactivation of the phosphatase receptor, resulting in sustained phosphorylation of its substrates, such as β -catenin and ALK (**Figure. 3**) (Maeda et al., 1996; Nagai et al., 2022; Perez-Pinera et al., 2007). Its absence causes early onset of oligodendrocyte differentiation and disruption of the perineuronal net (Eill et al., 2020; Kuboyama et al., 2012). While its expression is very limited across adult tissues, it is essential for gliomagenesis. In GB, PTPRZ1 takes part in cancer cell proliferation, migration, and invasiveness (Bourgonje et al., 2014; Qin et al., 2017; Ulbricht et al., 2006). Moreover, it contributes to angiogenesis and tumor radio-resistance (E et al., 2016; Lacore et al., 2022). Notably, depletion of PTPRZ1 results in significant impairment of glioblastoma cell sphere formation *in vitro* and delays tumor growth *in vivo*, indicating a strong association of PTPRZ1 with glioblastoma cell stemness (Fujikawa et al., 2017; Shi et al., 2017). Recent studies have utilized PTPRZ1 along with other markers, including CD133, ITGB8, CD44, and SOX2, to define GB stem cells (GSCs) in single-cell (sc) transcriptomic and flow cytometric analyses (Patel et al., 2014; Yang et al., 2022).

As found abundantly presented and considered a GSC marker, PTPRZ1 serves a potent target for eradicating GB from the cells responsible for tumor initiation and therapy resistance. Two peptides derived from the extracellular domain of PTPRZ1 were identified in MHC-I ligandomic analysis and used in immunization for the IMA950 trial along with other presented GAAs (Dutoit et al., 2012; Dutoit et al., 2018; Migliorini et al., 2019). Furthermore, besides the two peptides, in the GAPVAC-101 trial, four additional predicted immunogenic MHC-I peptides encoded in PTPRZ1, spanning both extracellular and intracellular domains, were employed for GB patient vaccination along with peptides of other GAAs and GSAs (Hilf et al., 2018). Out of the PTPRZ1 peptides in the GAPVAC-101 trial, only HLA-A*02-restricted PTPRZ1¹³⁴⁷⁻¹³⁵⁵ and PTPRZ1¹⁸¹⁴⁻¹⁸²² elicited immunogenicity in over 90% of vaccinated patients, and

multimer sorted- PTPRZ1¹⁸¹⁴⁻¹⁸²²-T cells demonstrated cytotoxicity against HLA-A*02⁺ GB cell lines with PTPRZ1 expression. However, the reactive TCRs for the two peptides PTPRZ1¹³⁴⁷⁻¹³⁵⁵ and PTPRZ1¹⁸¹⁴⁻¹⁸²², were not subsequently identified.

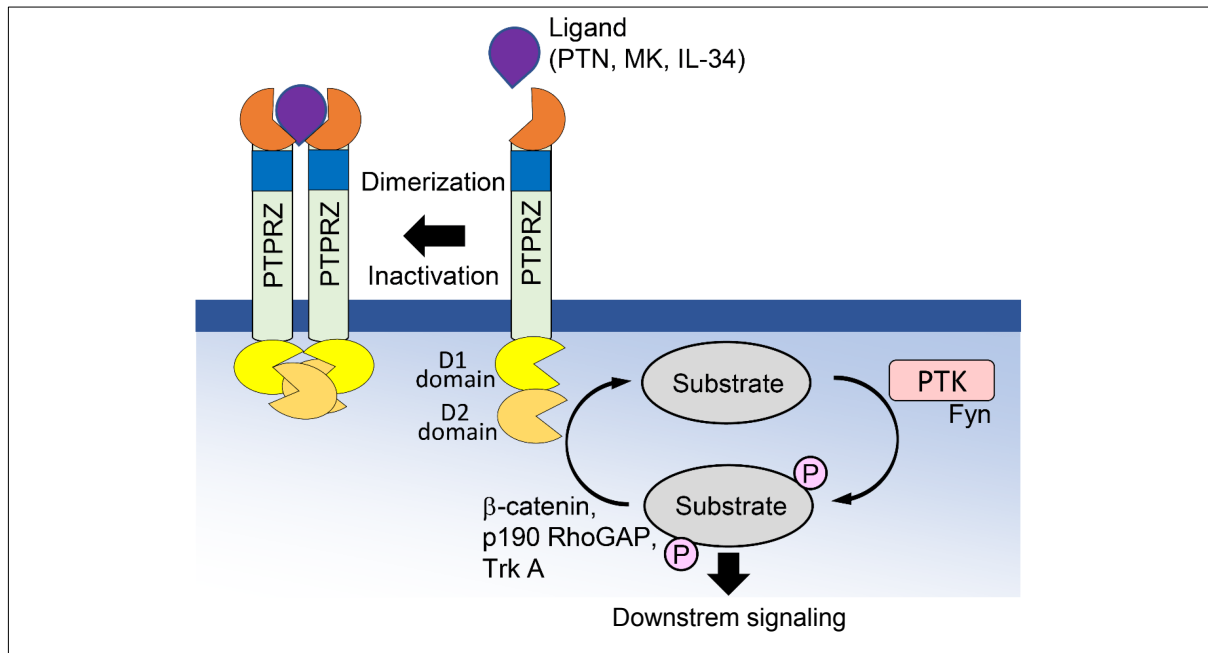


Figure 3: Known PTPRZ1 molecular interactions and downstream signaling

Modified from Nagai et al. (2022).

1.4 Cancer-reactive TCR discovery

To discover cancer-reactive TCRs, one can expand TILs with or without APCs. Since TILs are rich in tumor-reactive T cells, the likelihood of retrieving reactive TCRs is higher. The conventional TIL expansion method using high-dose IL-2 may not favor the proliferation of reactive T cells as these cells are often exhausted and/or dysfunctional within the TME (Scott et al., 2019), skewing towards other non-reactive TCR clonotypes (Poschke et al., 2020). A recent study has improved the efficiency and sensitivity of TIL expansion using engineered B cells to present a predicted panel of tumor antigens and to express cytokines and ligands to rejuvenate exhausted/dysfunctional TILs (Arnaud et al., 2021). Moreover, with advances in artificial intelligence (AI), a machine learning classifier, PredicTCR, was developed to identify individual tumor-reactive TILs based on gene expression from sc RNA sequencing (scRNA-seq) data, enabling accelerated personalized TCR-T cell therapy by circumventing laborious TCR testing (Tan et al., 2024). A caveat of these identified cancer-reactive TCRs from TILs or AI prediction is that the cognate antigen remains unknown unless further screened (Kohlgruber et al., 2024), posing a risk of on-target off-tumor effects.

Alternatively, one can expand reactive T cells against known tumor-derived antigens as shown in the studies for H3K27M, CICR215W, and NLGN4X (Boschert et al., 2024; Kilian et al., 2022; Krämer et al., 2024). It requires the *in vivo* priming and expansion of pre-existing reactive T cells in the host upon vaccination, and subsequent *in vitro* expansion and isolation with the peptides of interest. Such strategy is, however, limited by the need for patients to be immunized and develop immune response, which can be time-consuming and administrative burdensome, or by requiring a well-established MHC-humanized mouse strain. In addition, exogenous peptide-induced immunogenicity does not necessarily elicit a response against naturally processed and presented antigens (Viner et al., 1996). Oftentimes, several reactive TCRs are identified but must be validated for their reactivity against physiologically processed antigens, yet the therapeutic benefits of them require further investigation with various models. With known target epitopes, potential cross-reactivity can be predicted and examined in preclinical settings.

To alleviate the constraints of patient vaccination and engineered murine hosts, researchers have attempted to *in vitro* prime and expand rare reactive T cell clones from healthy donor peripheral blood using polarized autologous dendritic cells (DCs) loaded with epitopes of interest (Bozkus et al., 2021; Giannakopoulou et al., 2023). As exemplified, reactive T cells against frameshift mutations and recurrent driver mutations were expanded *in vitro* from healthy donors, and the TCR was further identified and tested in a TCR-T cell ACT regimen with preclinical murine models (Giannakopoulou et al., 2023; Roudko et al., 2020); nevertheless, the strategy was not yet shown possible to retrieve TAA-reactive T cells.

1.5 Tumoral MHCII expression and therapy efficacy

The TME is also a determinant of therapy outcome. MHC plays a fundamental role in tuning adaptive immunity (Guo et al., 2024); in cooperation with various cytokines upon MHCII-TCR interaction, naïve CD4⁺ T cells can become anti-tumoral subsets, such as T-helper 1 (Th1) and T follicular helper (Tfh), or pro-tumoral subsets, including T-helper 2 (Th2), T-helper 17 (Th17), and regulatory T cells (Treg) (**Figure. 4A**). Anti-tumoral CD4⁺ T cells are able to recruit/activate immune cells, reciprocally license CD8⁺ T cell functions through APCs, and, rarely, perform direct killing of the target cell. On the other hand, pro-tumoral CD4⁺ T cells promote immunosuppressive immune cells and suppress functions of APCs and effector cells (Guo et al., 2024; Khelil et al., 2022), leading to a loss of tumor control.

MHCII is predominantly expressed by APCs, such as DCs, B cells, and monocytes, as well as stromal cells (Bawden and Gebhardt, 2023; Kerdidani et al., 2022). Interestingly, recent evidence has revealed that cancer cells may express MHCII constitutively or upon stimulation by IFN γ (Axelrod et al., 2019). In small-cell lung cancers, MHCII is not expressed on tumor cells, but in non-small cell lung cancers, 38% of patients carry MHCII⁺ tumors (Yazawa et al., 1999). In colorectal cancer and prostate cancer, 76.5% and 60% of tumors express MHCII respectively (Michel et al., 2010; Younger et al., 2007). Notably, 30% of breast cancer patients and nearly 50% of melanoma patients have MHCII⁺ tumors that harbor more infiltration of immune cells and are responsive to immunotherapy interventions, as reflected in survival (Johnson et al., 2016; Oldford et al., 2006; Park et al., 2017). Potential interactions between tumoral MHCII and CD4⁺ T cells have been proposed but not independently validated yet (**Figure. 4B**); of note, unlike CD4⁺ T cells interacting with APCs, CD4⁺ T cells interacting with MHCII⁺ tumor cells do not involve co-stimulatory factors, and thereby, complete activation may not be elicited (**Figure. 4A&B**).

In glioma, myeloid MHCII has been in-depth investigated, concluded to be essential for proper T cell priming and tumor control (Kilian et al., 2023). It was observed that glioma MHCII expression does exist and is able to present neoantigens (Bunse et al., 2015; Soos et al., 2001). However, the role of tumoral MHCII in glioma is not elucidated. Furthermore, the intracellular signaling of MHCII, which is known in some APCs (Al-Daccak et al., 2004; Katikaneni and Jin, 2019), leads to activation and proliferation,

especially in the B cell-T cell context. Although the detailed molecular mechanism remains understudied, PKC and PTK are suggested to be involved, but it has not been validated in tumor cells. An observed outcome of MHCII intracellular signaling is cell death, and thereby, experimenters have targeted B cell malignancy with anti-MHCII antibodies (**Figure. 4C**) (Katikaneni and Jin, 2019; Nagy et al., 2002); despite the proapoptotic consequence of the antibody on tumor cells observed at bench side, the administration of it to refractory/relapsed B cell leukemia/lymphoma patients did not show therapeutic benefits (Schweighofer et al., 2012). It also remains unknown if CD4 TCR-tumoral MHCII would transduce intracellular signaling to result in target killing.

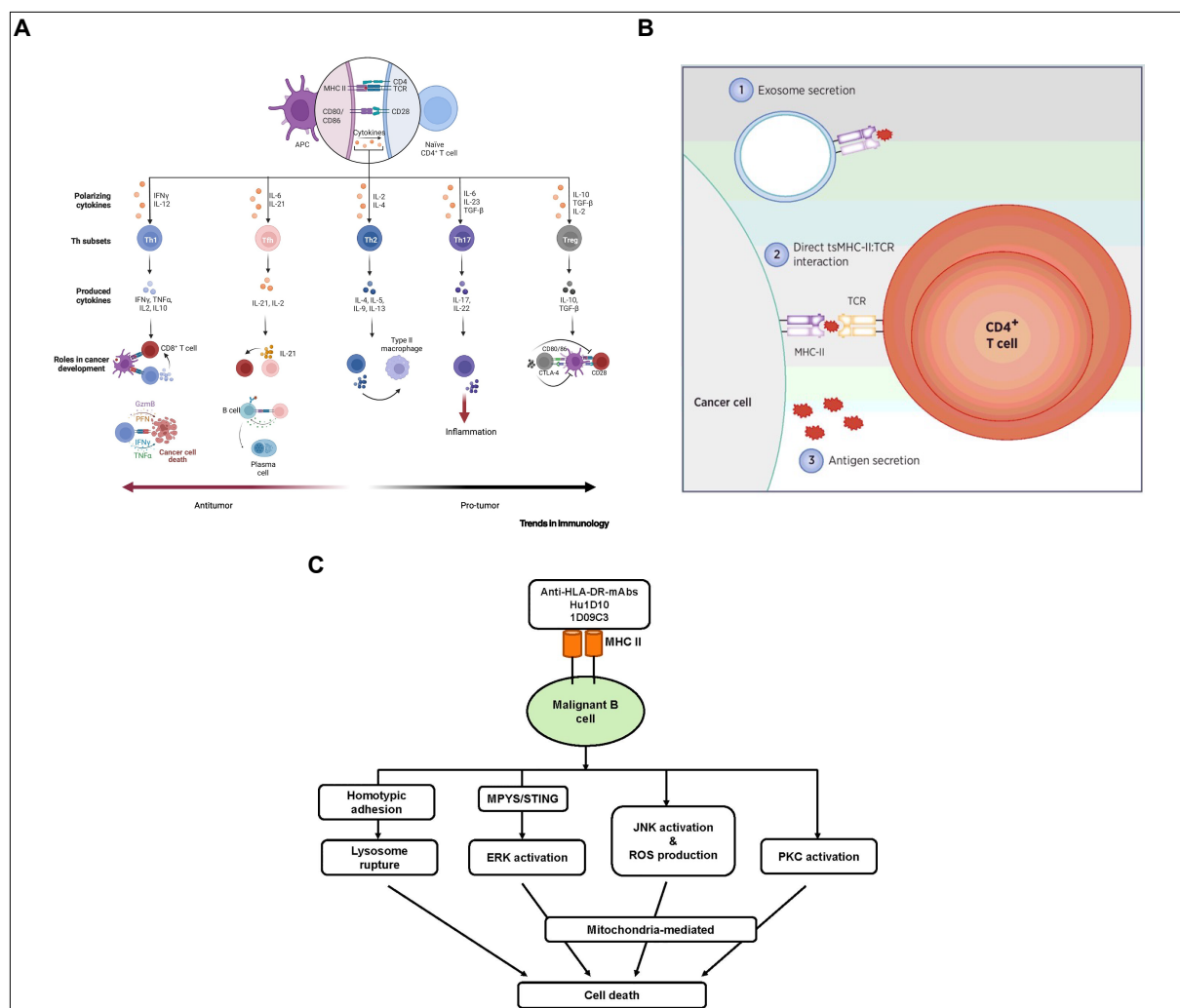


Figure 4: Outcomes of MHCII interaction through extracellular and intracellular signaling

A. CD4⁺ T cell differentiation into anti-tumoral or pro-tumoral subsets upon contact with APCs through TCR-MHCII axis. Adapted from Guo et al. (2024). **B.** Tumor cells interacting via MHCII with TCR of CD4⁺ T cells using distinct mechanisms. Modified from Axelrod et al. (2019). **C.** MHCII intracellular signaling leading to cell death after binding to antibodies. Adapted from Katikaneni and Jin (2019).

1.6 Objectives of the study

Within the study, MHC-dependent immunotherapy for gliomas is developed. As brain tumors rarely alter MHC expression and the antigen presentation machinery, and due to limited surface GSAs or GAAs for conventional CAR-T cell therapy (Bunse et al., 2022; Dhatchinamoorthy et al., 2021), targeting gliomas through the TCR-MHC axis may circumvent the challenges of treating the malignancy.

First objective is to retrieve and validate PTPRZ1-reactive TCR with the aid of available resources from vaccinated patient material from the GAPVAC-101 trial (Hilf et al., 2018). As PTPRZ1 is essential for gliomagenesis and represents GSCs (Bourgonje et al., 2014; Fujikawa et al., 2017; Patel et al., 2014; Qin et al., 2017; Shi et al., 2017; Ulbricht et al., 2006; Yang et al., 2022), targeting such GAA to combat GB presents great potential for disease control by eliminating cancer stem cells.

Second objective is to identify more TCRs for GB targeting candidate GAAs. As brain tumors do not harbor high mutation burden (Tian et al., 2015), targeting GAAs instead of GSAs is an alternative approach for TCR-T cell therapy for gliomas.

Third objective is to investigate the influences of glioma MHCII expression. Exemplified in other cancer entities, tumoral MHCII expression is associated with increased immune infiltrates, response to immunotherapy, and favorable prognosis (Johnson et al., 2016; Michel et al., 2010; Oldford et al., 2006; Park et al., 2017; Yazawa et al., 1999; Younger et al., 2007). Although functional tumoral MHCII expression is observed in gliomas (Bunse et al., 2015; Soos et al., 2001), its consequences on disease progression and its impacts on the TME and treatment efficacy have not been unveiled in brain tumors.

Namely, two main directions will be focused on: identifying and testing glioma-reactive TCRs, and elucidating glioma MHCII expression effects on tumor progression and therapy efficacy. Various models for TCR-T cell testing, different approaches of reactive TCR discovery, and state-of-the-art single-cell technology are employed.

2 Results

2.1 Targeting glioblastoma stem cells with a vaccine-induced patient-derived HLA-A*02-restricted TCR specific to the cancer-associated antigen PTPRZ1

2.1.1 *PTPRZ1* is exclusively overexpressed in glioma cells and associated with tumor purity and poor prognosis

To evaluate the extent of *PTPRZ1* association with gliomas, its expression at the transcript level was first analyzed using publicly available The Cancer Genome Atlas (TCGA) bulk RNA sequencing datasets for GB and low-grade glioma (LGG). In GB, *PTPRZ1* was significantly upregulated in tumors compared to adjacent normal samples (**Figure. 5A**). Whereas a main disadvantage of bulk sequencing is the mixed readout of all the cells in the tumor, including malignant, immune, and stromal cells, tumor ABSOLUTE purity was found to be mildly correlated with *PTPRZ1* (**Figure. 5B**) (Carter et al., 2012). Although *PTPRZ1* is a GAA, its expression was not associated with GB patient clinical survival (**Figure. 5B&C**). On the other hand, in LGG, similarly, *PTPRZ1* was highly expressed in tumors and even more prominent in higher disease grade tumors (**Figure. 5D**). Its mild positive correlation with tumor purity was again observed (**Figure. 5E**), and conversely, higher *PTPRZ1* expression denoted poor prognosis in LGG (**Figure. 5F**).

Results

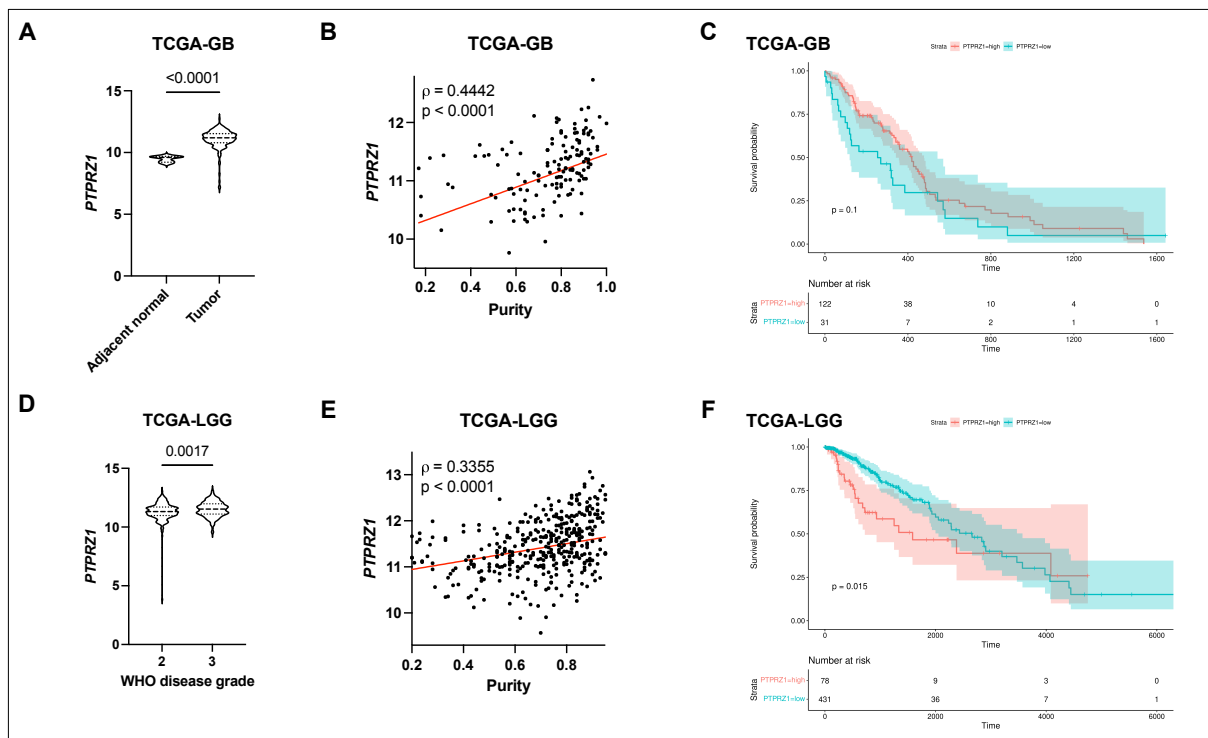


Figure 5: *PTPRZ1* expression and its association with tumor purity and prognosis in gliomas

A. *PTPRZ1* transcript levels in GB tumors and adjacent normal tissues. **B.** *PTPRZ1* correlation with GB tumor ABSOLUTE purity. **C.** Survival analysis of *PTPRZ1* high-expressing GB patients compared with low-expressing GB patients. **D.** *PTPRZ1* transcript levels in different grades of LGG tumors. **E.** *PTPRZ1* correlation with LGG tumor ABSOLUTE purity. **F.** Survival analysis of *PTPRZ1* high-expressing LGG patients compared with low-expressing LGG patients. **(A)** and **(D)** were analyzed with t-test. **(B)** and **(E)** were analyzed using Spearman correlation. **(C)** and **(F)** were performed with the log-rank test for survival analysis.

In order to detail *PTPRZ1* at high cellular resolution, previously published GB and IDH-mutant scRNA-seq datasets were interrogated (Nefel et al., 2019; Venteicher et al., 2017). In GB, *PTPRZ1* was exclusively expressed in malignant cells and not in immune cells such as T cells and macrophages, nor in normal glial cells, oligodendrocytes, and microglia (**Figure. 6A&B**). *PTPRZ1* expression in GB cancer cells varied slightly inter-individually, but upregulation was observed in all patients (**Figure. 6C**). In IDH-mutant gliomas, similar phenomena were observed that *PTPRZ1* was solely expressed in malignant cells and varied slightly across patients (**Figure. 6D-F**). To independently validate the findings, a paired glioma and stromal cell scRNA-seq dataset (n(GB)=16, n(IDH1-mutant glioma)=3, and n(pediatric high-grade glioma)=1, samples from the Neurosurgery Department at University Hospital Mannheim) was generated; briefly, surgically resected primary tumors were dissociated into single cells, followed by fluorescence-activated cell sorting (FACS) or magnetic-activated cell sorting (MACS) to enrich tumor cells and stromal cells separately (**Figure. 6G**, see **4 Materials and Methods**). The isolated cells were then subjected to scRNA-seq and primary cell line establishment. Different cell types were identified using canonical markers, and *PTPRZ1* was highly expressed in cancer cells, consistent with previous results (**Figure. 6H-J**). The upregulation of *PTPRZ1* in cancer cells was demonstrated across most of the patients with some variation (**Figure. 6K&L**). These observations reinforce that *PTPRZ1* is indeed a GAA that is highly and mostly exclusively overexpressed in malignant cells in gliomas, positively correlating to disease progression and tumor purity.

Results

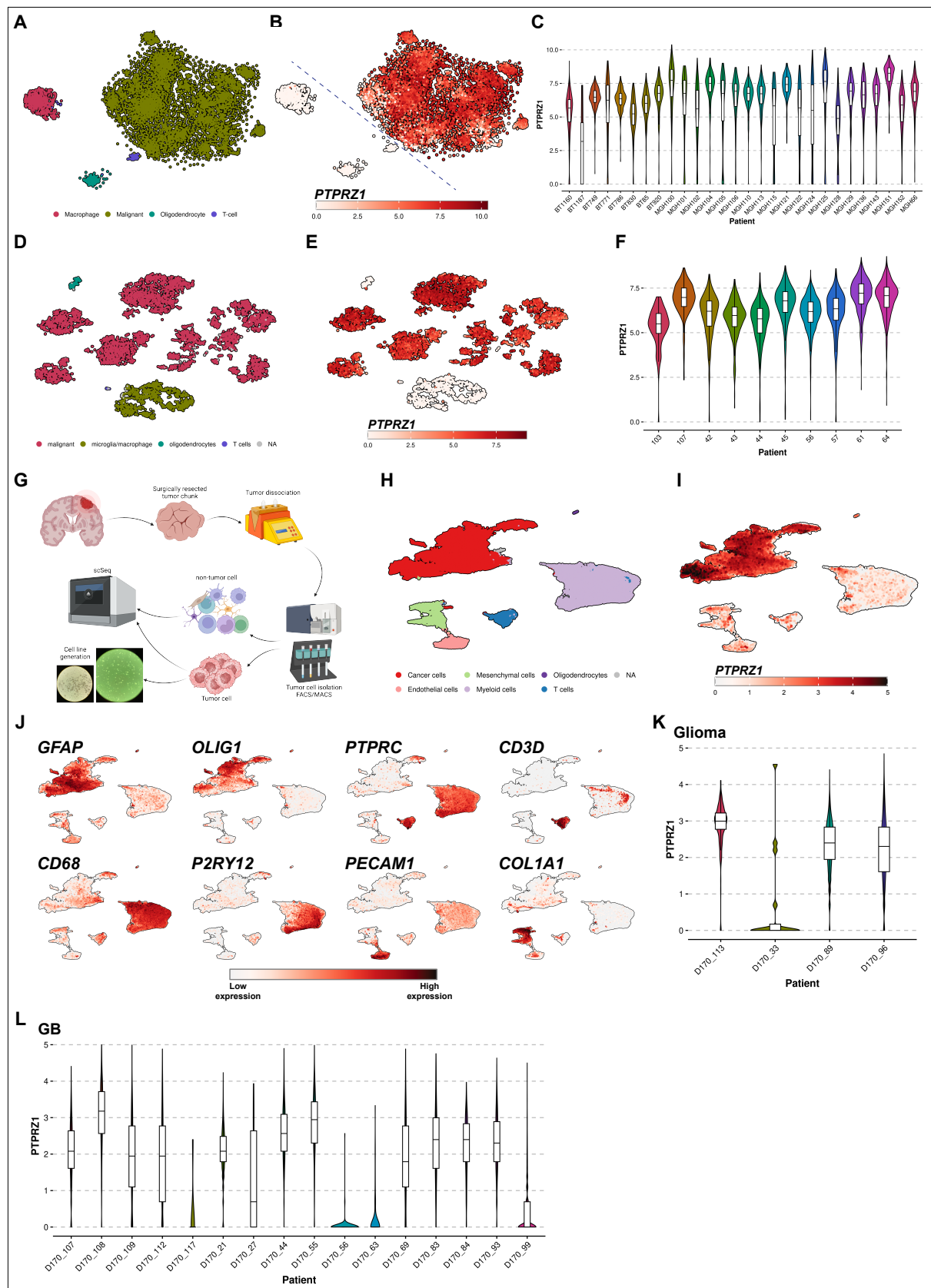


Figure 6: *PTPRZ1* expression at single-cell resolution in published and self-generated scRNA-seq datasets

A. Cell type annotation of GB tumors in a t-SNE plot. Dataset from Neftel et al. (2019). **B.** *PTPRZ1* expression in different cells from **(A)**. **C.** Individual *PTPRZ1* levels in malignant cells from **(A)**. **D.** Cell type annotation of IDH-mutant gliomas in a t-SNE plot. Dataset from Venteicher et al. (2017). **E.** *PTPRZ1* expression in different cells from **(D)**. **F.** Individual *PTPRZ1* levels in malignant cells from **(D)**. **G.** Schematic of tumor processing and cell enrichment for single-cell sequencing and cell line establishment. **H.** Cell type annotation of collected patient samples in a UMAP plot. **I.** *PTPRZ1* expression in different cells from **(H)**. **J.** Canonical marker expression of single cells in **(H)**. **K.** Individual *PTPRZ1* levels in IDH1-mutant glioma and pediatric high-grade glioma cancer cells. **L.** Individual *PTPRZ1* levels in GB cancer cells.

2.1.2 PTPRZ1 is abundantly expressed at protein levels and dominantly presented on MHCI

Apart from the transcript level, n=20 matched primary and recurrent GB samples were collected from the Pathology Department at Heidelberg University to evaluate protein abundance. Patient-individual PTPRZ1 levels were apparent without temporal alterations between primary and recurrent tumors (**Figure. 7A&B**). In concordance with the transcriptomic data, using GFAP to depict tumor purity, the frequency of PTPRZ1⁺ cells positively correlated with GFAP⁺ cells (**Figure. 7A&C**). To address whether the protein abundance translated to increased presentation on MHC, untargeted HLA class I (HLAI) ligandomics was conducted. PTPRZ1-derived epitopes were found among the most presented HLA I ligands across generated primary GB cell lines (**Figure. 6G & 7D**). Several shared PTPRZ1-derived epitopes were presented in all three cell lines; particularly, one PTPRZ1-derived epitope, PTPRZ1¹⁸¹⁴⁻¹⁸²², which was targeted in the GAPVAC-101 trial, was among the overlapping ligands (**Figure. 7E**). The data here describe that PTPRZ1 is overexpressed not only at the transcription level but also at the protein level in GB. The high abundance of PTPRZ1 protein expression thereby results in dominant epitope presentation on MHCI.

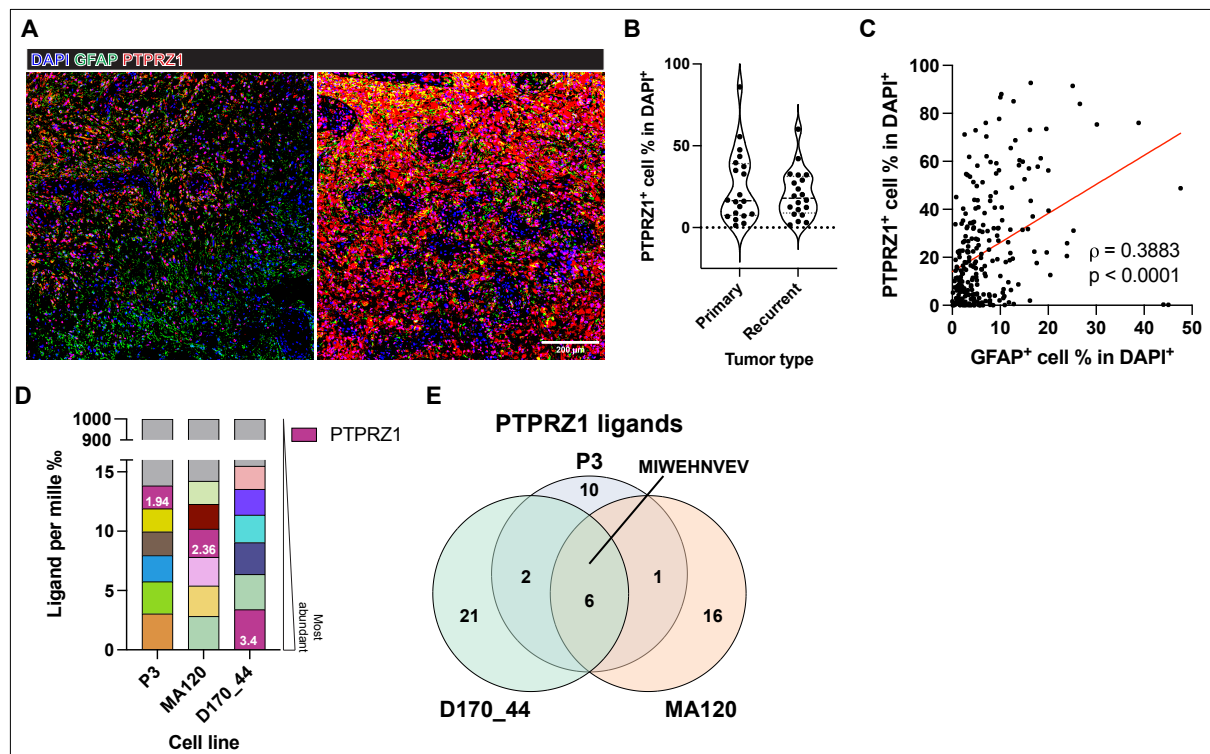


Figure 7: Protein expression of PTPRZ1 and its presentation on MHC I in GB

A. Immunofluorescence staining of the GAA PTPRZ1 and the surrogate marker for tumor cells, GFAP, on matched primary and recurrent GB tumors. **B.** Patient-individual average PTPRZ1⁺ cell frequencies. **C.** PTPRZ1⁺ cell frequency correlation with GFAP⁺ cell frequency of each tumor piece evaluated. **D.** Presented ligands on MHC I across three primary GB cell lines, ranked according to gene-specific epitope abundance. **E.** PTPRZ1-derived epitopes of the examined cell lines. PTPRZ1¹⁸¹⁴⁻¹⁸²², MIWEHNVEV, was commonly presented on all cell lines. **(B)** was analyzed with paired t-test. **(C)** was performed with Spearman correlation.

2.1.3 *PTPRZ1* is associated with distinct cellular states and GB stem cells

Distinct cellular states were previously demonstrated in GB (**Figure. 8A**) (Nefitel et al., 2019), and *PTPRZ1* expression was revealed to be prominent in astrocyte-like (AC-like) and oligodendrocyte-progenitor-like (OPC-like) GB cells (**Figure. 8B**), positively correlated with their module scores but not correlated with the module scores of the other two cellular states, neural-progenitor-like (NPC-like) and mesenchymal-like (MES-like) (**Figure. 8C&D**). As *PTPRZ1* was reported to contribute to cancer cell stemness (Fujikawa et al., 2017; Shi et al., 2017), GSC module scores were analyzed and found to be positively correlated with *PTPRZ1* expression (**Figure. 8E**). To validate the results, GB cellular states of our scRNA-seq dataset were illustrated using the defined gene sets from Nefitel et al. (2019) (**Figure. 8F**). Consistently, higher *PTPRZ1* expression was identified in AC-like and OPC-like GB cells (**Figure. 8G**). Comparable to the previous work (Nefitel et al., 2019), the distribution of cell states differed across patients, yet *PTPRZ1* was uniformly more pronounced in AC-like and OPC-like cells (**Figure. 8H&I**). A GSC score for each GB cell was derived from the defined gene set in Patel et al. (2014) and was again found to be positively correlated with *PTPRZ1* expression (**Figure. 8J**). Additionally, TCGA-GB tumors were grouped according to dominant GB cell states (**Figure. 8K**), and similar conclusions were made (**Figure. 8L**). Collectively, these transcriptomic analyses indicate that *PTPRZ1* expression correlates positively with AC-like and OPC-like GB cellular states and GB stemness.

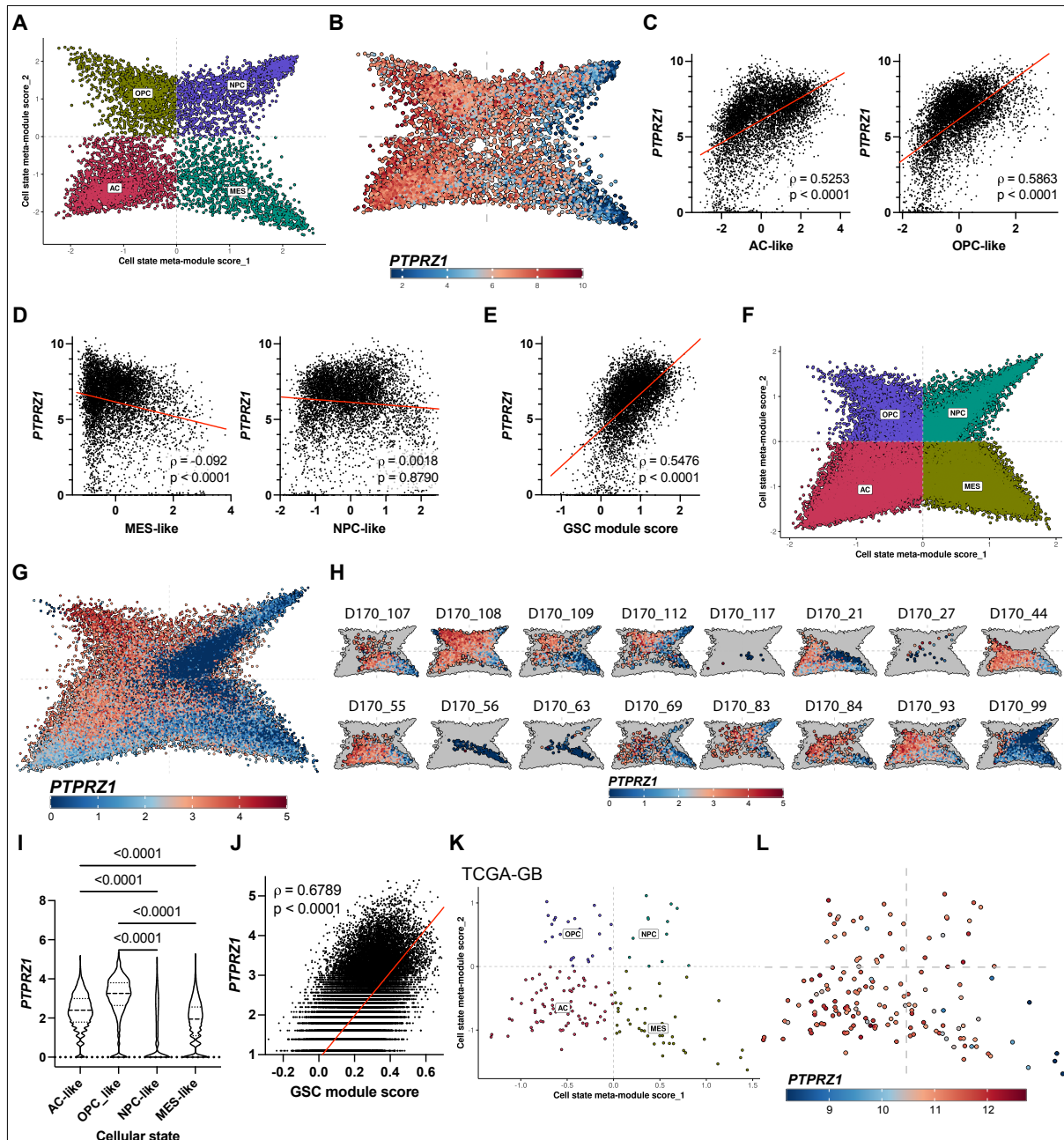


Figure 8: Correlation of *PTPRZ1* expression with GB cellular states and stemness

A. Cellular states of GB malignant cells from **Figure 6A**. The module scores were directly retrieved from the published work (Neftel et al., 2019). **B.** *PTPRZ1* expression in distinct GB cellular states from **(A)**. **C.** Correlation of *PTPRZ1* with AC-like and OPC-like module scores. **D.** Correlation of *PTPRZ1* with MES-like and NPC-like module scores. **E.** Correlation of *PTPRZ1* with GSC module scores calculated with the gene set from Patel et al. (2014). **F.** Cellular states of GB cancer cells from **Figure 6H**, calculated with the gene sets from Neftel et al. (2019). **G.** *PTPRZ1* expression in distinct GB cellular states from **(F)**. **H.** Patient-individual distribution of distinct GB cellular states with *PTPRZ1* expression color-coded. **I.** *PTPRZ1* expression across four GB cellular states from **(F)**. **J.** Correlation of *PTPRZ1* with GSC module score of GB cancer cells from **Figure 6H**. **K.** Cellular states of bulk TCGA-GB tumors. **L.** *PTPRZ1* expression in distinct GB cellular states from **(K)**. All correlation tests were performed with

Spearman. (I) was analyzed with one-way ANOVA multiple comparison corrected with Holm-Šidák method.

2.1.4 A vaccine-induced T cell receptor binds to intracellularly processed and presented PTPRZ1¹⁸¹⁴⁻¹⁸²² without evidence of off-target reactivity

To discover therapeutic PTPRZ1-reactive TCRs, PBMCs were retrieved from a female HLA-A*02⁺ GAPVAC-101 patient, pt.16, who had undergone 11 APVAC1 vaccinations and 8 APVAC2 vaccinations at the time of sample collection with a favorable clinical course, showing immune responses to the examined PTPRZ1 peptides (**Figure. 9A**) (Hilf et al., 2018). Reactive T cells were sorted following *in vitro* restimulation with PTPRZ1¹³⁴⁷⁻¹³⁵⁵ or PTPRZ1¹⁸¹⁴⁻¹⁸²² peptide then subjected to sc TCR sequencing (scTCR-seq). The TCR repertoire of the sorted T cells for PTPRZ1¹³⁴⁷⁻¹³⁵⁵ was polyclonal while the one for PTPRZ1¹⁸¹⁴⁻¹⁸²² was uni- to oligo-clonal, with the top CDR3 comprising 75.09% and the second top 19.76% of the repertoire (**Figure. 9A**). Notably, the top CDR3 for PTPRZ1¹⁸¹⁴⁻¹⁸²² consisted of one β chain paired with two different α chains. Subsequently, the dominant TCRs for both peptides were cloned into a novel non-viral, non-integrating episomal scaffold matrix attachment region (S/MAR) DNA vector (Bozza et al., 2021). To avoid mispairing with endogenous human TCRs and to enhance pairing stability, constant regions of TCR α and β chains were murinized (Cohen et al., 2006). To validate reactivity, TCRs were electroporated into Jurkat cells carrying NFAT, AP-1, and NF- κ B reporters or electroporated along with a plasmid encoding a reporter into Jurkat cells (**Figure. 9B**). TCR surface expression was identified within the first 48 hours post-transfection (**Figure. 9C**). TCR-Jurkat cells were then cocultured with peptide-loaded presenter cells for 24 hours. For PTPRZ1¹³⁴⁷⁻¹³⁵⁵, none of the tested dominant TCRs were reactive to peptide-loaded target cells (**Figure. 9D&E**). In contrast, one out of the top two TCRs for PTPRZ1¹⁸¹⁴⁻¹⁸²² demonstrated strong reactivity against peptide-loaded presenters (**Figure. 9F**). Hence, the identified reactive TCR for PTPRZ1¹⁸¹⁴⁻¹⁸²² was subsequently further interrogated.

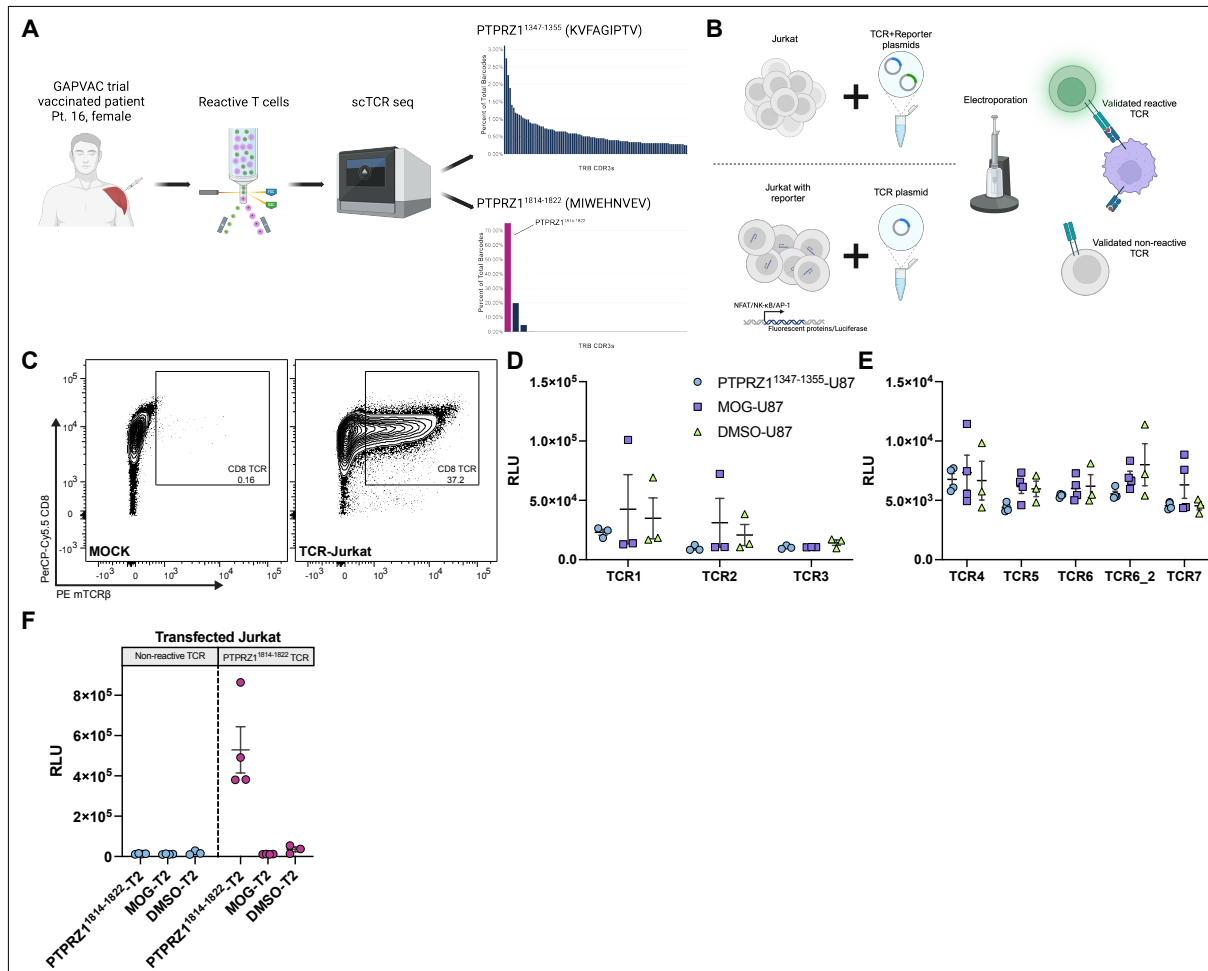


Figure 9: Identification of PTPRZ1-reactive TCR

A. Schematic workflow illustrating the sorting and sequencing of PTPRZ1-reactive T cells upon stimulation with PTPRZ1 epitopes of interest, with clonotype plots showing dominant TCRs. The later identified reactive TCR is highlighted. **B.** Validation of dominant TCR clonotypes from (A) using Jurkat cells transfected with a TCR and a reporter plasmid (top panel) or Jurkat reporter cells transfected with a TCR plasmid (bottom panel). **C.** Contour plot showing TCR transfection efficiency 48 hours post-electroporation. **D&E.** Luminescence reporter signal of Jurkat cells transfected with TCRs for PTPRZ1¹³⁴⁷⁻¹³⁵⁵ upon overnight coculture with PTPRZ1¹³⁴⁷⁻¹³⁵⁵-loaded presenter cells. **F.** Luminescence reporter signal of Jurkat cells transfected with TCRs for PTPRZ1¹⁸¹⁴⁻¹⁸²² after overnight coculture with PTPRZ1¹⁸¹⁴⁻¹⁸²²-loaded target cells.

Results

Notably, exogenous peptides do not necessarily induce immunogenicity against naturally processed and presented antigens (Viner et al., 1996). Therefore, it is essential to assess whether the peptide vaccine-induced TCR is indeed reactive to the antigen that is endogenously processed and presented. Since the complete open reading frame (ORF) of *PTPRZ1* is large (~7kbp), the establishment of a stable cell line overexpressing it failed (data not shown). To circumvent this challenge, the tandem minigene (TMG) approach was employed. A well characterized HLA-A*02⁺ GB cell line, U87, was engineered to stably express TMG encoding antigens of interest derived from the GAPVAC-101 and IMA950 trials, including the aforementioned *PTPRZ1* antigens (**Figure. 10A&B** and **Table. 1**) (Hilf et al., 2018; Migliorini et al., 2019). Upon coculture with U87 TMG cells, TCR-Jurkat cells also presented strong reporter activity (**Figure. 10C**), indicating that the identified TCR is able to recognize the intracellularly processed and presented antigen *PTPRZ1*¹⁸¹⁴⁻¹⁸²².

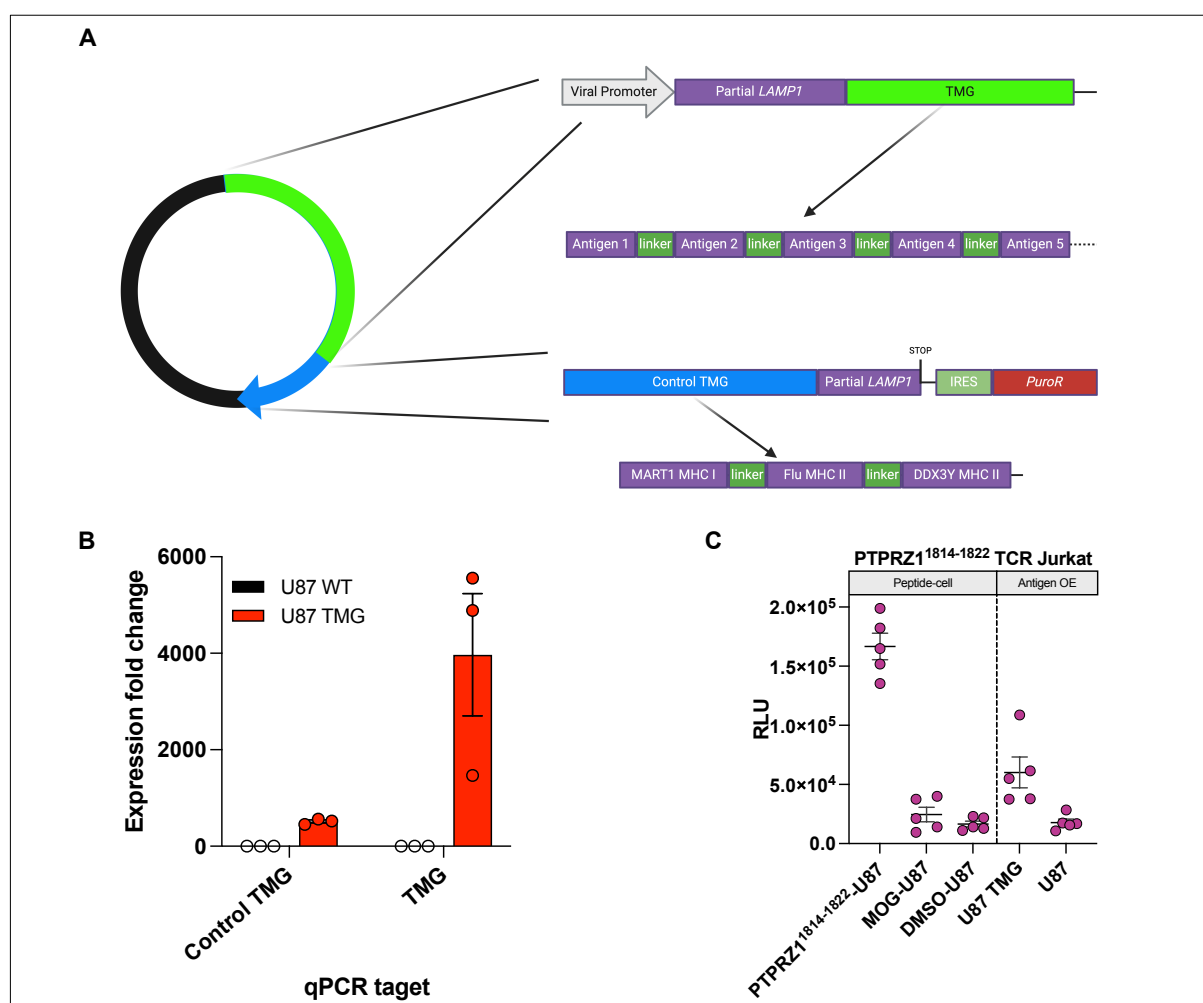


Figure 10: Tandem minigene cell line establishment and assessment of TCR recognition against intracellularly processed antigen

A. Tandem minigene design covering antigens of interest and control antigens for validation. The full list of antigens encoded can be referred to in **Table. 1**. **B.** RT-qPCR confirming TMG expression. **C.** Luminescence reporter signal following overnight coculture with peptide-loaded or antigen-expressing target cells.

TMG	aa sequence	Synonym in the GAPVAC-101
PTPRZ1 ¹⁸¹⁴⁻¹⁸²²	MIWEHNVEV	PTP-013
BCA	ALWAWPSEL	BCA-002
FAB7	TFGDVVAV	-
NRCAM	GLWHHQTEV	NRCAM-001
IGF2BP3	KIQEILTQV	-
PTPRZ1	AIIDGVESV	PTP-003
PTPRZ1 ¹³⁴⁷⁻¹³⁵⁵	KVFAGIPTV	PTP-005
TNC	AMTQLLAGV	-
CSP	TMLARLASA	-
CHI	SLWAGVVVL	-
NLGN4X	NLDTLMTYV	NLGN4X-001
Control TMG		
MART1 MHC I	ELAGIGILTV	-
Flu MHC II	PKYVKQNTLKLAT	-
DDX3Y MHC II	CPPHIENFSDIDMGEIIMGN	-

Table 1: Antigens encoded in TMG

Next, the safety profile of the PTPRZ1¹⁸¹⁴⁻¹⁸²² TCR was evaluated, critical for clinical translation. PTPRZ1 is barely expressed across adult normal tissues (Dutoit et al., 2012; TheHumanProteinAtlas, 2024), and the TCR was isolated from an immunized patient without notable adverse events (Hilf et al., 2018); therefore, the TCR had undergone thymic selection, making both off-target and on-target off-tumor toxicities unlikely, and thus, the reactive T cell carrying the TCR could circulate in the periphery safely and later be retrieved. To nevertheless assess potential off-targets, ARDitox was applied, an *in silico* AI-facilitated prediction tool for off-target TCR binding (Pienkowski et al., 2023). A panel of potential off-targets for the PTPRZ1¹⁸¹⁴⁻¹⁸²² TCR was generated with various off-target-specific safety and presentation scores (**Figure. 11A** and **Table. 2**). No high-risk (safety score < 3) potential off-targets were predicted while 12 low-risk (safety score > 3) off-targets with relevant presentation probabilities on HLA-A*02 were predicted. In a subsequent Jurkat reporter assay, no reactivity against any of these 12 potential off-targets was observed (**Figure. 11B**). Together, these data reveal a patient-derived vaccine-induced PTPRZ1¹⁸¹⁴⁻¹⁸²²-reactive TCR

Results

that binds to both exogenous and intracellularly processed and presented antigen on MHC I without interaction with AI-predicted potential off-targets.

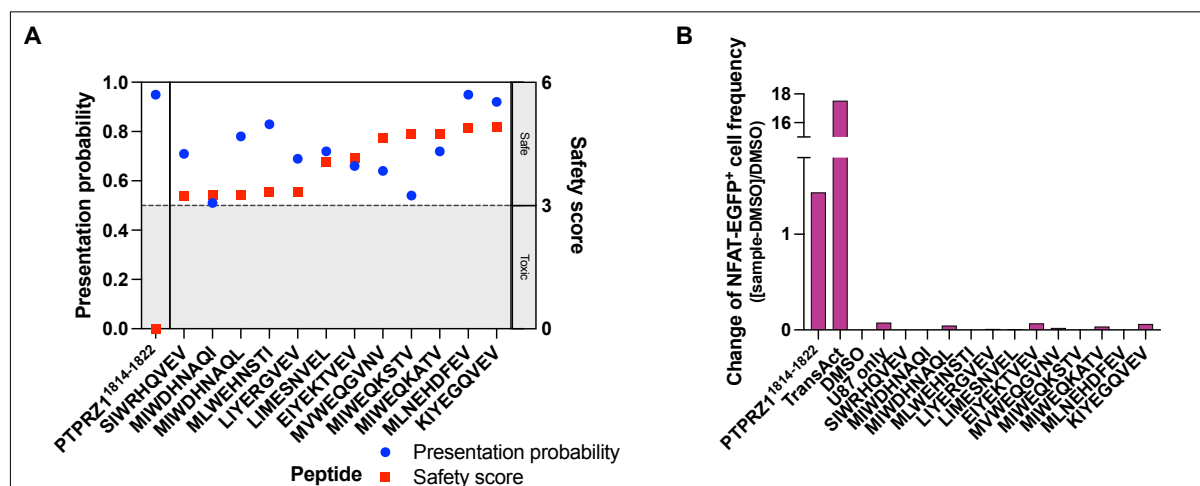


Figure 11: PTPRZ1¹⁸¹⁴⁻¹⁸²² TCR off-target reactivity evaluation

A. *In silico* AI-predicted off-targets of the identified PTPRZ1-reactive TCR with presentation probability indicated by blue circles and safety score indicated by red squares. Presentation probability predicts whether the peptide is presented on MHC, and lower safety score denotes a higher likelihood of cross-reactivity. The full list of off-targets can be referred to in **Table 2**. **B.** Fluorescence reporter signal of TCR-Jurkat cells upon overnight coculture with various peptide-loaded target cells.

aa sequence	Corresponding gene	Safety score	Presentation score
MIWEHNVEV	PTPRZ1	0	0.95
SIWRHQVEV	ZBTB21	3.24	0.71
MIWDHNAQI	PTPRG	3.26	0.51
MIWDHNAQL	PTPRZ1	3.26	0.78
MLWEHNSTI	PTPRF/D	3.33	0.83
LIYERGVEV	SLC45A2	3.33	0.69
LIMESNVEL	CEP44	4.05	0.72
EIYEKTVEV	CYFIP1/2	4.15	0.66
MVWEQGVNV	PTPN14	4.65	0.64
MIWEQKSTV	PTPN13	4.75	0.54
MIWEQKATV	PTPRC	4.75	0.72
MLNEHDFEV	BRCA1	4.88	0.95
KIYEGQVEV	RPL5	4.9	0.92

Table 2: ARDitox predicted off-target safety score and presentation score

2.1.5 PTPRZ1¹⁸¹⁴⁻¹⁸²² TCR acts antigen-specifically and facilitates orchestration of antigen-reactive CD4⁺ and CD8⁺ primary T cells

Next, whether the discovered PTPRZ1¹⁸¹⁴⁻¹⁸²² TCR could elicit effector functions in primary human T cells was evaluated. A GMP-compatible retroviral system commonly used in the clinic for CAR-T cell manufacture was used to transduce the TCR with constant regions murinized (Sauer et al., 2021). Assessed by flow cytometric analysis of murine constant TCR β chain surface expression frequency, transduction efficiency was reproducibly around 85% for both experimental PTPRZ1¹⁸¹⁴⁻¹⁸²² TCR and control Influenza (Flu) TCR, targeting the HLA-A*02-restricted epitope GILGFVFTL (**Figure. 12A**). Without further enrichment, TCR surface expression was maintained without frequency decrease 20 days post-transduction *in vitro* (**Figure. 12B**). Of note, the culture conditions here using IL-7 and IL-15 for stimulation and maintenance, instead of conventional IL-2 stimulation, favored the expansion of CD8⁺ T cells (**Figure. 12C**) (Meyran et al., 2023). Longitudinal subtyping of CD8⁺ TCR-T cells into stem cell memory (T_{SCM}, CD45RA⁺ CD62L⁺), central memory (T_{CM}, CD45RA⁻ CD62L⁺), effector memory (T_{EM}, CD45RA⁻ CD62L⁻), and CD45RA⁺ effector memory (T_{EMRA}, CD45RA⁺ CD62L⁻) revealed a long-lasting and predominant adaptation to a T_{SCM} phenotype over 3 weeks *in vitro* regardless of TCR expression (**Figure. 12D**). In contrast to a previous study (Meyran et al., 2023), a T_{SCM}-abundant engineered T cell product could still be produced even without enrichment of naïve T cells.

Results

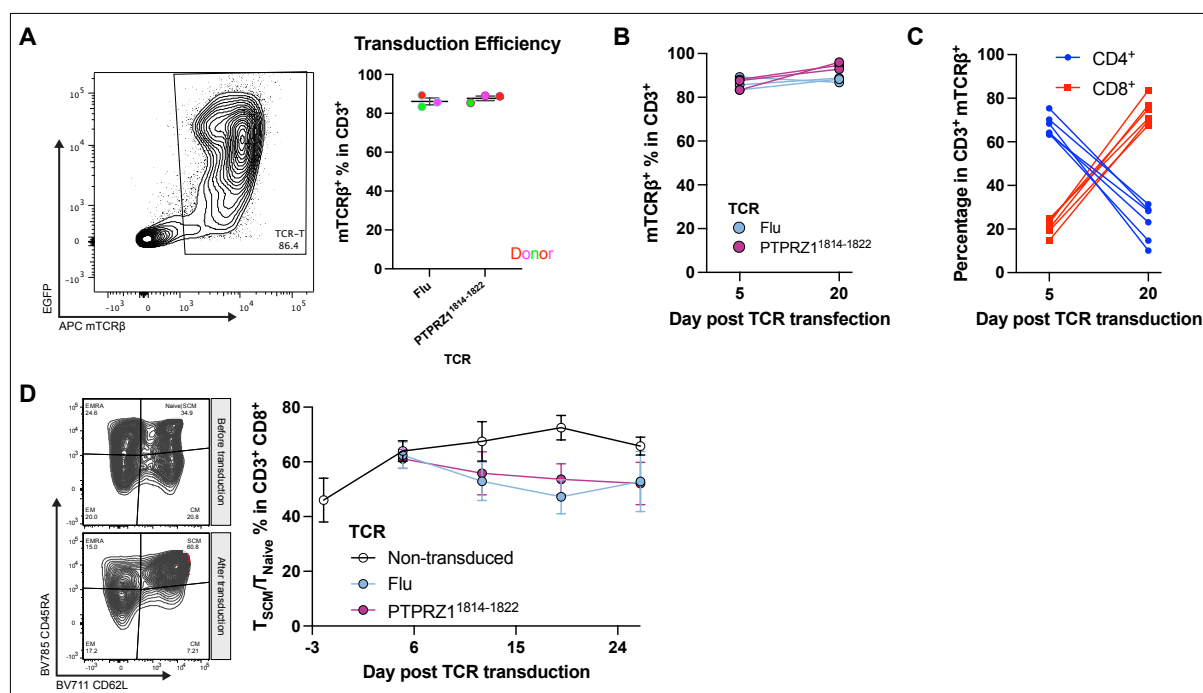


Figure 12: Characterization of TCR-engineered primary human T cell product

A. Transduction efficiency monitored by surface murine constant TCR β chain. **B.** Longitudinal observation of TCR surface expression. **C.** Longitudinal tracking CD4 $^+$ and CD8 $^+$ T cell percentages. **D.** Longitudinal subtyping CD8 $^+$ T cells.

The generated TCR-T cells were then cocultured with various target cells. Only upon contact with cognate peptide-loaded target cells or U87 TMG did CD8 $^+$ TCR-T cells become activated, as indicated by canonical activation markers and effector cytokines and proteins (**Figure. 13A-C**). Importantly, the primary HLA-A*02 $^+$ GB P3 cell line, which endogenously expresses *PTPRZ1* (Hilf et al., 2018), also activated CD8 $^+$ PTPRZ1¹⁸¹⁴⁻¹⁸²² TCR-T cells (**Figure. 13A**). Cytotoxicity was determined by measuring LDH release or counting cells by flow cytometry. PTPRZ1¹⁸¹⁴⁻¹⁸²² TCR-T cells demonstrated antigen-specific, dose-dependent cytotoxic function with an optimal E:T ratio of 2:1 (**Figure. 13D&E**).

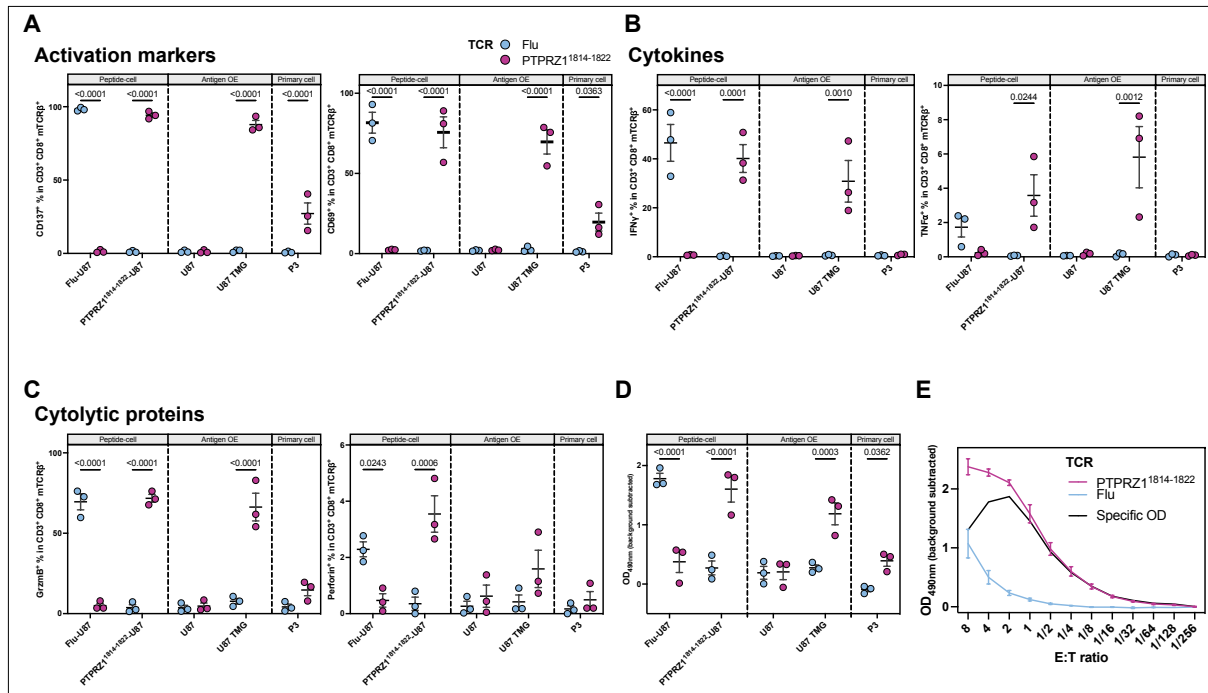


Figure 13: Activation of CD8⁺ TCR-T cells and cytotoxicity upon antigen recognition

A. Activation marker (CD137 and CD69)-positive frequencies in CD8⁺ TCR-T cells. **B.** Cytokine (IFN γ and TNF α)-secreting CD8⁺ TCR-T cell frequencies. **C.** Cytolytic protein (Granzyme B and Perforin)-expressing CD8⁺ TCR-T cell frequencies. **D.** Detection of LDH released into the medium after 24h coculture of TCR-T cells and target cells. **E.** Titration of E:T ratio with TCR-T cells and U87 TMG, measured by LDH release. 1 unit is 75×10^3 cells. Specific OD is OD_{PTPRZ1}-OD_{Flu}. (A)-(D) were analyzed with two-way ANOVA multiple comparison corrected with Holm-Šidák method.

The TCR-T cell manufacturing process transduced both CD4⁺ and CD8⁺ T cells. As a recent study suggests that cytotoxic CD4⁺ CAR-T cells facilitate long-term tumor control (Melenhorst et al., 2022), CD4⁺ TCR-T cells were subsequently examined. Even without the co-receptor CD8, the TCR elicited activation in CD4⁺ T cells in an antigen-dependent fashion (**Figure. 14A-C**). Moreover, additional irradiation of tumor cells *in vitro* resulted in further exacerbated activation of CD4⁺ TCR-T cells and increased target cell lysis without enhancement of CD8⁺ TCR-T cell activation (**Figure. 14C-F**).

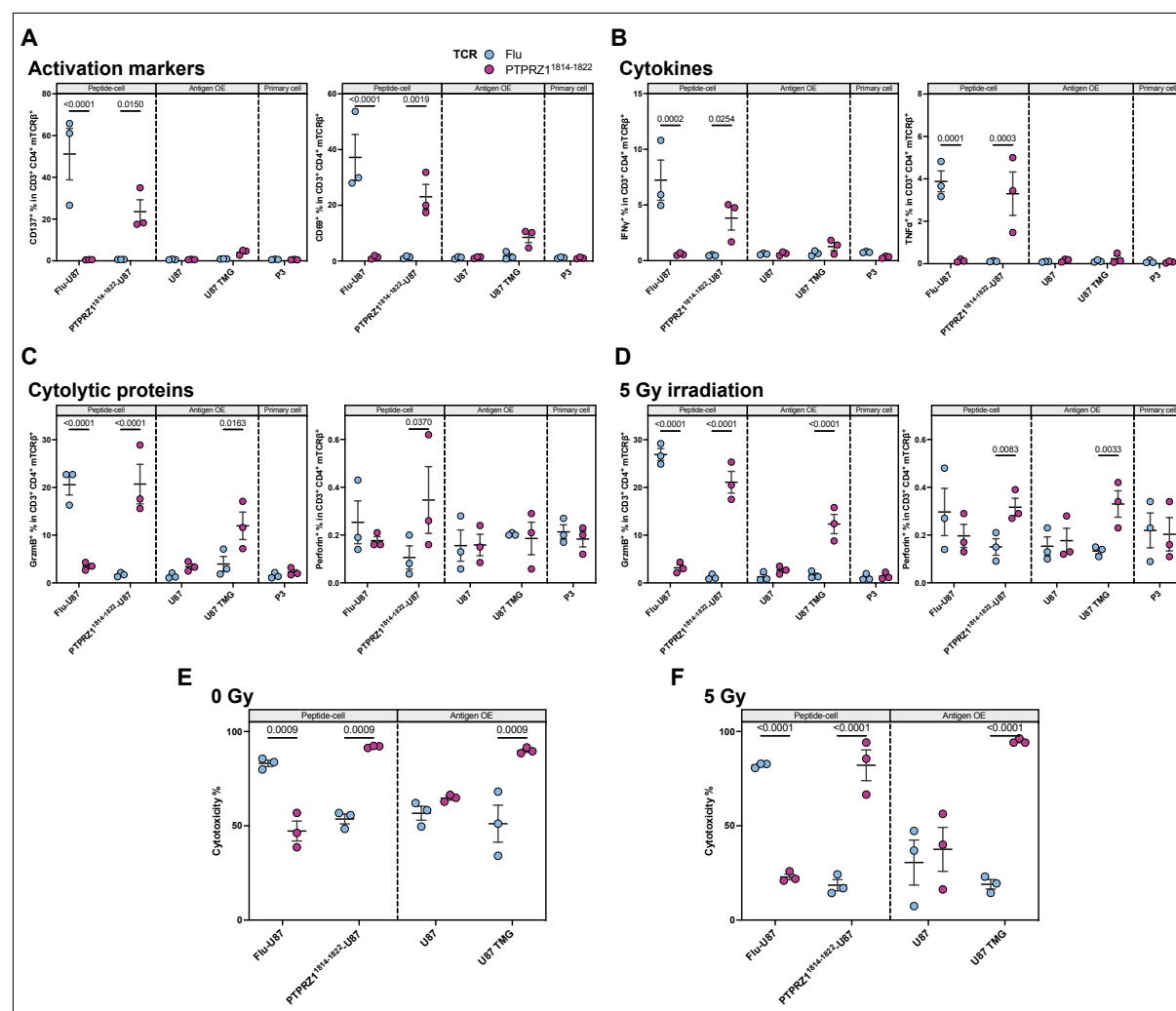


Figure 14: Activation of CD4⁺ TCR-T cells and effects of additional irradiation on tumor cells

A. Activation marker-positive frequencies in CD4⁺ TCR-T cells. **B.** Cytokine-secreting CD4⁺ TCR-T cell frequencies. **C.** Cytolytic protein-expressing CD4⁺ TCR-T cell frequencies. **D.** Cytolytic protein-expressing CD4⁺ TCR-T cell frequencies upon coculture with 5 Gy-irradiated target cells. **E.** Cytotoxicity of various tumor cells after 24h coculture with TCR-T cells, measured by flow cytometric cell counting. **F.** Cytotoxicity of 5 Gy-irradiated target cells after 24h coculture with TCR-T cells. All were analyzed with two-way ANOVA multiple comparison corrected with Holm-Šidák method.

Although cytolytic proteins were elevated in CD4⁺ TCR-T cells, it remained unclear if they encountered target cells directly to execute cytotoxicity or supported neighboring cytotoxic CD8⁺ TCR-T cells. Thus, the role of CD4⁺ T cells engineered with the CD8-restricted PTPRZ1¹⁸¹⁴⁻¹⁸²² TCR in the context of tumor cell lysis was further unraveled. CD4⁺ or CD8⁺ TCR-T cells were enriched with MACS after TCR transduction (**Figure 15A**). Following MACS, high-purity CD4⁺ or CD8⁺ TCR-T cells were obtained (**Figure 15B&C**). As expected, serial dilution of CD4⁺ TCR-T cells in comparison to that of CD8⁺ TCR-T cells revealed that CD4⁺ T cells play a minor role in target cell killing

(Figure. 15D&E). However, a moderate increase in cytotoxicity was observed when both CD4⁺ and CD8⁺ T cells carried the reactive TCR compared to the combination of reactive CD8⁺ T cells with non-reactive CD4⁺ T cells (Figure. 15F). To sum up, these data show that the identified PTPRZ1¹⁸¹⁴⁻¹⁸²² TCR can function antigen-specifically in human primary T cells and suggest a differential but synergistic role for CD4⁺ and CD8⁺ T cells following antigen-specific activation via the reactive TCR.

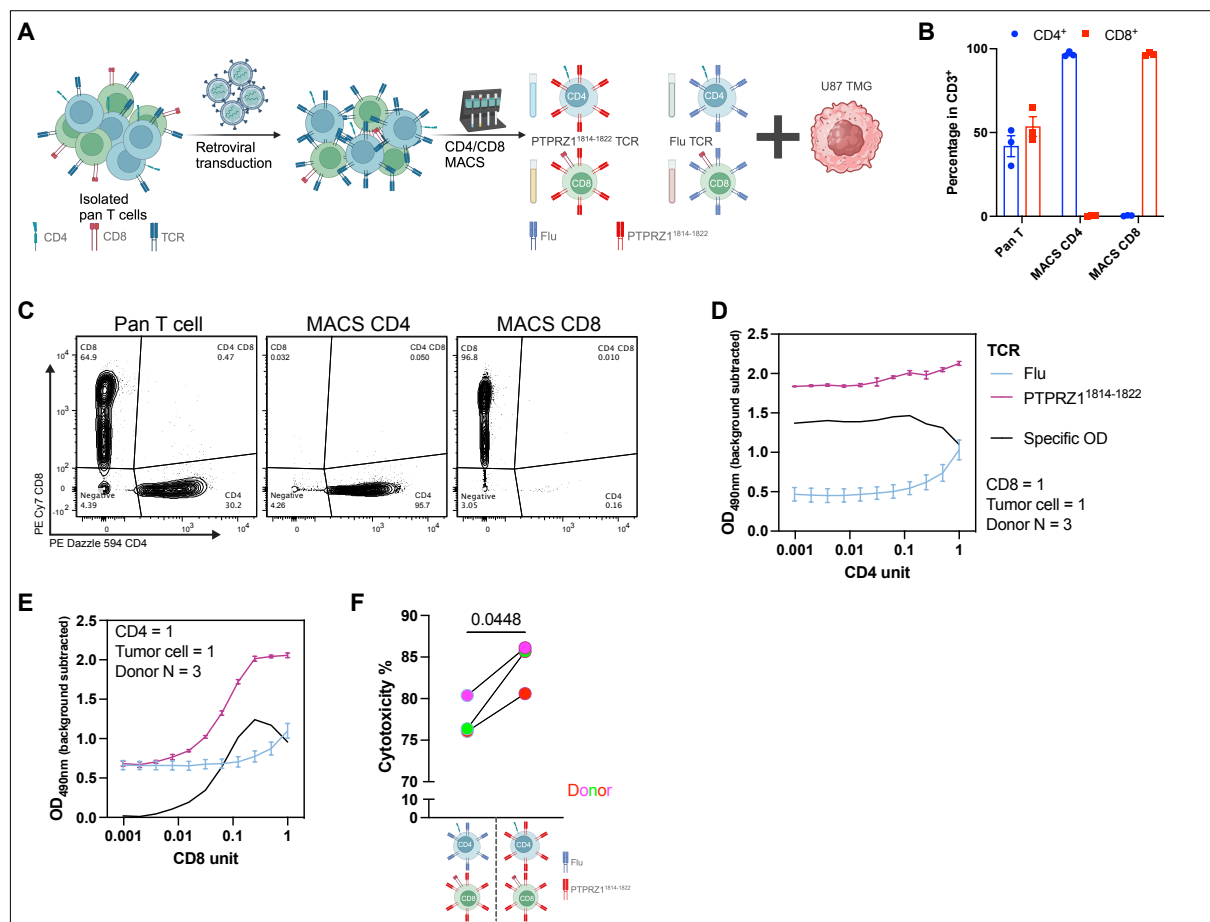


Figure 15: Detailing the role of CD4⁺ T cells carrying the CD8-restricted TCR

A. Workflow to enrich CD4⁺ or CD8⁺ TCR-T cells post-transduction with MACS. **B.** Bar plot showing purity after MACS enrichment. **C.** Contour plot showing percentages of CD4⁺ and CD8⁺ TCR-T cells upon MACS. **D.** Cytotoxicity upon serial diluting CD4⁺ T cells. **E.** Cytotoxicity upon serial diluting CD8⁺ T cells. 1 unit equals to 75×10^3 cells in **(D)** and **(E)**, and specific OD is $OD_{PTPRZ1} - OD_{Flu}$. **F.** Cytotoxicity of the target cell using reactive CD8⁺ T cells with either reactive or non-reactive CD4⁺ T cells, measured by cell counting through flow cytometry. **(F)** was analyzed with paired t-test.

2.1.6 PTPRZ1¹⁸¹⁴⁻¹⁸²² TCR-T cells are efficacious in controlling experimental flank and brain tumors

To investigate the therapeutic potential of the PTPRZ1¹⁸¹⁴⁻¹⁸²² TCR *in vivo* without the influential factors of brain tumors such as the BBB, U87 TMG cells were subcutaneously (s.c.) inoculated in the flanks of immunodeficient mice, followed by two doses of intravenous (i.v.) TCR-T cell administration (**Figure. 16A**). Following ACT with PTPRZ1¹⁸¹⁴⁻¹⁸²² TCR-T cells, flank tumors regressed over time while control mice without treatment or those treated with control Flu TCR-T cells showed sustained tumor growth and met termination criteria by day 40 post-tumor inoculation (**Figure. 16B-D**). Despite initial tumor regression, some PTPRZ1¹⁸¹⁴⁻¹⁸²² TCR-T cell-treated animals experienced tumor recurrence starting from day 42 onwards, yet by the predefined experimental endpoint, 33.33% (3 out of 9) of PTPRZ1¹⁸¹⁴⁻¹⁸²² TCR-T cell-treated animals remained tumor-free, reflected in prolonged survival (**Figure. 16C&D**).

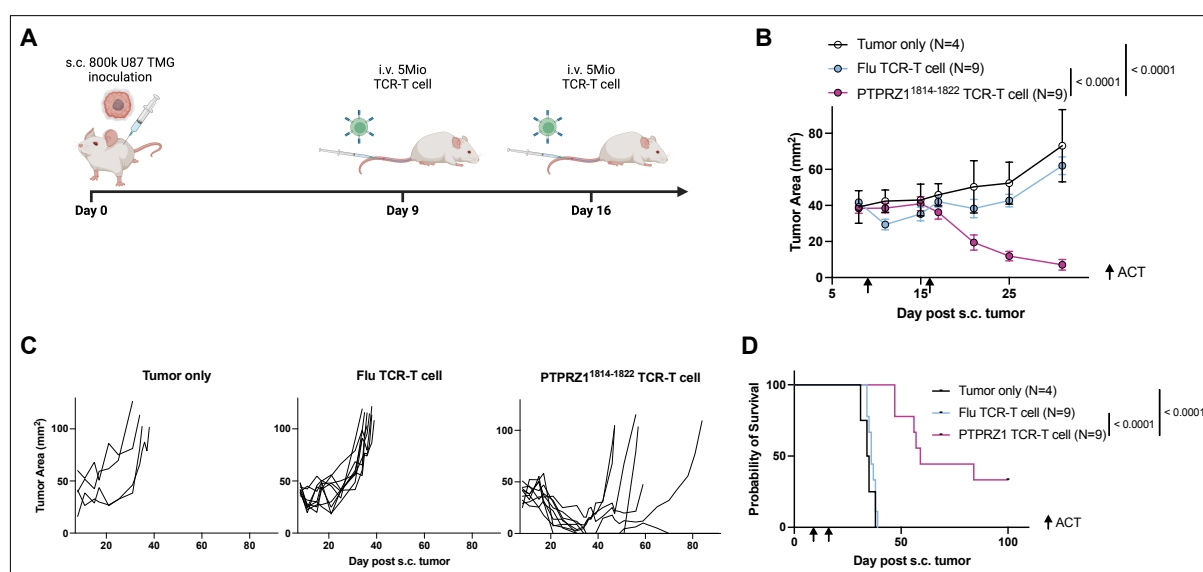


Figure 16: Intravenous ACT of PTPRZ1¹⁸¹⁴⁻¹⁸²² TCR-T cells in a flank tumor model

A. Workflow of i.v. ACT on s.c. tumor model. **B.** Longitudinal s.c. tumor growth monitoring. **C.** Individual s.c. tumor growth under each treatment. **D.** Overall survival of s.c. tumor-bearing mice treated with i.v. ACT. (**B**) was analyzed with nonlinear regression. (**D**) was analyzed with Log-rank test.

As the TCR was proven to be effective in controlling flank solid tumors, its potency in the context of brain tumors was subsequently assessed. To deliver engineered cell products, several routes were considered, including systemic i.v., local i.cv., and intratumoral (i.t.) administration (Guzman et al., 2023). However, as the brain tumor microenvironment is immunosuppressive and due to the presence of the BBB (see **1.2 Immunotherapy for brain tumors**), i.v. and i.t. routes are not optimal, risking ACT T cells being suppressed or not entering the tumor entity at all. As previously mentioned in **1.3 Brain tumor-derived antigens**, repeated systemic i.v. CAR-T cell delivery does not result in GB control in a phase I trial, not even in combinatorial treatment with ICB (Bagley et al., 2024a). Indeed, when PTPRZ1¹⁸¹⁴⁻¹⁸²² TCR-T cells were i.v. delivered twice into mice bearing intracranial U87 TMG tumors (**Figure. 17A**), no therapeutic effect was observed (**Figure. 17B**). Hence, the ACT regime was adapted to two doses of i.cv. ACT following one dose of i.v. ACT (**Figure. 17C**). Notably, by combined i.v. and i.cv. ACT of PTPRZ1¹⁸¹⁴⁻¹⁸²² TCR-T cells, mice showed preclinical response (**Figure. 17D&E**). 5 out of 7 (71.4%) PTPRZ1¹⁸¹⁴⁻¹⁸²² TCR-T cell-treated, tumor-bearing mice responded radiographically to ACT while tumors of control-treated mice continued to grow (**Figure. 17E**). Only PTPRZ1¹⁸¹⁴⁻¹⁸²² TCR-T cell-treated mice (4 out of 7, 57.1%) survived till the experimental endpoint (**Figure. 17F&G**). One out of the survivors remained tumor-free macroscopically while the others experienced tumor recurrence (**Figure. 17F**).

Results

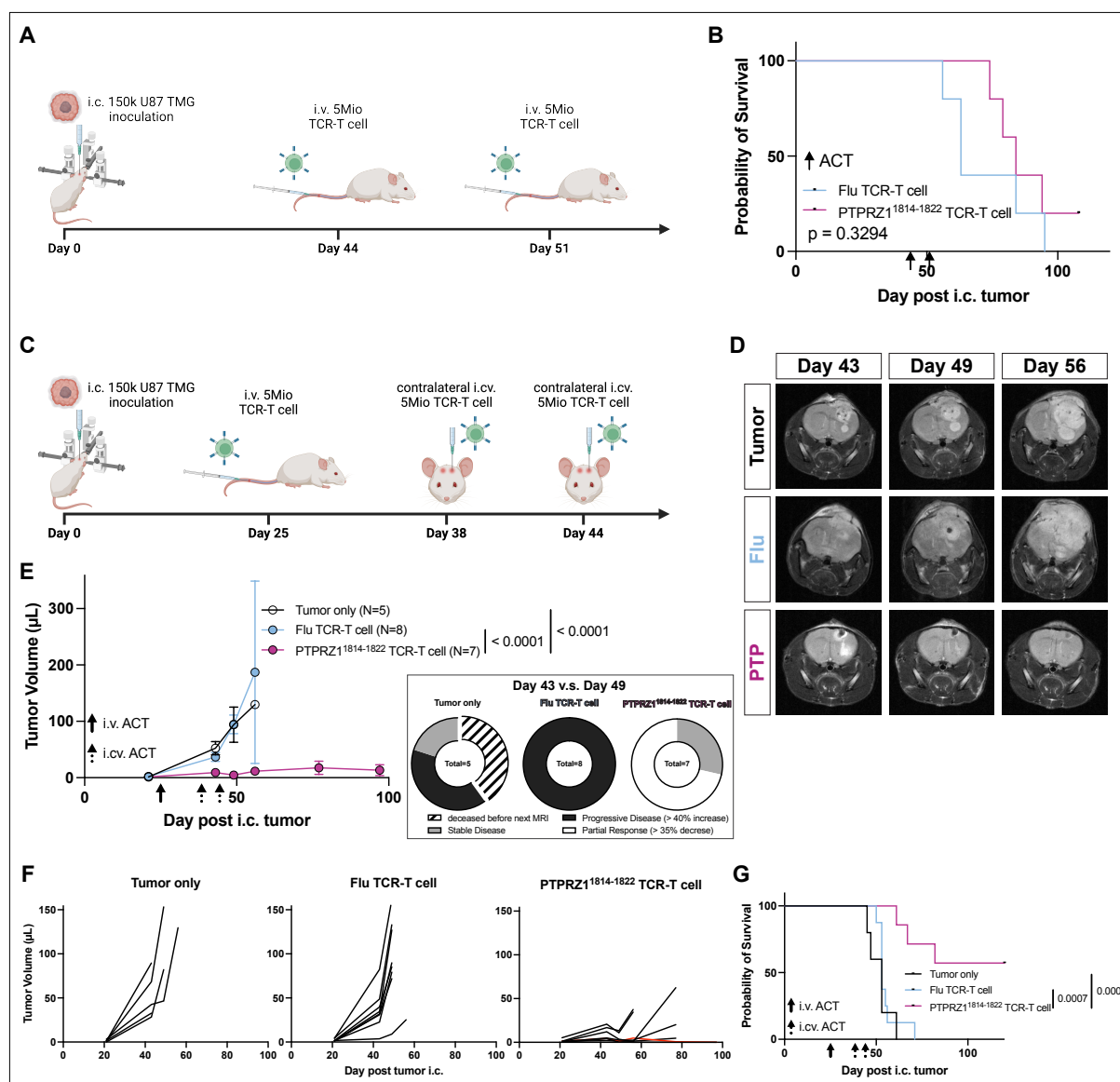


Figure 17: Intravenous and intracerebroventricular delivery of PTPRZ1¹⁸¹⁴⁻¹⁸²² TCR-T cells in an experimental brain tumor model

A. Workflow of i.v. ACT on i.c. tumor model. **B.** Overall survival of i.c. tumor-bearing mice treated with i.v. ACT. **C.** Workflow of i.v. and i.cv. ACT on i.c. tumor model. **D.** I.c. tumor imaging with preclinical MRI. **E.** Longitudinal monitoring of i.c. tumor size with MRI and assessment of radiographic response upon ACT treatment using criteria from Aslan et al. (2020). **F.** Individual i.c. tumor growth curves under each treatment. Red-colored line denotes the survivor mouse with complete regression. **G.** Overall survival of i.c. tumor-bearing mice treated with i.v. and i.cv. ACT. **(B)** and **(G)** were analyzed with Log-rank test. **(E)** was analyzed with nonlinear regression.

To profile the ACT T cells *in vivo*, cheek blood was collected three weeks post-first i.v. ACT. TCR-T cells were detected in all mice receiving ACT (**Figure. 18A**). Adoptive transfer of different CD8⁺ T cell subsets is known to affect T cell engraftment and T cell effector functions. Paradoxically, ACT with more stem-like or central memory T cells outperforms other CD8⁺ subsets as they retain self-renewal capacity, but nonetheless, have less cytotoxic and cytokine-releasing capacity (Berger et al., 2008; Hinrichs et al., 2011; McLellan and Ali Hosseini Rad, 2019). Engrafted T cells were thereby characterized with flowcytometry. Comparable to *in vitro* expanded TCR-T cells (**Figure. 12D**), grafted T cells maintained T_{SCM}-dominant phenotype (**Figure. 18B**). No difference in absolute TCR-T cell number or in population frequencies was observed when comparing therapeutic TCR-T cell-treated with control TCR-T cell-treated mice (**Figure. 18A&B**), indicating that the engraftment and CD8⁺ T cell subset maintenance were independent of cognate antigen encounter *in vivo*. Next, the tumor recurrence mechanism was interrogated (**Figure. 17F**). To decipher if in recurrent tumors, dormant GB cells regained proliferative capacity when reactive TCR-T cells were no longer present within the GB microenvironment (Min and Lee, 2023; Phan and Croucher, 2020), or if MHC and/or antigen loss occurred to facilitate immune surveillance evasion (Dhatchinamoorthy et al., 2021; Jhunjunwala et al., 2021), tumors reaching preclinical termination criteria or the experimental endpoint were post-mortem analyzed. Transferred human T cells were detected in the tumor in mice treated with PTPRZ1¹⁸¹⁴⁻¹⁸²² TCR-T cells (**Figure. 18C&D**), even after 76 days the following the last ACT (**Figure. 18E**). In addition, MHCI expression was maintained in recurrent tumors (**Figure. 18C**). Therefore, TMG expression was examined with RNAscope™, and its transcript levels were greatly diminished in the recurrent tumor (**Figure. 18F&G**). Collectively, these data evidence that the identified PTPRZ1¹⁸¹⁴⁻¹⁸²² TCR-T cells are therapeutic against experimental brain tumors via i.v. and i.c.v. administration; intriguingly, the reactive TCR-T cell product persists in the tumor microenvironment, and the relapse in this model is driven by downregulation of the synthetic gene TMG. On the contrary, as previously shown, *PTPRZ1* expression remains stable throughout disease progression (**Figure. 7B**). Likewise, the MHC and antigen processing/presentation machinery are rarely disrupted in GB (Dhatchinamoorthy et al., 2021).

Results

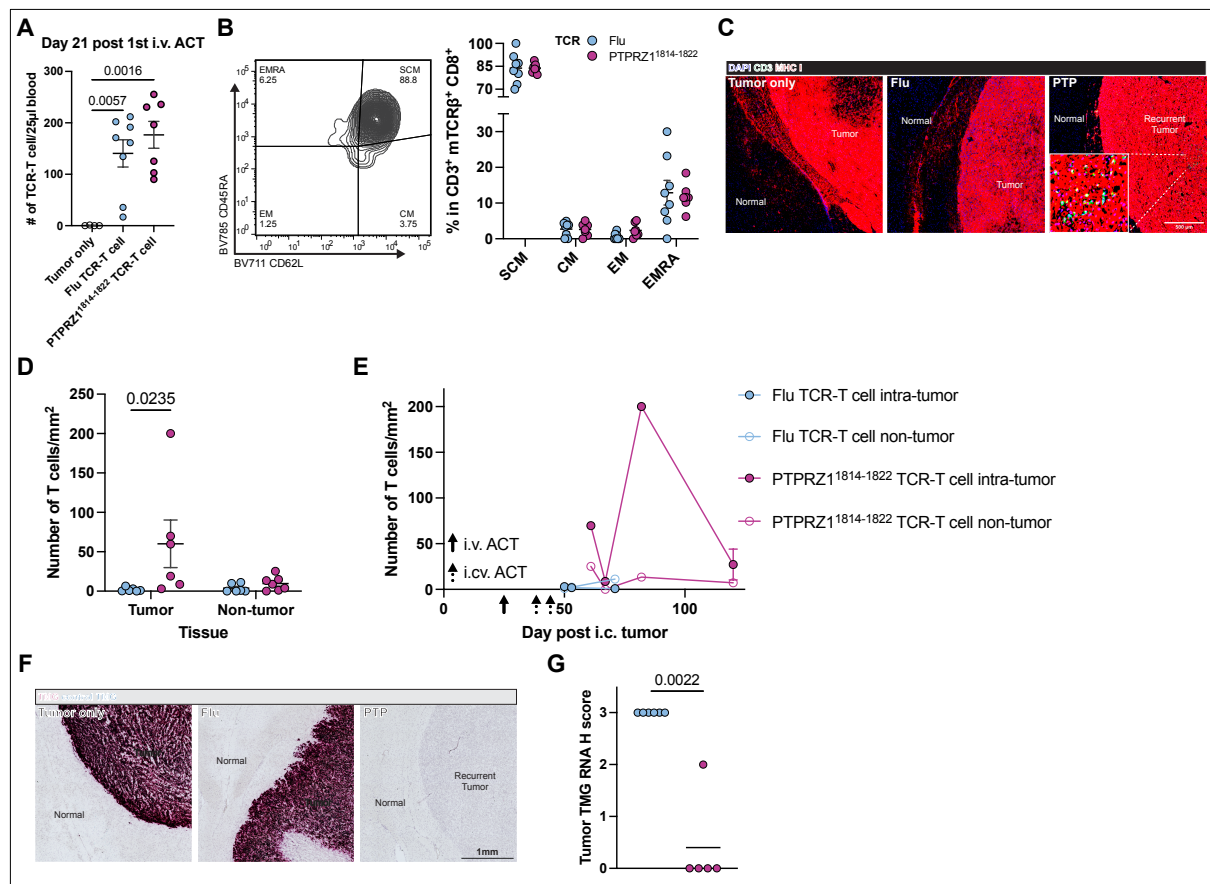


Figure 18: Profiling transferred T cells and investigating recurrence mechanism

A. TCR-T cell number in different treatment groups per 25 µl cheek blood. **B.** Characterization of CD8⁺ TCR-T cell subsets in the cheek blood. **C.** Immunofluorescence staining to identify transferred human T cells and MHC I expression. **D.** Quantification of human T cell numbers in tumoral or non-tumoral areas from (C). **E.** Human T cell numbers of samples collected at different timepoints upon termination or experimental endpoint. **F.** RNAscope™ staining to identify synthetic TMG transcript expression. **G.** Quantification of TMG expression in the tumor from (F). (A) was performed with one-way ANOVA multiple comparison corrected with Holm-Šidák method. (B) and (D) were analyzed with two-way ANOVA multiple comparison corrected with Holm-Šidák method. (G) was conducted with non-parametric t-test.

2.1.7 PTPRZ1¹⁸¹⁴⁻¹⁸²² TCR targets all examined patient-derived HLA-A*02⁺ GB spheroid cell lines, especially the stem-like slow-cycling cell

To evaluate PTPRZ1¹⁸¹⁴⁻¹⁸²² TCR-T cell potency on primary GB, patient-derived GB cell lines were established following previously described protocols of tumor cells isolated via FACS or MACS (**Figure. 6G**) (Ratliff et al., 2022). The generated primary GB cell lines were maintained in serum-free medium and cultured in spheroids to preserve stemness. In order to benchmark the cytotoxicity of PTPRZ1¹⁸¹⁴⁻¹⁸²² TCR-T cells against primary GB cell lines, they were cocultured with one of the first established HLA-A*02⁺ GB cell lines, D170_44, and with the already established P3 cell line. The cytotoxicity was confirmed as shown by the fact that D170_44 was lysed comparably to P3 by PTPRZ1¹⁸¹⁴⁻¹⁸²² TCR-T cells (**Figure. 19A**). Again, both CD8⁺ and CD4⁺ PTPRZ1¹⁸¹⁴⁻¹⁸²² TCR-T cells were activated by the primary GB cell lines (**Figure. 19B&C**). Slow-cycling GB cells are considered stem-like as they have the potential for tumor initiation, therapy resistance, and generation of large numbers of progeny (Deleyrolle et al., 2011; Hoang-Minh et al., 2018; Yang et al., 2022). As PTPRZ1 was defined as a GSC marker and highly associated with GSC scores (**Figure. 8E&J**, see **1.3.1 GB-associated antigen and GB stem cell marker: PTPRZ1**), PTPRZ1¹⁸¹⁴⁻¹⁸²² TCR-T cells were hypothesized to preferentially target the stem-like slow-cycling cells (SCCs). To delineate SCCs, primary GB cell lines were labeled with a fluorescent dye, and the top 10% dye-retaining cells after expansion were considered SCCs while the rest were defined as fast-cycling cells (FCCs). Upon coculture with PTPRZ1¹⁸¹⁴⁻¹⁸²² TCR-T cells, dye-retaining SCCs and dye-losing FCCs were enumerated by flow cytometry to assess differential cytotoxicity (**Figure. 19D**). Indeed, in the first 5 hours of coculture, PTPRZ1¹⁸¹⁴⁻¹⁸²² TCR-T cells favorably killed SCC while after 24 hours, both SCCs and FCCs were killed significantly at a comparable degree (**Figure. 19E**), suggesting a preferential anti-tumor activity on stem-like SCCs.

Results

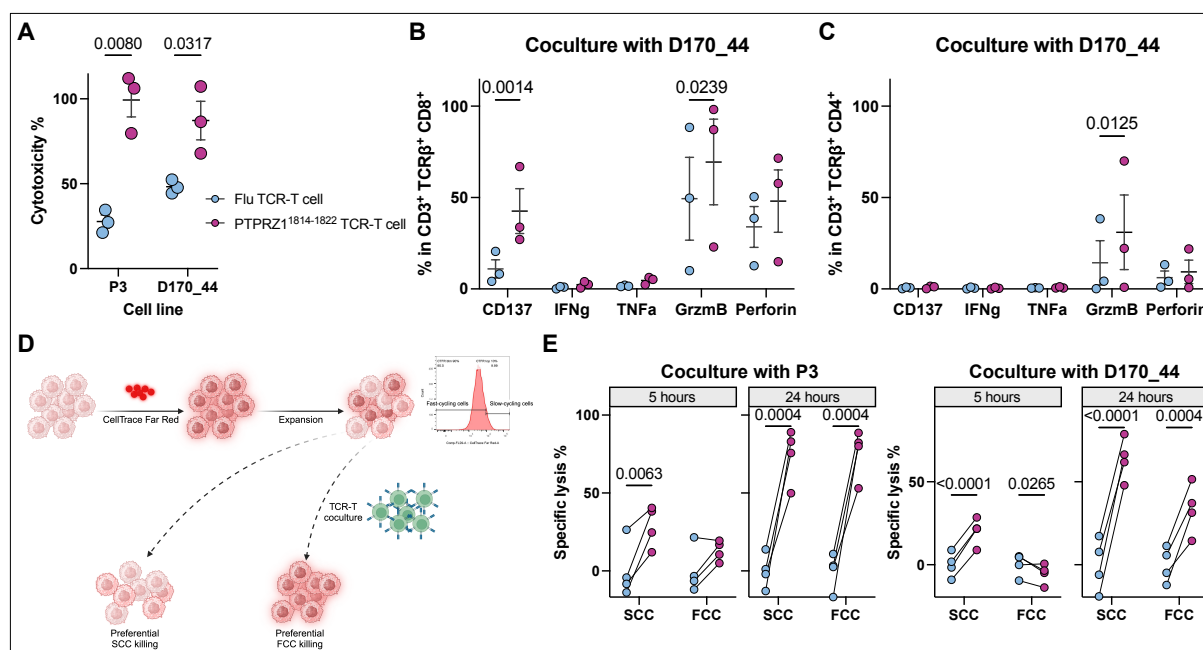


Figure 19: Preferential killing of stem-like slow-cycling cells by PTPRZ1¹⁸¹⁴⁻¹⁸²² TCR-T cells

A. Cytotoxicity of primary GB cell lines by TCR-T cells. **B.** Activation of CD8⁺ TCR-T cells, shown by expression frequencies of various markers. **C.** Activation of CD4⁺ TCR-T cells, shown by expression frequencies of various markers. **D.** Experimental design to assess preferential killing by TCR-T cells on dye-retaining SCCs or dye-losing FCCs. **E.** Cytotoxicity of SCCs and FCCs upon short-term (5h) or long-term (24h) coculture with TCR-T cells. Specificity was calculated by subtraction of mean values of Flu TCR-T cells treated samples for each timepoint and target cell. **(A)-(C)** and **(E)** were analyzed with two-way ANOVA multiple comparison corrected with Holm-Šidák method.

Furthermore, to demonstrate HLA-A*02-dependency and assess the breadth of anti-tumor activity by PTPRZ1¹⁸¹⁴⁻¹⁸²² TCR, we established 5 additional primary GB cell lines, of which MA120, MA140, and D170_108 were HLA-A*02⁺, and MA108 and MA118 were HLA-A*02⁻ (**Figure. 20A**). Upon coculture, PTPRZ1¹⁸¹⁴⁻¹⁸²² TCR-T cells exclusively killed all HLA-A*02⁺ lines (**Figure. 20B**). Primary HLA-A*02⁺ GB cell lines led to activation of CD8⁺ PTPRZ1¹⁸¹⁴⁻¹⁸²² TCR-T cells at varying degrees and additionally activated CD4⁺ PTPRZ1¹⁸¹⁴⁻¹⁸²² TCR-T cells in a moderate fashion (**Figure. 20C-E**). Conversely, HLA-A*02⁻ GB cell lines did not elicit any activation nor were lysed (**Figure. 20B-E**). Together, these data demonstrate that PTPRZ1¹⁸¹⁴⁻¹⁸²² TCR can broadly and specifically target HLA-A*02⁺ GB primary cell lines (5 out of 5) with a preference for stem-like SCCs.

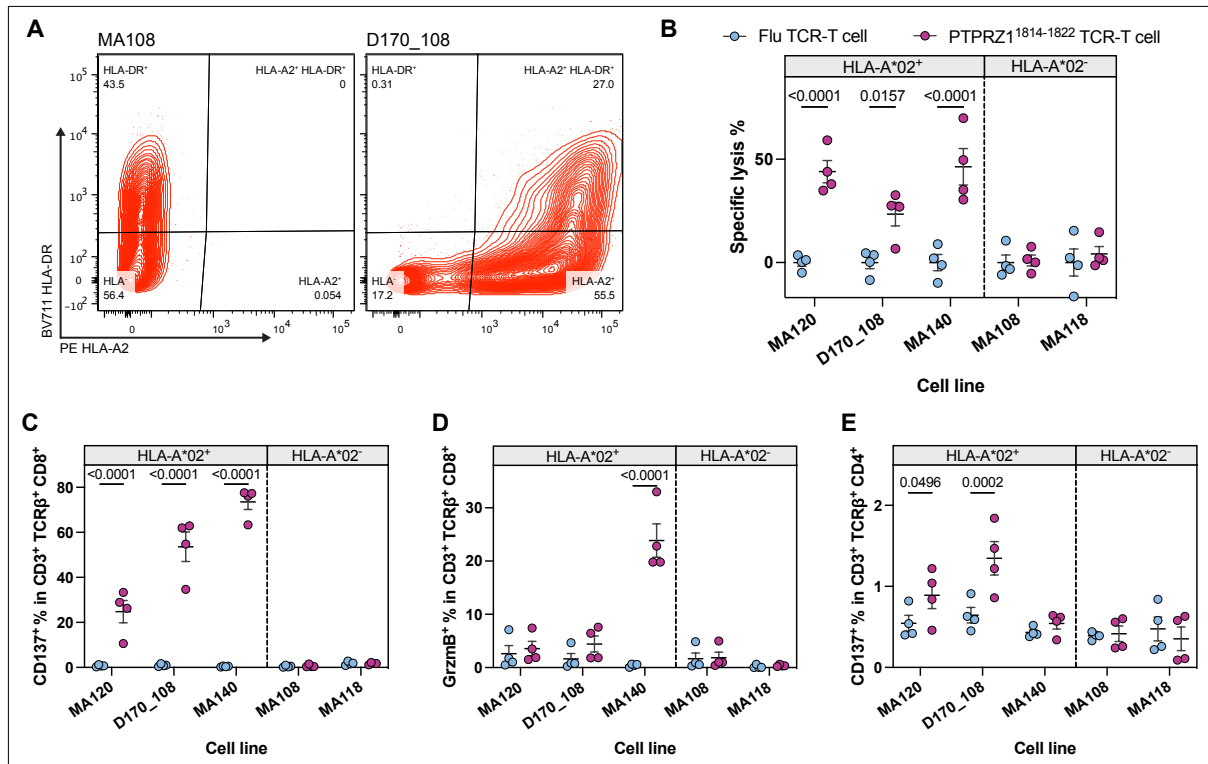


Figure 20: HLA-A*02-dependency of PTPRZ1¹⁸¹⁴⁻¹⁸²² TCR and its coverage

A. Representative contour plot showing cell line positivity for HLA-A*02. **B.** Cytotoxicity of TCR-T cells on a panel of established cell lines. Specificity was calculated by subtracting mean values of Flu TCR-T cell-treated samples for each timepoint and target cell. **C.** Activation marker-positive frequency of CD8⁺ TCR-T cells upon coculture with a panel of primary cell lines. **D.** Effector protein-expressing frequency of CD8⁺ TCR-T cells upon coculture with a panel of primary cell lines. **E.** Activation marker-positive frequency of CD4⁺ TCR-T cells upon coculture with a panel of primary cell lines. All analyses here were performed with two-way ANOVA multiple comparison corrected with Holm-Šidák method.

2.1.8 PTPRZ1¹⁸¹⁴⁻¹⁸²² TCR-T cells partly control tumors in patient-derived xenograft model in combinatorial therapy

As PTPRZ1¹⁸¹⁴⁻¹⁸²² TCR-T cells showed reactivity and cytotoxic capability against primary GB cell lines (**Figure. 19 & 20**), their potency in treating tumors in patient-derived xenograft (PDX) models was explored. Primary HLA-A*02⁺ GB cell lines were i.c. inoculated into immunodeficient mice and treated with ACT regimen. Again, i.v. route delivering therapeutic TCR-T cell product did not result in tumor regression even after five treatments (**Figure. 21A**). In contrast to the U87 TMG *in vivo* orthotopic model (**Figure. 17C-G**), i.v. and i.cv. delivery of PTPRZ1¹⁸¹⁴⁻¹⁸²² TCR-T cells did not control the tumor in the PDX model (**Figure. 21B**). In parallel, with a newly established cell line, D170_44, tumors were not controlled after treatment with i.cv. administration of PTPRZ1¹⁸¹⁴⁻¹⁸²² TCR-T cells (**Figure. 21C**). The affectlessness of the treatment in these PDX models was likely due to the physiological upregulation of endogenous PTPRZ1 expression, unlike the artificial overexpression of the cognate epitope in the U87 TMG model, reflected in different levels of PTPRZ1¹⁸¹⁴⁻¹⁸²² TCR-T cell activation (**Figure. 13A & 20C**). To promote antigen processing and presentation machinery to enhance the probability of TCR-T cell interacting with primary GB cells, irradiation was implemented (Punnaitinont et al., 2020). Five-Gy irradiation was applied locally to the tumor-bearing hemisphere after i.v. ACT and a day before the first i.cv. ACT. Irradiation itself greatly delayed the tumor growth and prolonged the survival, and with the addition of therapeutic TCR-T cell treatment, the benefits were further exacerbated (**Figure. 21D**), indicating that although the endogenous upregulated *PTPRZ1* level in primary GB cells is not sufficient to elicit therapeutic potential of PTPRZ1¹⁸¹⁴⁻¹⁸²² TCR-T cells, an intervention boosting antigen processing/presentation can facilitate TCR-T cell treatment efficacy *in vivo*.

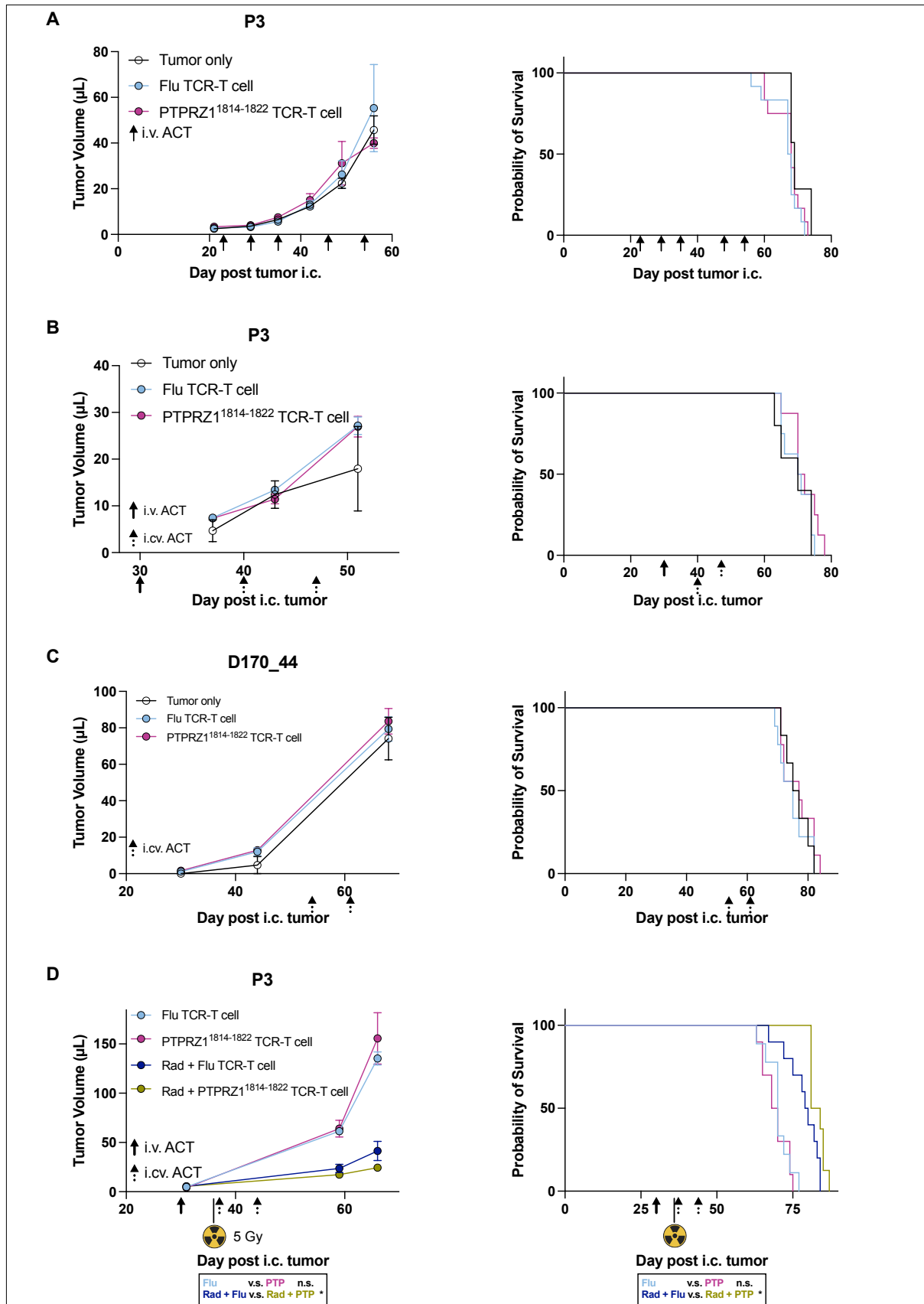


Figure 21: Patient-derived xenograft models treated with PTPRZ1¹⁸¹⁴⁻¹⁸²² TCR-T cells

A. Tumor growth and survival monitoring of a PDX model inoculated with the P3 cell line and treated with five doses of i.v. ACT. **B.** Tumor growth and survival monitoring of a PDX model inoculated with the P3 cell line and treated with one dose of i.v. ACT and two additional doses of i.cv. ACT. **C.** Tumor growth and survival monitoring of a PDX model inoculated with the D170_44 cell line and treated with two doses of i.cv. ACT. **D.** Tumor growth and survival monitoring of a PDX model inoculated with the P3 cell line and treated with one dose of i.v. ACT, followed by 5 Gy local irradiation on the tumor-bearing hemisphere and additional two doses of i.cv. ACT. All tumor growth was monitored with preclinical MRI and analyzed with nonlinear regression. All survival analyses were conducted with Log-rank test.

2.1.9 *PTPRZ1*¹⁸¹⁴⁻¹⁸²² TCR-T cells impact GB cellular state distribution and target GB stemness in individual patient tumor organoids

As previously shown, *PTPRZ1* is higher expressed in AC-like and OPC-like cells and associated with GB stemness (**Figure. 8B-E & G-J**). Whether *PTPRZ1*-prominent subsets of malignant cells were preferentially targeted by *PTPRZ1*¹⁸¹⁴⁻¹⁸²² TCR-T cells was investigated. To reconstitute and maintain tumor multicellular structures, individual patient tumor organoids (IPTO) were employed using induced pluripotent stem cell (iPSC)-derived cerebral organoids (**Figure. 22A**). IPTOs from three HLA-A*02⁺ GB patients were treated with TCR-T cells and interrogated with scRNA-seq. GB cells and immune cells were identified based on the absence of *EGFP* and the presence of *B2M* expression, as host feeder organoid cells were engineered to be EGFP-expressing and B2M-deficient (**Figure. 22B**). The GB malignant cell cluster expressed high levels of *PTPRZ1* (**Figure. 22C**). Upon *PTPRZ1*¹⁸¹⁴⁻¹⁸²² TCR-T cell treatment, the malignant cell frequency decreased (**Figure. 22D**), and average *PTPRZ1* expression levels in malignant cells were lowered (**Figure. 22E**). To visualize cellular states, the module scores of each malignant cell were calculated with the aforementioned gene sets (**Figure. 22F**) (Neftel et al., 2019). Concordant to previous results (**Figure. 8B&G**), *PTPRZ1* was associated with AC-like tumor cells (**Figure. 22F**). After *PTPRZ1*¹⁸¹⁴⁻¹⁸²² TCR-T cell treatment, AC-like score and AC-like tumor cell frequency were reduced significantly (**Figure. 22G&H**). Corroborating previous findings, a positive correlation between GSC score and *PTPRZ1* was observed (**Figure. 22I**), and *PTPRZ1*¹⁸¹⁴⁻¹⁸²² TCR-T cells coculture led to a drop of GSC cell frequency (**Figure. 22J**). In summary, the results once again confirm that in addition to being upregulated in GB, *PTPRZ1* is more highly expressed in AC-like cells and

GSCs, and demonstrate that these *PTPRZ1*¹⁸¹⁴⁻¹⁸²² GB cells are favorably targeted by *PTPRZ1*¹⁸¹⁴⁻¹⁸²² TCR-T cells.

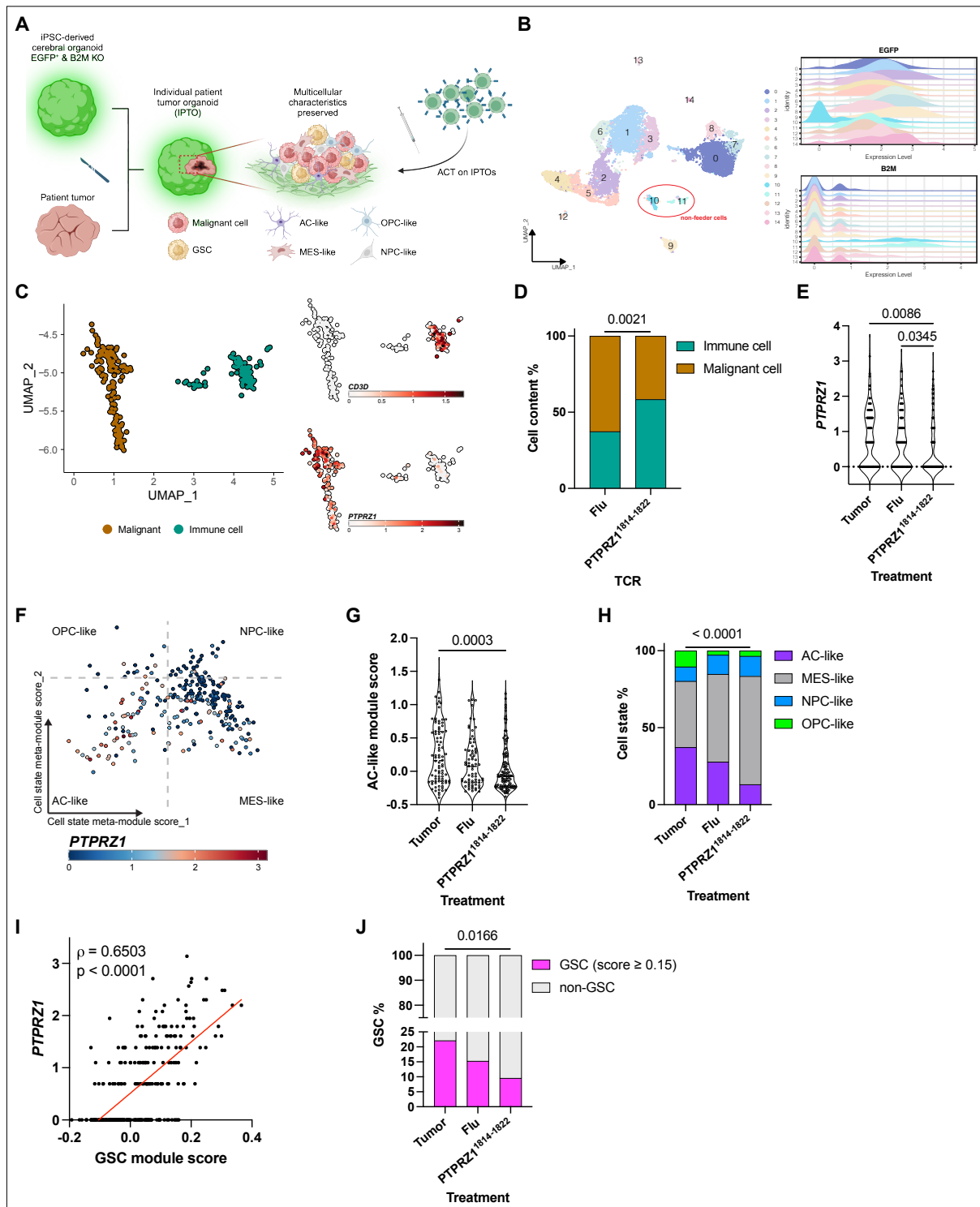


Figure 22: Preferential targeting GB subsets by the *PTPRZ1*¹⁸¹⁴⁻¹⁸²² TCR-T cell

A. IPTO generation from three HLA-A*02⁺ GB samples to reconstitute multicellular characteristics and treatment with TCR-T cells. **B.** UMAP plot of all cells collected upon the treatment with ridge plots showing *EGFP* and *B2M* expression to identify non-feeder cells. **C.** UMAP plot of malignant cells and

Results

immune cells derived from **(B)** with their marker expression on the right. **D.** Frequency of cell content in IPTOs upon TCR-T cell treatment. **E.** *PTPRZ1* expression after TCR-T cell treatment. **F.** Cellular states of generated and treated IPTOs with *PTPRZ1* expression. **G.** AC-like module score of malignant cells after TCR-T cell treatment. **H.** Distinct cell state frequency in malignant cells after TCR-T cell treatment. **I.** Correlation of *PTPRZ1* expression and GSC module score in malignant cells in IPTOs. **J.** Frequency of GSCs upon TCR-T cell treatment. Cells score over 0.15 in the GSC module score are defined as GSCs here. **(D)**, **(H)**, and **(J)** were analyzed with Fisher's exact test. **(E)** and **(G)** were performed with one-way ANOVA multiple comparison corrected with Holm-Šidák method. **(I)** was conducted with Spearman correlation.

2.2 Developing TCRs against glioblastoma-associated antigens

2.2.1 Glioblastoma-associated antigen selection and immunogenic epitope prediction

To expand the coverage of TCR-T cell therapy for GB, additional TCRs targeting other GAAs were aimed for development. Firstly, more GAAs had to be identified. GB and normal samples were collected and bulk RNA-sequenced, and several candidate GAAs were shortlisted and validated through RT-qPCR (**Figure. 23A**). These candidates were further filtered based on their expression across normal adult tissues. Ultimately, four transcription factors—GSX1, GSX2, HOXD13, and ZNF560—were selected to proceed. Interestingly, the first three candidates are homeobox genes that are expressed and essential in segmentation during embryonic development (Hubert and Wellik, 2023). Recent studies have further revealed that homeobox gene expression is often dysregulated in cancers, contributing to disease malignancy (Yadav et al., 2024). GSX1 and GSX2 are among the earliest transcription factors expressed in neuronal progenitors (Pei et al., 2011). GSX1 has been associated with gastric cancer patient prognosis (Chen et al., 2019), and GSX2 was found to be overexpressed in pancreatic cancers (Zhuang et al., 2021). HOXD13 is required for limb development, particularly in the early and late stages of limb morphogenesis (Brison et al., 2014; Zhao et al., 2007). However, HOXD13 role in cancers is differential: in prostate, pancreatic, and breast cancers, it is associated with favorable prognosis and suppresses disease progression (Cantile et al., 2009; Xu et al., 2021; Zhong et al., 2015); in colon cancer, it is overexpressed and linked to poor prognosis by influencing cell proliferation and invasion through transcriptionally promoting PTPRN2 expression (Yin and Guo, 2021). On the other hand, ZNF560 is also a transcription factor that is typically expressed solely in reproductive systems which are immune-privileged (TheHumanProteinAtlas, 2024). While ZNF560 functions and target genes remain mysterious, it has been reported to be associated with poor prognosis in leukemia (Wang et al., 2022), and mutations in ZNF560 are associated with longer survival in lung adenocarcinoma (Cho et al., 2018). In brain tumors, apart from bulk RNA-seq, TCGA data confirmed that these candidates were overexpressed in GB cancerous tissues, and *GSX1* and *GSX2* were even higher expressed in grade 3 LGG

Results

compared to grade 2 (**Figure. 23B**). In addition, out of these candidate GAAs, *GSX2* and *HOXD13* were associated with poor prognosis in GB patients (**Figure. 23C&D**).

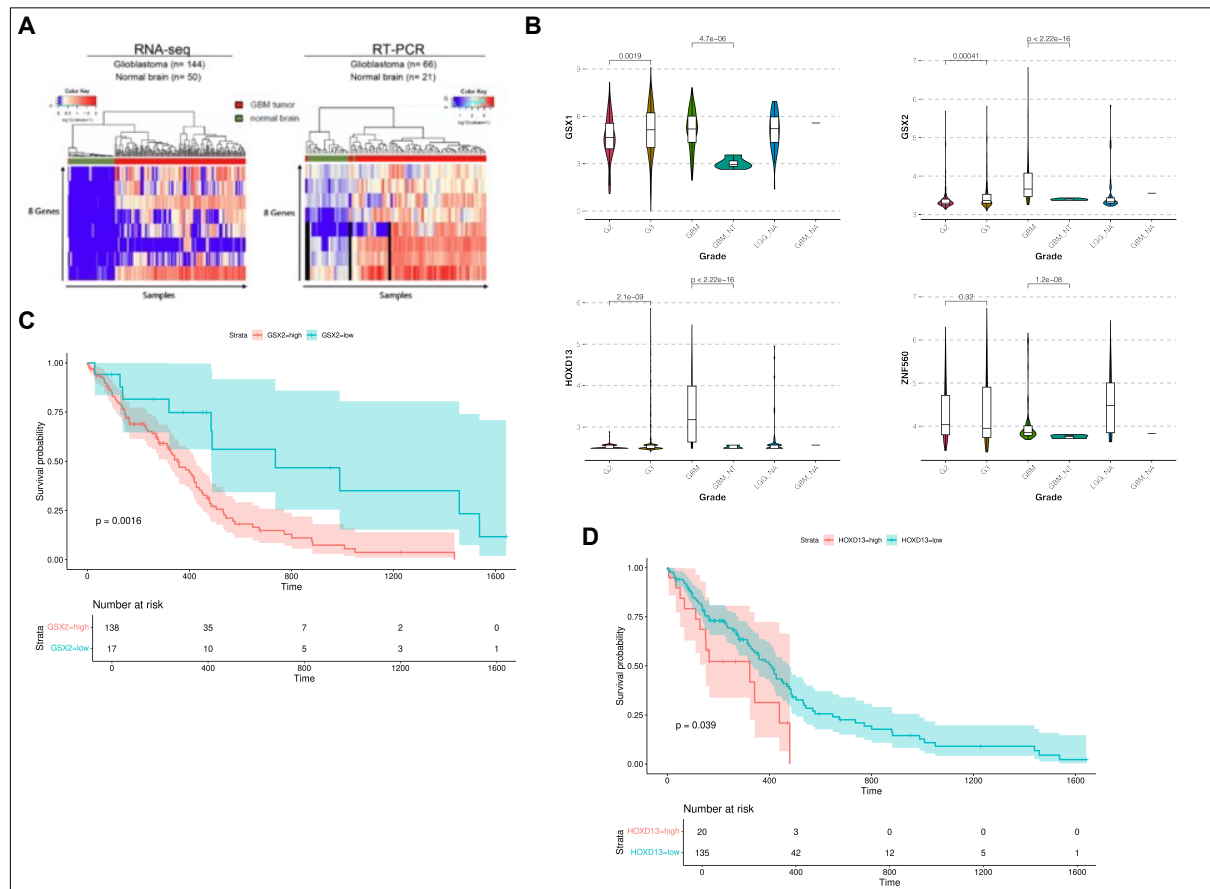


Figure 23: Candidate GAA selection and characterization in brain tumors

A. Bulk RNA-seq and RT-qPCR comparing GB and normal samples for GAA shortlisting. **B.** Candidate GAA expression in brain tumors in TCGA datasets. **C.** Survival analysis based on differential *GSX2* expression. **D.** Survival analysis based on differential *HOXD13* expression. (**B**) was analyzed with t-test. (**C**) and (**D**) were performed with Log-rank test.

With GAAs shortlisted, their immunogenic epitopes for the common MHC I allele HLA-A*02 were subsequently predicted using a machine learning-facilitated tool, NetMHCpan-4.1 (Reynisson et al., 2020a), and those for the common MHC II allele HLA-DRB1*0101 were predicted with NetMHCIIpan-4.0 (Reynisson et al., 2020b). The epitopes that were not shared by other proteins (blast.ncbi.nlm.nih.gov/Blast.cgi) and had top EL scores (derived and trained from mass-spectrometry eluted ligand data) were next selected (**Figure. 24A&B** and **Table. 3 & 4**). In order to discover reactive TCRs, the humanized A2.DR1 mouse strain (see **4 Materials and Methods**) was used as it is knockin with common human HLA alleles, HLA-A*0201, HLA-DRA*0101, and HLA-DRB1*0101, ensuring that the developed TCRs would be reactive to peptide-HLA complexes. A previous immunization strategy was adapted and modified to include two peptides per vaccine, aiming to mitigate mouse usage and to develop TCRs for as many predicted immunogenic epitopes as possible (**Figure. 24C**) (Kilian et al., 2022). In sham vaccinated mice, no auto-reactivity was observed for MHC II epitopes (**Figure. 24D**). Furthermore, with the T2 peptide binding assay, it was confirmed that predicted MHC I peptides were able to bind to HLA-A*02 (**Figure. 24E**). No peptide was excluded, and subsequently, the predicted epitopes were used for vaccination.

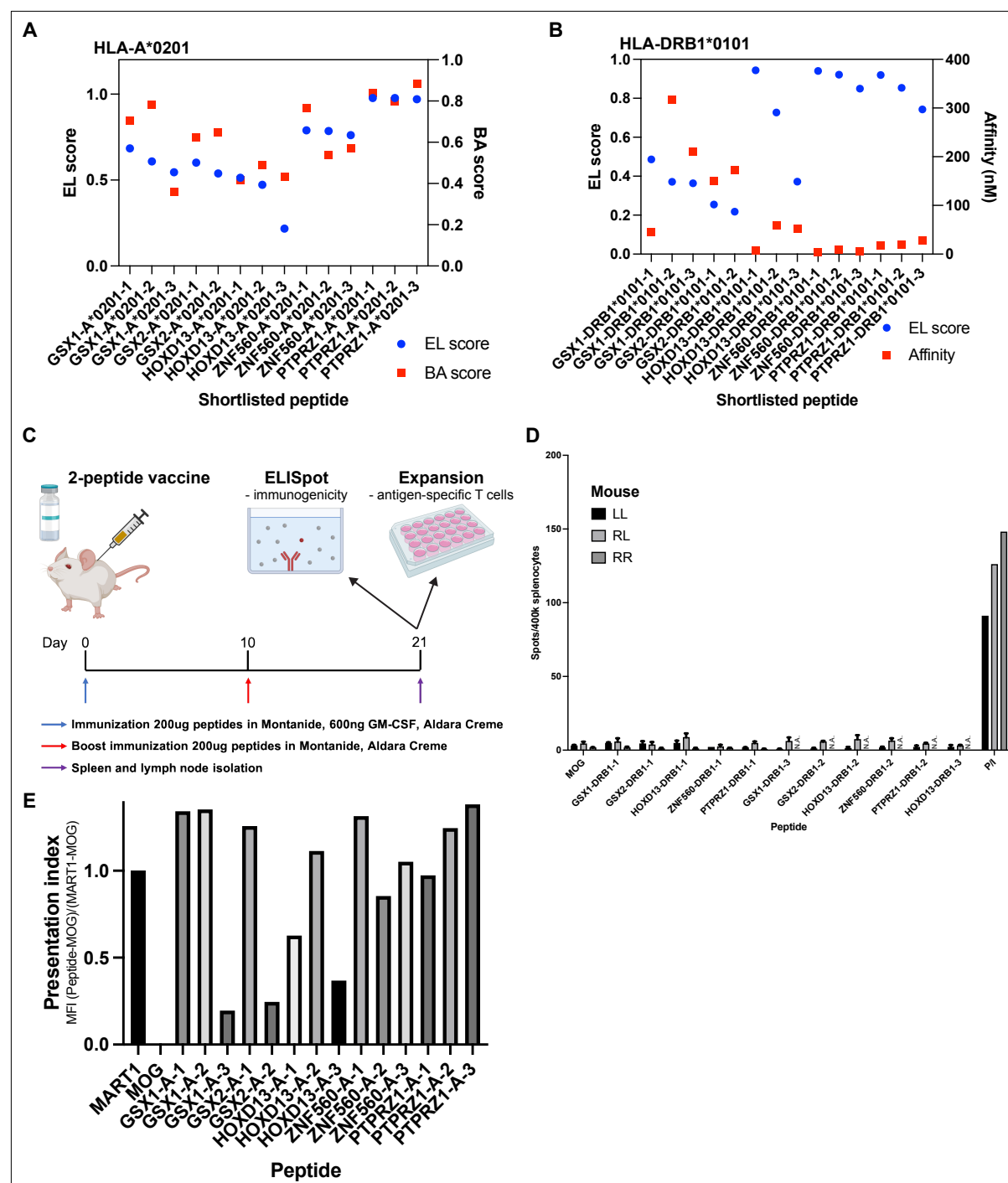


Figure 24: Immunogenic epitope prediction and auto-reactivity and peptide binding validation

A. *In silico* predicted immunogenic epitopes of candidate GAAs for the HLA-A*0201 allele with elution (EL) and binding affinity (BA) scores illustrated. Specific sequences and score values can be referred to in **Table 3**. **B.** *In silico* predicted immunogenic epitopes of GAAs for the HLA-DRB1*0101 allele with EL score and binding affinity indicated. Specific sequences and score values can be referred to in **Table 4**. **C.** Modified vaccination strategy incorporating two peptides in one immunization. The developed immunogenicity would be validated with ELISpot, and the antigen-reactive T cells would be *in vitro* expanded. **D.** Auto-reactivity test of MHCII peptides with splenocytes from sham-vaccinated mice with ELISpot assay. **E.** Validation of predicted MHCII epitope binding to HLA-A*0201+ β 2M-deficient T2 cells.

MART1 peptide serves as a positive control for peptide binding while MOG peptide is MHCII-restricted and serves as a negative control.

Name	Peptide	EL-score	BA-score
GSX1-A*0201-1	FLVDSLVLREA	0.6849	0.7039
GSX1-A*0201-2	ALYQTSYPL	0.6088	0.7834
GSX1-A*0201-3	NLSEKQVKI	0.5454	0.3577
GSX2-A*0201-1	GMPPPLVMSV	0.6014	0.6234
GSX2-A*0201-2	RLRRIEIATYL	0.5382	0.6491
HOXD13-A*0201-1	NLSERQVTI	0.5134	0.4156
HOXD13-A*0201-2	ALNQPDMCV	0.4723	0.4895
HOXD13-A*0201-3	HVPGYIDMV	0.2176	0.4319
ZNF560-A*0201-1	ALWQDNFCL	0.789	0.7669
ZNF560-A*0201-2	ILLDPVQRNL	0.785	0.5397
ZNF560-A*0201-3	SLYNKTSTI	0.7611	0.5709
PTPRZ1-A*0201-1	KVFAGIPTV	0.9775	0.8389
PTPRZ1-A*0201-2	AIIDGVESV	0.9773	0.7973
PTPRZ1-A*0201-3	MIWEHNVEV	0.9703	0.8817

Table 3: Shortlisted NetMHCpan-4.1-predicted immunogenic epitopes of GAAs for HLA-A*0201

Name	Peptide	EL-score	Affinity (nM)
GSX1-DRB1*0101-1	EIATYLNLSSEKQVKI	0.486544	45.6559774
GSX1-DRB1*0101-2	KGAVGAEGGLAAGRP	0.37141	316.746594
GSX1-DRB1*0101-3	PHALHGLSPGACHAR	0.364021	210.622322
GSX2-DRB1*0101-1	PPLVMSVSGPGCPSR	0.254968	149.354434
GSX2-DRB1*0101-2	VDSLIIKDTSRPAPS	0.217975	173.224017
HOXD13-DRB1*0101-1	RHEAYISMEGYQSWT	0.94345	6.80946959
HOXD13-DRB1*0101-2	VPGYIDMVSTFGSGE	0.726989	59.3100291
HOXD13-DRB1*0101-3	KLQLKELENEYAINK	0.37222	52.611132
ZNF560-DRB1*0101-1	GKSFRLLILNVQVQRK	0.940595	3.92009554
ZNF560-DRB1*0101-2	QEFWKIQTSNGIQMD	0.921636	9.77962102
ZNF560-DRB1*0101-3	GKAFASFSARIAHLK	0.849938	6.09610192
PTPRZ1-DRB1*0101-1	ENNFSVQPTHVSQA	0.919857	18.4561949
PTPRZ1-DRB1*0101-2	RVGISSLSGEGTDYI	0.853531	19.9158763
PTPRZ1-DRB1*0101-3	PVLLKSESSHQVPS	0.742726	27.621031

Table 4: Shortlisted NetMHCIIpan-4.0-predicted immunogenic epitopes of GAAs for HLA-DRB1*0101

2.2.2 GAA-reactive CD4⁺ T cell identification and expansion

To start, since the antigen-reactive murine CD4⁺ T cell expansion protocol was well-established (Schumacher et al., 2014), and because GSX2 was not only overexpressed but also associated with poor prognosis (**Figure. 23B&C**), GSX2 MHCII peptides were first employed. Following immunization (**Figure. 24C**), immunogenicity against the epitope GSX2-DRB1-1 was observed in three out of four vaccinated mice (**Figure. 25A**). Murine DCs from A2.DR1 mice expressing co-stimulatory molecules were *in vitro* differentiated from bone marrow cells to expand rare antigen-reactive T cells (**Figure. 25B**). With peptide-loaded irradiated DCs, after one round of stimulation, antigen-reactive CD4⁺ T cells were greatly expanded *in vitro* (**Figure. 25C**). As IFN γ was specific, an IFN γ secretion assay was utilized to identify and FACS-isolate antigen-specific IFN γ -secreting CD4⁺ T cells (**Figure. 25D**). The sorted CD4⁺ T cells were then subjected to scTCR-seq, and their clonotype appeared rather uni- to oligo-clonal, indicating specific expansion of antigen-reactive CD4⁺ T cells (**Figure. 25E**). Some TCRs were even shared across individual animals (**Figure. 25F**). To authenticate the TCR reactivity, the most dominant TCR was cloned and validated with a Jurkat reporter assay mentioned before (**Figure. 9B**), and it showed strong reactivity against the cognate peptide-loaded DCs (**Figure. 25G**). With this promising result, more peptides were applied in the A2.DR1 mouse vaccination. For GSX1 MHCII epitopes, GSX1-DRB1-1 elicited more notable immunogenicity across mice while GSX1-DRB1-3 induced minor but observable immunogenicity (**Figure. 25H**). In the meantime, for HOXD13 MHCII epitopes, HOXD13-DRB1-1 elicited strong immunogenicity while HOXD13-DRB1-3 did not evoke any reactivity (**Figure. 25I**). This phenomenon for both GAAs is likely due to peptide affinity; as GSX1-DRB1-1 and HOXD13-DRB1-1 have higher EL scores and better affinity (**Figure. 24B**), they bind to MHCII with an advantage while the other peptides with lower affinities could not compete for binding under the same vaccination regimen and thus failed to elicit specific T cell responses. Together, it is demonstrated that predicted immunogenic MHCII epitopes for GAAs can indeed elicit T cell responses following immunization, and the antigen-specific CD4⁺ T cells can be expanded *in vitro* and isolated. Further assays are required to assess the therapeutic potential of the identified GSX2-reactive CD4-restricted TCR and to develop more GAA-reactive TCRs.

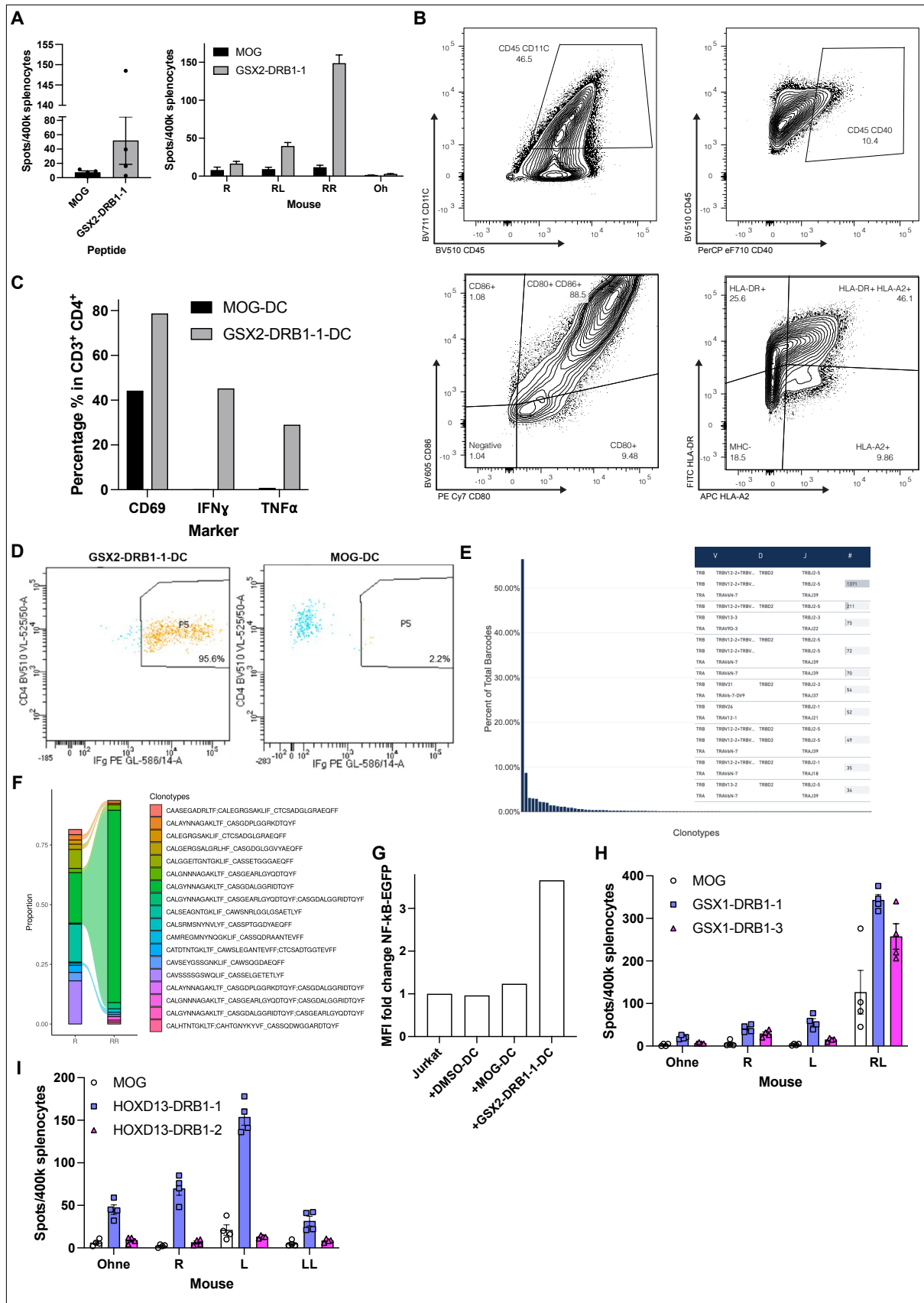


Figure 25: Identification and isolation of GAA-reactive CD4⁺ T cell in A2.DR1 mice

A. Immunogenicity against GSX2-DRB1-1 following vaccination in four mice. **B.** A2.DR1 DC *in vitro* differentiation from bone marrow cells and characterization. **C.** Activation marker-positive frequencies of CD4⁺ T cells after expansion with peptide-loaded irradiated DCs. **D.** IFN γ secretion assay used to sort antigen-reactive CD4⁺ T cells following antigen-specific expansion. **E.** Clonotype plot of sorted antigen-reactive CD4⁺ T cells from (**D**). **F.** Shared TCR clonotypes between two individual vaccinated A2.DR1 mice. **G.** Validation of the dominant TCR from (**E**) with Jurkat reporter cells mentioned in **Figure. 9B**. **H.** Immunogenicity against GSX1 MHCII epitopes upon two-peptide vaccination. **I.** Immunogenicity against HOXD13 MHCII epitopes upon two-peptide vaccination.

2.2.3 GAA-reactive CD8⁺ T cell identification and expansion

To discover CD8-restricted TCRs for GAAs, A2.DR1 mice were vaccinated with predicted immunogenic MHCI epitopes. As no protocol for antigen-specific CD8⁺ T cells was established, several published methods were explored. The first attempt was adapted from Wölfl and Greenberg (2014) with T2 cells as APCs; however, this method ended up expanding CD4⁺ T cells (**Figure. 26A**). The next attempt further modified the protocol and used peptide-loaded DCs as APCs cocultured with MACS-enriched CD8⁺ T cells after vaccination. The modified protocol not only enlarged CD8⁺ T cell population but also expanded antigen-reactive CD8⁺ T cells (**Figure. 26B&C**). With the established workflow to expand antigen-reactive CD8⁺ T cells, more A2.DR1 mice were subsequently vaccinated with predicted MHCI epitopes. For both GSX1 and ZNF560, only the higher EL-score/affinity epitopes, GSX1-A-1 and ZNF560-A-1, elicited strong immunogenicity while the ones with lower affinity did not (**Figure. 26D&E**). Again, this is likely due to MHC binding competition when included in the same immunization regimen, similar to MHCII peptide vaccination outcomes (**Figure. 25H&I**). As immunogenicity was developed upon vaccination, antigen-specific CD8⁺ T cells were subsequently expanded following the established protocol. Antigen-reactive CD8⁺ T cells were FACS-isolated and subjected to scTCR-seq (**Figure. 26F**). The TCR clonotype of sorted CD8⁺ T cells appeared rather oligoclonal, an indication of antigen-specific expansion (**Figure. 26G**). Additional assays are essential to validate the reactivity of the dominant TCRs and to showcase their therapeutic potential.

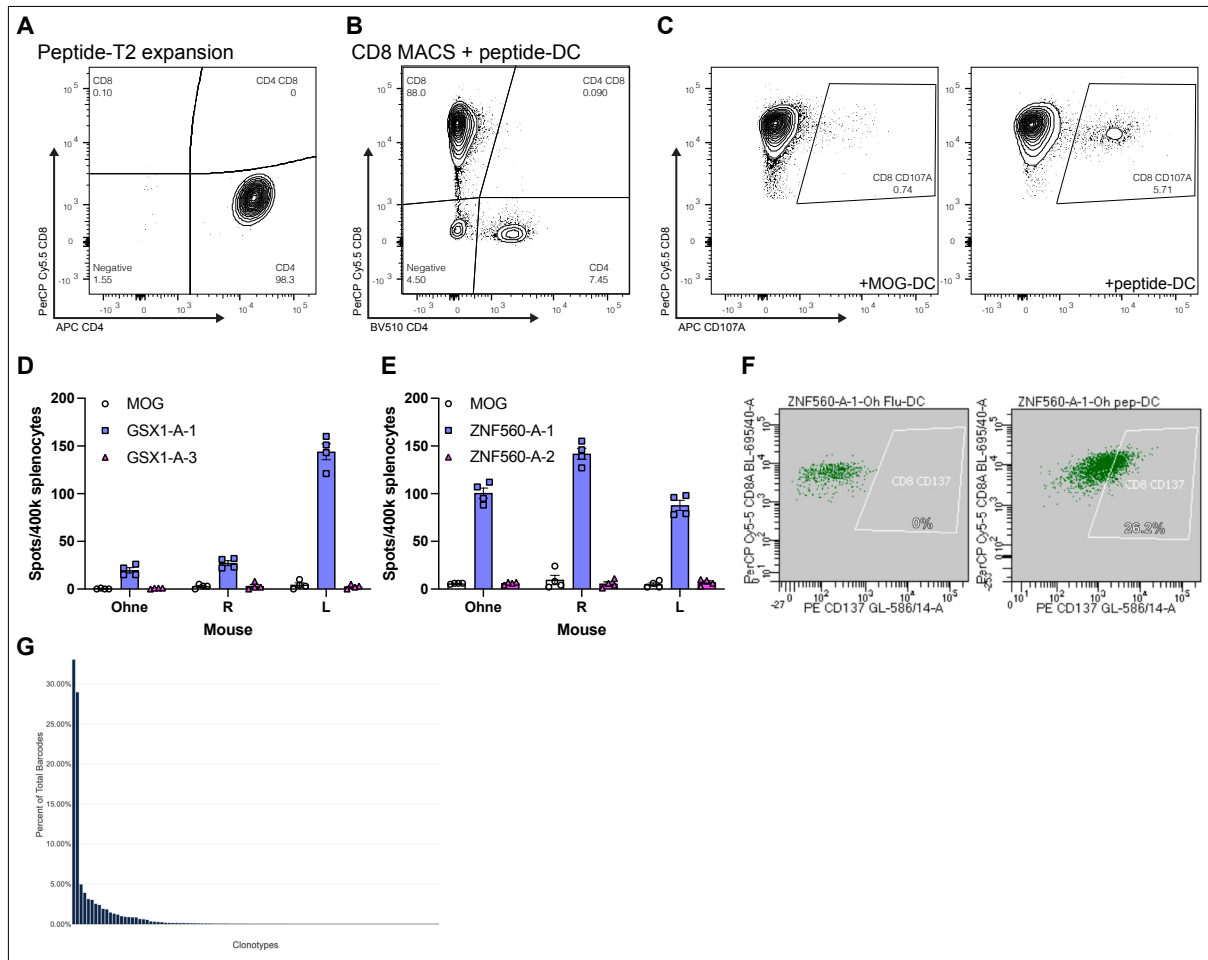


Figure 26: Identification and isolation of GAA-reactive CD8⁺ T cell with A2.DR1 mice

A. Protocol adapted from Wöfl and Greenberg (2014) to expand antigen-reactive CD8⁺ T cells with T2 cells. **B.** Modified protocol from (A) with MACS-enriched CD8⁺ T cells stimulated with peptide-loaded DCs. **C.** Antigen-specific reactivity of expanded T cells from (B). **D.** Immunogenicity against GSX1 MHC I epitopes upon two-peptide vaccination. **E.** Immunogenicity against ZNF560 MHC I epitopes upon two-peptide vaccination. **F.** FACS to sort expanded antigen-reactive CD8⁺ T cells. **G.** Clonotype plot of sorted antigen-reactive CD8⁺ T cells from (F).

2.2.4 *In vitro* vaccination expanding antigen-reactive T cells from healthy donors

To restrain the consumption of animals and to avoid labor-intensive safety profiling for using A2.DR1 mouse-derived TCRs, the potential of directly retrieving reactive TCRs from healthy donors was explored. Since HLA-A*0201 could be rapidly identified using flow cytometry, MHC I epitopes restricted to HLA-A*0201 were first employed. In accordance with a previously developed protocol (Bozkus et al., 2021), PBMCs were freshly isolated and HLA-typed from healthy donor blood (**Figure. 27A**), followed by one-day APC differentiation and eight-day antigen-specific stimulation and expansion. Restimulation with the cognate peptide was performed for 24 hours before analyzing antigen-specific T cell frequency. As a proof-of-concept, the commonly used immunogenic peptide Flu, the GAPVAC-101 trial-proven immunogenic peptide PTPRZ1¹⁸¹⁴⁻¹⁸²², and the A2.DR1 mouse-shown immunogenic epitope GSX1-A-1 were first used. Upon restimulation, a marginal increase of antigen-reactive CD8⁺ T cell frequency was observed for Flu and PTPRZ1¹⁸¹⁴⁻¹⁸²² peptides but not for GSX1-A-1 (**Figure. 27B**). In alignment with the previous study (Bozkus et al., 2021), not all healthy donors harbor pre-existing reactive T cell clones to be expanded *in vitro*, and the extent of expansion is limited to around 20%. More optimized workflow should be developed to more efficiently expand rare antigen-reactive T cell clones. Alternatively, the protocol requiring a large number of PBMCs and peptide-MHC multimers could be attempted (Giannakopoulou et al., 2023). Additionally, *in vitro* vaccination for antigen-reactive CD4⁺ T cells is still in need of exploration.

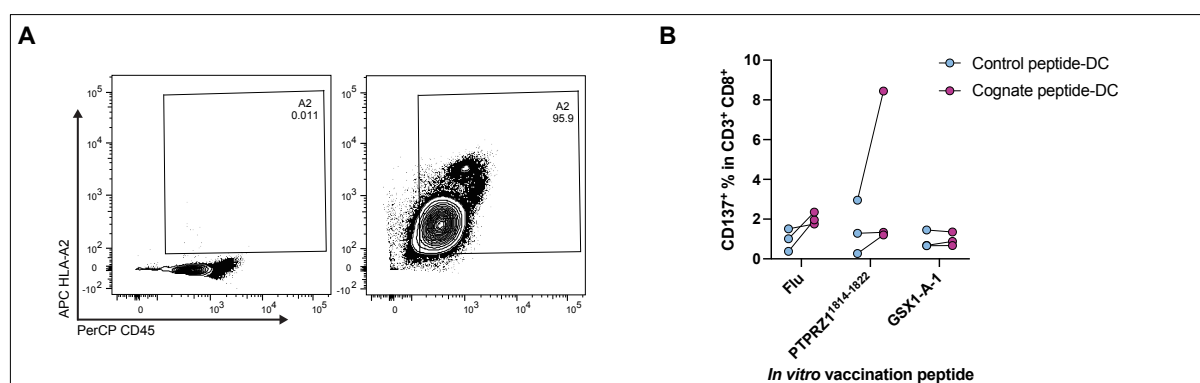


Figure 27: *In vitro* vaccination

A. HLA typing healthy donors with flow cytometry. **B.** Activated CD8⁺ T cell frequencies upon restimulation with control or cognate peptide used for initial stimulation. **(B)** was analyzed with two-way ANOVA multiple comparison corrected with Holm-Šidák method.

2.3 Glioma MHCII expression and its effects on immunotherapy

2.3.1 A subset of gliomas express MHCII

To understand tumoral MHCII role in gliomas, firstly, its expression in brain tumors was evaluated with immunofluorescence staining on samples from the Pathology Department in Heidelberg University (**Figure. 28A**). Typically, MHCII expression was present on immune cells (CD68⁺ cells) yet was also observed on some tumor cells (GFAP⁺ cells) in some patients, particularly those with higher-grade gliomas (**Table. 5**). Apart from protein levels, tumoral MHCII expression was also observed at the transcription level. In IDH-mutant gliomas (Venteicher et al., 2017), a rare population of tumor cells expressed MHCII (**Figure. 28B**). In GB (Neftel et al., 2019; Patel et al., 2014), a population of tumor cells expressing MHCII was also identified (**Figure. 28C&D**). In our glioma scRNA-seq data, some tumor cells were found to express MHCII as well (**Figure. 28E**), and certain established GB primary cell lines maintained MHCII expression (**Figure. 20A**). These findings confirm that MHCII can indeed be expressed by glioma cells as mentioned in **1.5 Tumoral MHCII expression and therapy efficacy**.

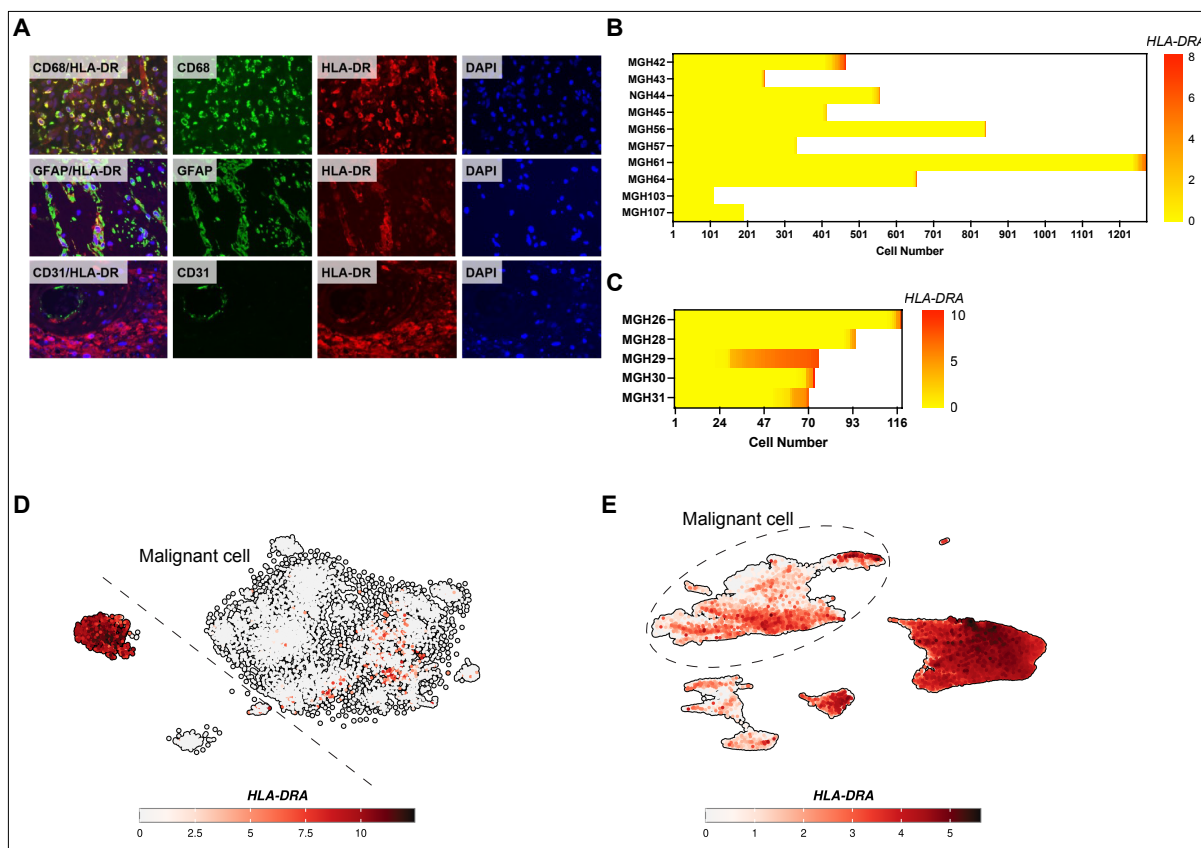


Figure 28: Glioma MHCII expression at protein and transcript levels

A. Immunofluorescence staining of gliomas showing the expression of CD68 (Monocyte lineage marker, e.g. microglia), CD31 (endothelial cell marker), and GFAP (glioma marker). **B.** IDH-mutant astrocytoma cells expressing *HLA-DR* from scRNA-seq data in Venteicher et al. (2017). **C.** GB tumor cells expressing *HLA-DR* from scRNA-seq data in Patel et al. (2014). **D.** t-SNE plot showing GB malignant cells and non-tumor cells with *HLA-DR* expression from scRNA-seq data in Neftel et al. (2019). **E.** UMAP plot of our glioma scRNA-seq data showing *HLA-DR* expression in various cells.

WHO	n	HLA-DR ⁺ Microglia	Percentage %	HLA-DR ⁺ Tumor	Percentage %
O II	13	10	77	0	0
O III	11	11	100	0	0
OA II	3	3	100	0	0
OA III	3	1	33	2	67
A I	7	7	100	0	0
A III	22	20	91	2	9
GB	23	16	70	7	30

O: Oligodendroglioma; OA: Oligoastrocytoma; A: Astrocytoma

Table 5: Frequency of MHCII expression in gliomas

2.3.2 Glioma MHCII expression is associated with poor prognosis and immune infiltration

To unveil the impact of glioma MHCII expression, TCGA data were employed as the sample number was ample and clinical data were documented. However, only bulk RNA-seq data were available. In order to deconvolute tumoral MHCII expression in each tumor, all MHCII genes were summarized, and immune cell markers, *PTPRC* and *ITGAM*, were included to normalize immune cell composition using *singscore* R package (Foroutan et al., 2018), resulting in a tumoral HLAI score for each tumor. Strikingly, tumoral MHCII appeared to be a poor prognostic factor in LGG patients, especially in those with IDH1 mutations (**Figure. 29A**). Molecular analyses revealed that higher tumoral HLAI score was associated with interferon responses in line with previous findings (**Figure. 29B**) (Axelrod et al., 2019). Additionally, the tumoral HLAI score was associated with immune cell infiltration as indicated by several marker gene expression. *CD3E*, representing T cells, was more highly expressed in tumors with high tumoral HLAI scores (**Figure. 29C**); nonetheless, it was not due to more infiltration of either CD4⁺ or CD8⁺ T cells but rather a collective consequence as shown with *CD4* and *CD8A* expression (**Figure. 29D**). Moreover, *ADGRE1*, representing macrophages, was higher in tumors with high tumoral HLAI scores, but no difference was observed in *AIF1*, a microglia marker (**Figure. 29E**). Immune cell infiltration was also described in MHCII⁺ melanomas (Johnson et al., 2016), and an immune checkpoint molecule, PD-L1, was upregulated along with MHCII expression. Similarly, in tumors with high tumoral HLAI scores in LGG, immune checkpoint molecules, *CTLA4* and *PDCD1*, were more highly expressed (**Figure. 29F**). Together, these data suggest that glioma MHCII expression, although resulting in more immune infiltration, is associated with disease progression.

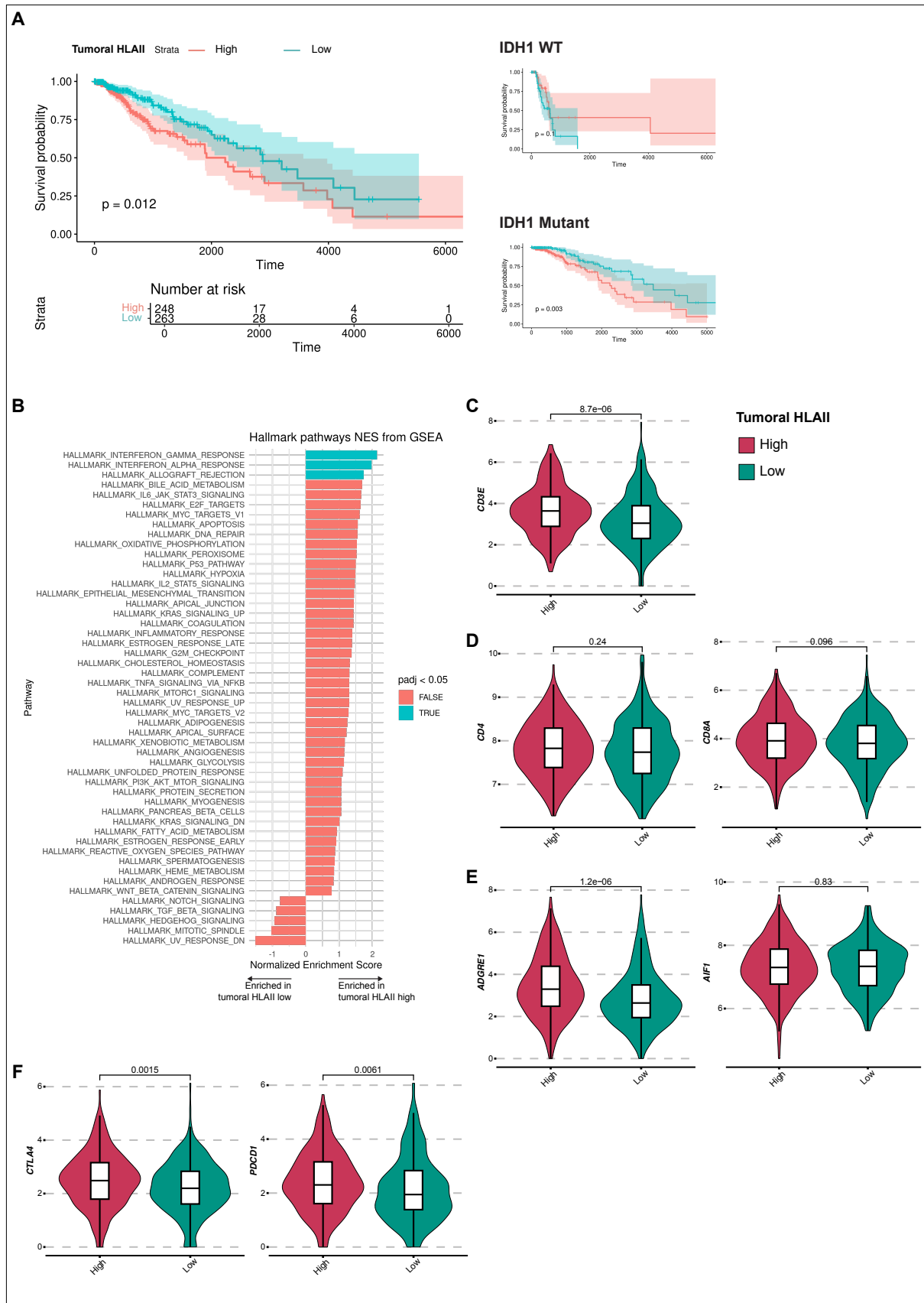


Figure 29: Clinical and molecular impacts of glioma MHCII expression in LGG

A. Survival analyses of LGG patients with high and low tumoral HLAII scores and with or without IDH1 mutations. **B.** Gene set enrichment analysis (GSEA) of differentially expressed genes (DEGs) between high and low tumoral HLAII score tumors. **C.** *CD3E* (T cells) expression in tumors with different tumoral HLAII scores. **D.** *CD4* and *CD8A* expression in tumors with different tumoral HLAII scores. **E.** *ADGRE1* (F4/80, macrophages) and *AIF1* (IBA1, microglia) expression in tumors with different tumoral HLAII scores. **F.** *CTLA4* and *PDCD1* checkpoint molecule expression in tumors with different tumoral HLAII scores. **(A)** was conducted with Log-rank test. **(C)-(F)** were analyzed with t-test.

2.3.3 Glioma MHCII is functional

To model the above findings, a murine glioma model cell line, GL261, was utilized. The cell line did not express MHCII at baseline but became MHCII⁺ when stimulated with IFN γ (**Figure. 30A**). In order to model MHCII⁻ and MHCII⁺ gliomas, GL261 was further engineered. Using CRISPR-Cas9 technology, the murine MHCII was maneuvered to be knocked out (KO). A single clone *H2-Ab1* KO line, ID5, was generated from GL261 and validated with IFN γ stimulation (**Figure. 30A**). In parallel, an oligoclonal line with *H2-Ab1* KO was generated with antibiotic selection, yet the *H2-Ab1* KO^{oligo} line did not completely lose the ability to express MHCII even after a round of FACS enrichment (**Figure. 30B**). On the other hand, both chains of MHCII from the C57BL/6 mouse strain were cloned (**Figure. 30C**), and the construct was then used to generate GL261 cell line overexpressing MHCII (H2-A or I-A) and a cell line of ID5 with rescued MHCII expression (**Figure. 30D**). Interestingly, MHCII overexpression (OE) in these cell lines led to a marginal increase in Ki67, proliferative marker, and PD-L1 expression (**Figure. 30E**), implying that MHCII intracellular signaling may be present in solid tumor cancer cells. To assess whether the transgenic MHCII was functional in terms of interacting with CD4⁺ T cells, the cell lines were loaded with OVAII peptide and cocultured with OTII CD4⁺ T cells, and only the lines with MHCII OE or rescued expression induced OTII CD4⁺ T cell activation (**Figure. 30F**). Here glioma cells modelling MHCII⁻ and MHCII⁺ tumors are established.

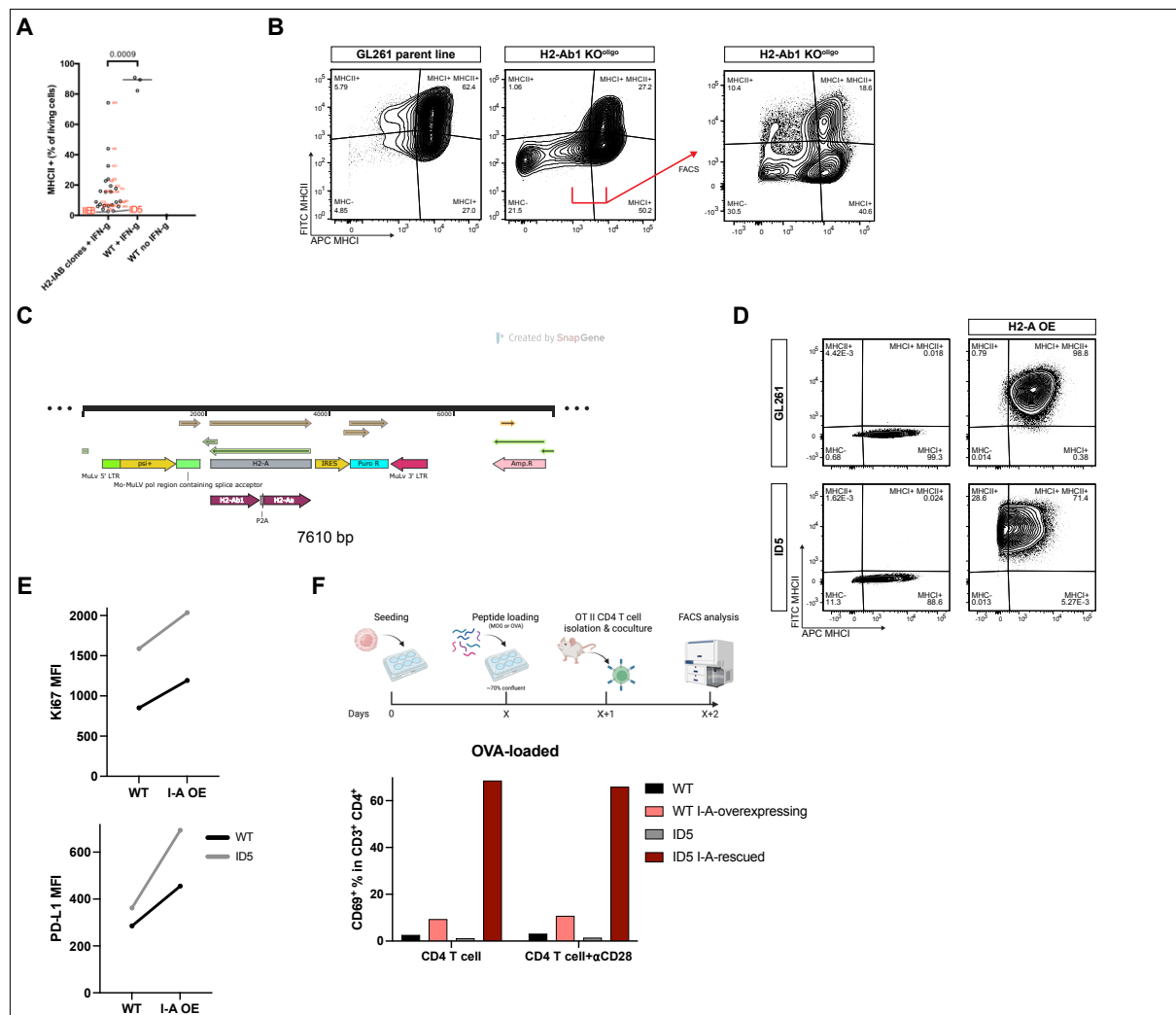


Figure 30: Generation of MHCII⁻ and MHCII⁺ murine glioma cell lines with GL261

A. Gesicle-based CRISPR-Cas9-mediated *H2-Ab1* KO with IFN γ stimulation to validate single clone MHCII depletion. **B.** CRISPR-Cas9-mediated *H2-Ab1* KO with antibiotic selection to generate an oligoclonal cell line with incomplete MHCII KO even after FACS enrichment of MHCII⁻ cells. **C.** Construct design harboring both chains of the C57/BL6 mouse MHCII with puromycin to select stable cell lines. **D.** Overexpression and rescue of MHCII expression with the construct from (C). **E.** Ki67 and PD-L1 intensity levels in parental lines and lines stably expressing MHCII. **F.** Validation of the function of transfected MHCII with OVAII and OTII CD4⁺ T cells.

2.3.4 Glioma MHCII does not promote disease progression but attracts immune cells

With model cell lines established, findings in human gliomas were attempted to be recapitulated (**Figure. 30**). GL261 and I-A-expressing cells were i.c. inoculated into C57BL/6 mice; however, no tumor growth nor survival difference was observed with MHCII expression though MHCII expression intrinsically led to more proliferation (**Figure. 30E & 31A**). As gliomas with high tumoral HLAII scores had more immune infiltration and higher expression of immune checkpoint molecules (**Figure. 29C-F**), immune surveillance might be influenced and evaded. A model with immune surveillance against GL261 using the model antigen SIINFEKL was demonstrated (Kilian et al., 2022). Mice orthotopically inoculated with the SIINFEKL-expressing cell line spontaneously developed antigen-reactive CD8⁺ T cells and required myeloid MHCII in the microenvironment to facilitate activation of CD4⁺ T cells to prevent CD8⁺ T cell dysfunction for tumor control. In addition, I-A expression intrinsically led to higher PD-L1 expression (**Figure. 30E**). It was then hypothesized that glioma MHCII would act as a decoy to engage and stall CD4⁺ T cells, stopping the prevention of CD8⁺ T cell dysfunction, leading to loss of tumor control. Nevertheless, although SIINFEKL cells grew slower *in vivo* due to the immune control, I-A-expressing SIINFEKL tumors did not escape immune surveillance and still grew slower (**Figure. 31B**).

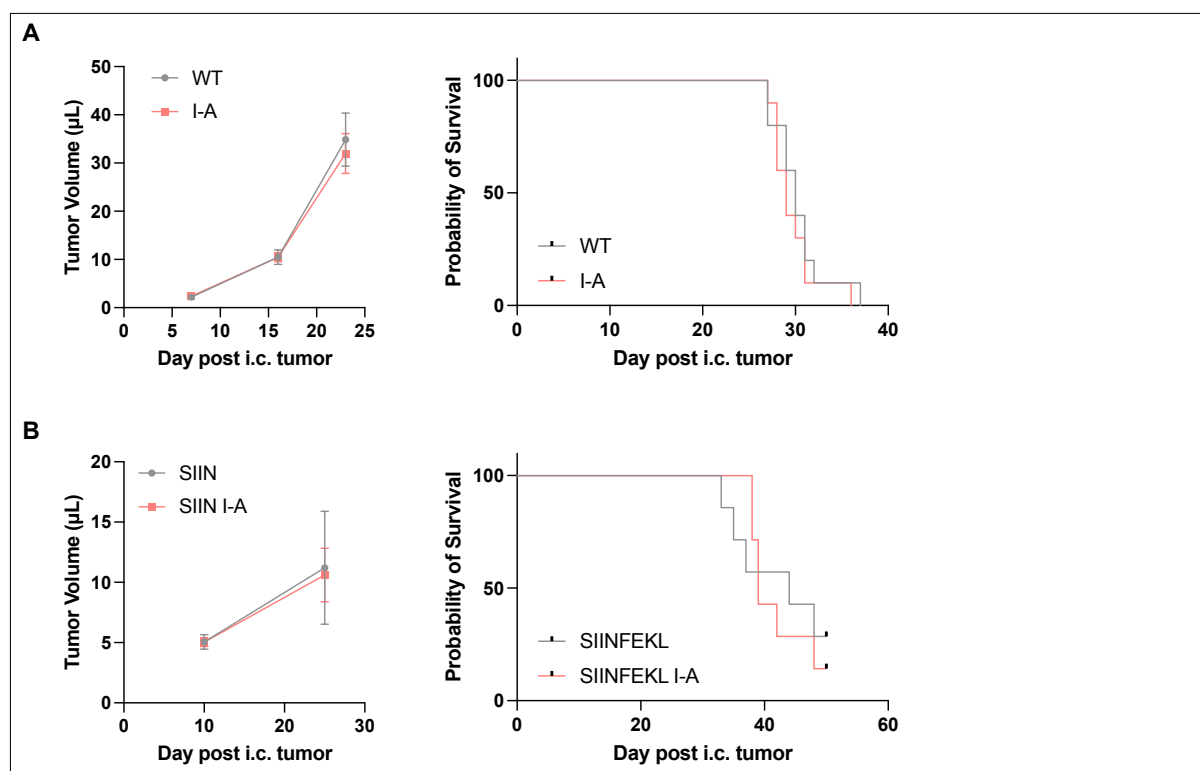


Figure 31: Glioma MHCII expression impacts in *in vivo* mouse models

A. C57BL/6 mice i.c. orthotopically inoculated with WT GL261 and I-A-expressing GL261 cells. **B.** C57BL/6 mice i.c. orthotopically inoculated with GL261 SIINFEKL and I-A-expressing GL261 SIINFEKL cells. Tumor growth curves were analyzed with nonlinear regression, and survival analyses were conducted with Log-rank test.

Despite no preclinical phenotype difference, the immune microenvironment was profiled to validate the molecular analysis results (**Figure. 29B-F**). With glioma MHCII expression, it was found that more CD4⁺ T cells were present while CD8⁺ T cells only showed marginal increase (**Figure 32A**), partly in consistence with the human data (**Figure. 29C&D**). Moreover, no difference in activation, exhaustion/dysfunction, and stemness was observed in CD4⁺ T cells while CD8⁺ T cells were less proliferative in MHCII⁺ gliomas (**Figure. 32B&C**). As mentioned, MHCII-CD4⁺ T cell interaction results in CD4⁺ T cell differentiation into various subsets (see **1.5 Tumoral MHCII expression and therapy efficacy**); therefore, CD4⁺ T cell differentiation was evaluated, and only the master regulator T-BET frequency was marginally decreased in CD4⁺ T cells in I-A-expressing gliomas (**Figure. 32D**). Besides T cells, innate immune cells were assessed, and macrophage cell numbers were increased in I-A-expressing gliomas while microglia cell numbers remained unchanged in concordance with the human

results (**Figure. 29E & 32E**). Together, these data partly recapitulate the findings in human gliomas, suggesting that glioma MHCII indeed leads to more T cell and macrophage infiltration, yet the functional alterations of the effector cells require further detailing.

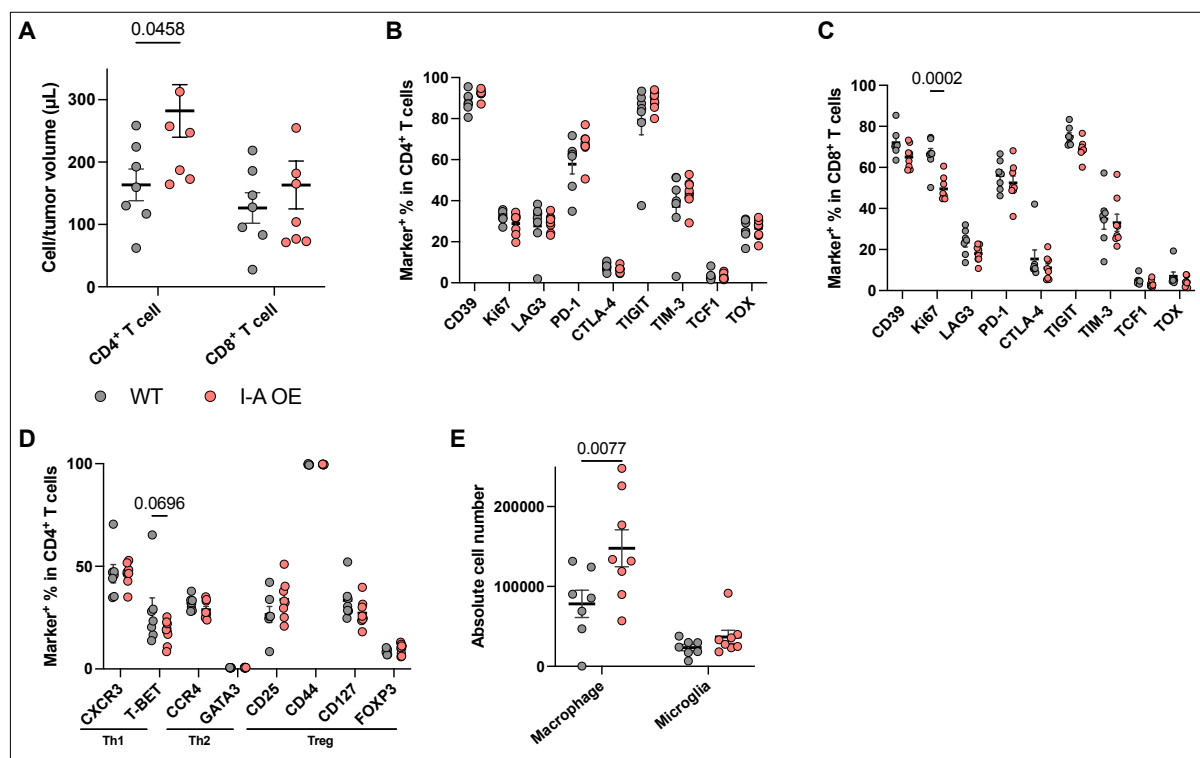


Figure 32: Immune microenvironment alteration in I-A-expressing gliomas

A. CD4⁺ and CD8⁺ T cell numbers in the TME in WT and I-A-expressing GL261 tumors from **Figure. 31A**. **B&C.** Marker-positive frequencies in CD4⁺ and CD8⁺ T cells from **(A)**. CD39 denotes TILs and also exhaustion. Ki67 is a proliferative marker. LAG3, PD-1, CTLA-4, TIGIT, and TIM-3 are exhaustion markers. TCF1 is a T cell stemness marker. TOX is a T cell dysfunction marker. **D.** Differentiation of CD4⁺ T cells from **(A)**. **E.** Macrophage and microglia cell numbers in the TME. All were analyzed with two-way ANOVA multiple comparison corrected with Holm-Šidák method.

2.3.5 Glioma MHCII induces immune checkpoint molecules intrinsically and extrinsically and expands but exhausts reactive T cells

In order to understand the functional consequences of glioma MHCII, an *in vitro* coculture assay was set up with established cell lines (**Figure. 30**), cognate OVA peptide (and control MOG peptide), and OTII T cells (**Figure. 33A**). The impacts on tumor cells were first examined. With the cognate OVA peptide loaded on glioma MHCII, tumor cells were not killed by antigen-reactive T cells (**Figure. 33B**). Strikingly, OVA-loaded I-A-expressing tumor cells were further stimulated to express more MHC upon contact with the antigen-reactive T cells (**Figure. 33C**). As observed before (**Figure. 30E**), I-A expression already resulted in increased PD-L1 expression, and with interaction with antigen-reactive T cells, the expression was further exacerbated (**Figure. 33D**), indicating that MHCII intracellular signaling is present in tumor cell and is further exaggerated upon TCR-MHC interaction.

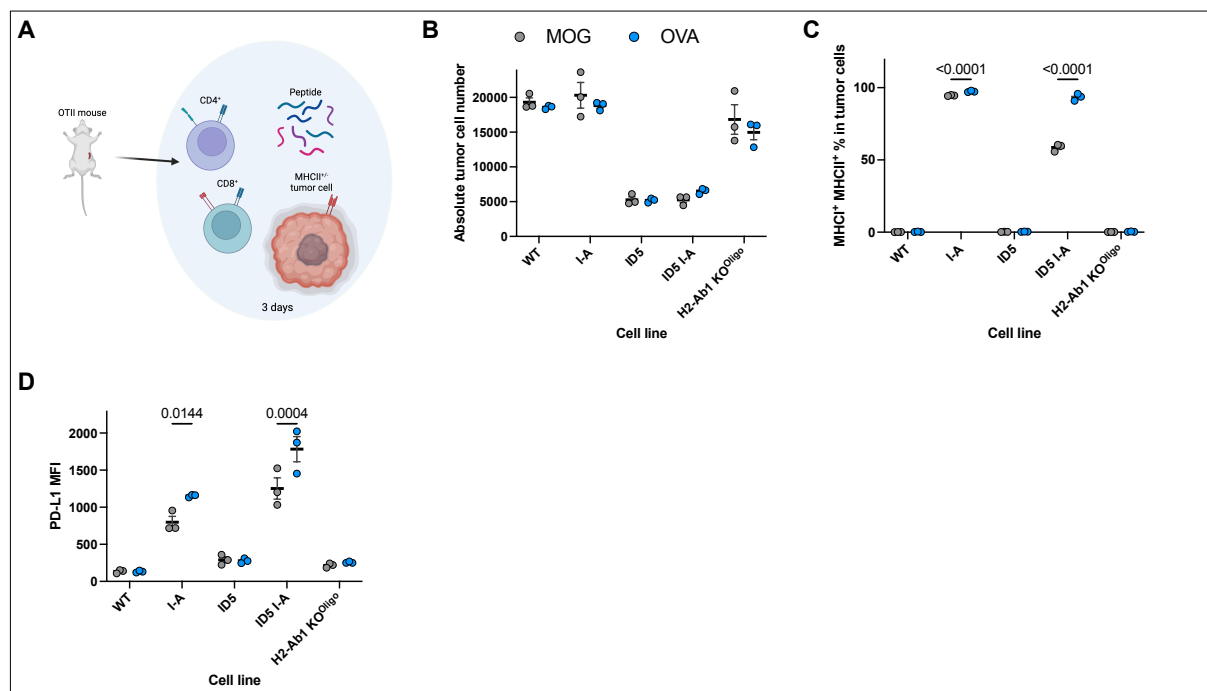


Figure 33: Glioma MHCII expression functional effects on tumor cells

A. Coculture setup with OTII T cells and established cell lines loaded with cognate or control peptide. **B.** Tumor cell number after 3 days of coculture with the peptides and OTII T cells. **C.** MHCII and MHCII double-positive cell frequency upon coculture. **D.** PD-L1 expression levels after coculture. **(B)-(D)** were analyzed with two-way ANOVA multiple comparison corrected with Holm-Šidák method.

Results

T cells in the coculture were also characterized (**Figure. 33A**). CD4⁺ T cell numbers were increased upon contact with OVA-loaded I-A-expressing cells due to proliferation (**Figure. 34A&B**). Exhaustion markers in T cells were evaluated, including PD-1, CTLA-4, LAG3, and TIGIT, and their frequencies in CD4⁺ T cells were all elevated when the cognate peptide OVA and glioma MHCII were present in the culture (**Figure. 34C-F**). In contrary to *in vivo* results, CD4⁺ T cell differentiation was affected upon encounter with OVA-glioma MHCII; specifically, differentiation into Th1, Th2, and Treg subsets was promoted (**Figure. 34G-I**).

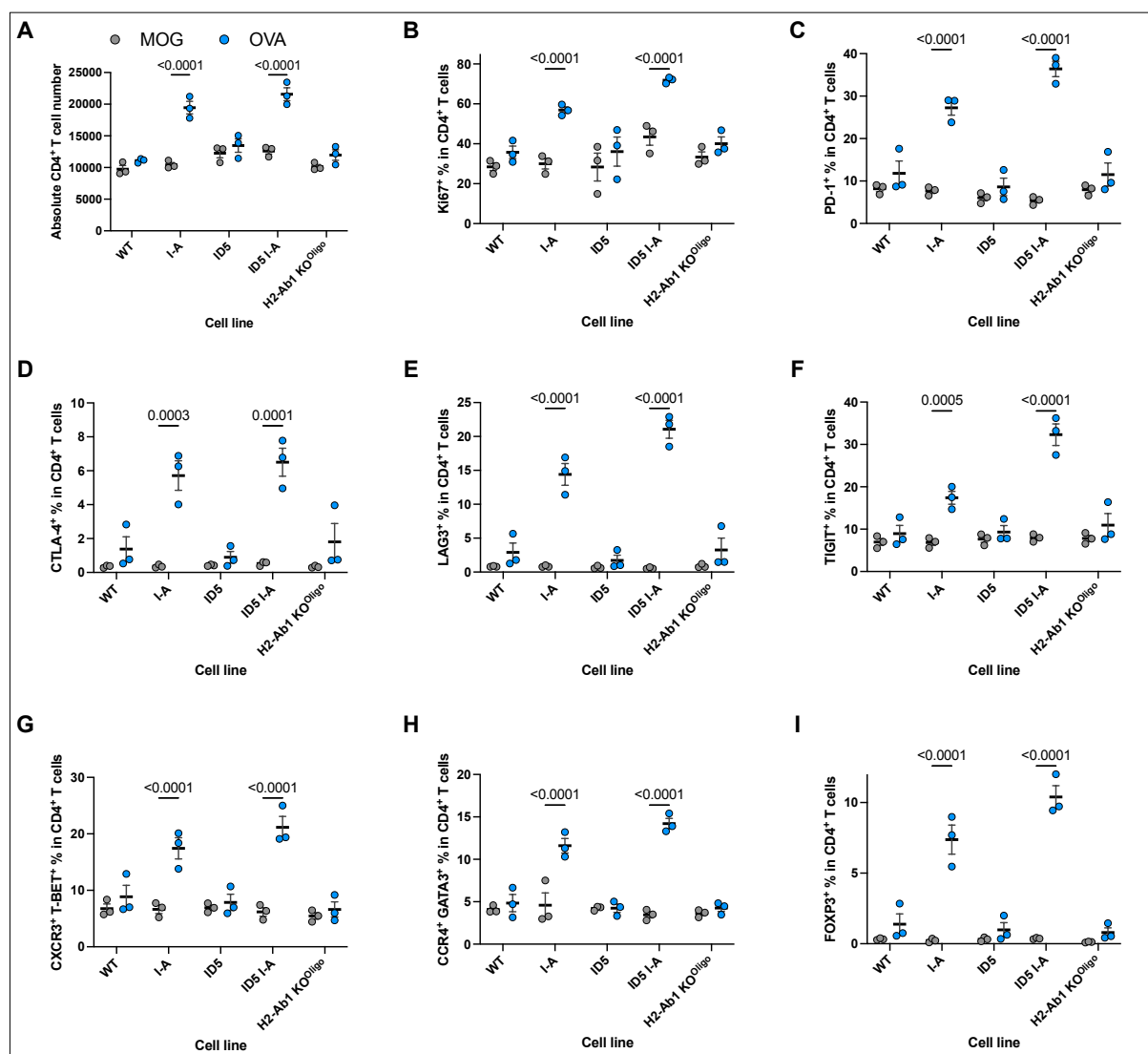


Figure 34: Glioma MHCII expression functional effects on CD4⁺ T cells

A. CD4⁺ T cell number after 3 days of coculture with peptides and established cell lines. **B.** Ki67-positive frequency of CD4⁺ T cell upon coculture. **C-F.** Exhaustion marker (PD-1, CTLA-4, LAG3, and TIGIT)-positive CD4⁺ T cell frequencies after coculture. **G-I.** CD4⁺ T cell subset (Th1, Th2, and Treg)

frequencies upon coculture. All were analyzed with two-way ANOVA multiple comparison corrected with Holm-Šidák method.

On the other hand, OTII CD8⁺ T cells that carried the antigen-reactive TCR but lacked the co-receptor CD4 were also in the culture and assessed. Unlike OTII CD4⁺ T cells, the CD8⁺ T cell did not increase in number nor change in proliferative capacity upon contact with the cognate peptide OVA and MHCII (**Figure. 35A&B**). Nevertheless, similar to CD4⁺ T cells, exhausted CD8⁺ T cell frequencies were increased after encountering OVA-MHCII (**Figure. 35C-E**).

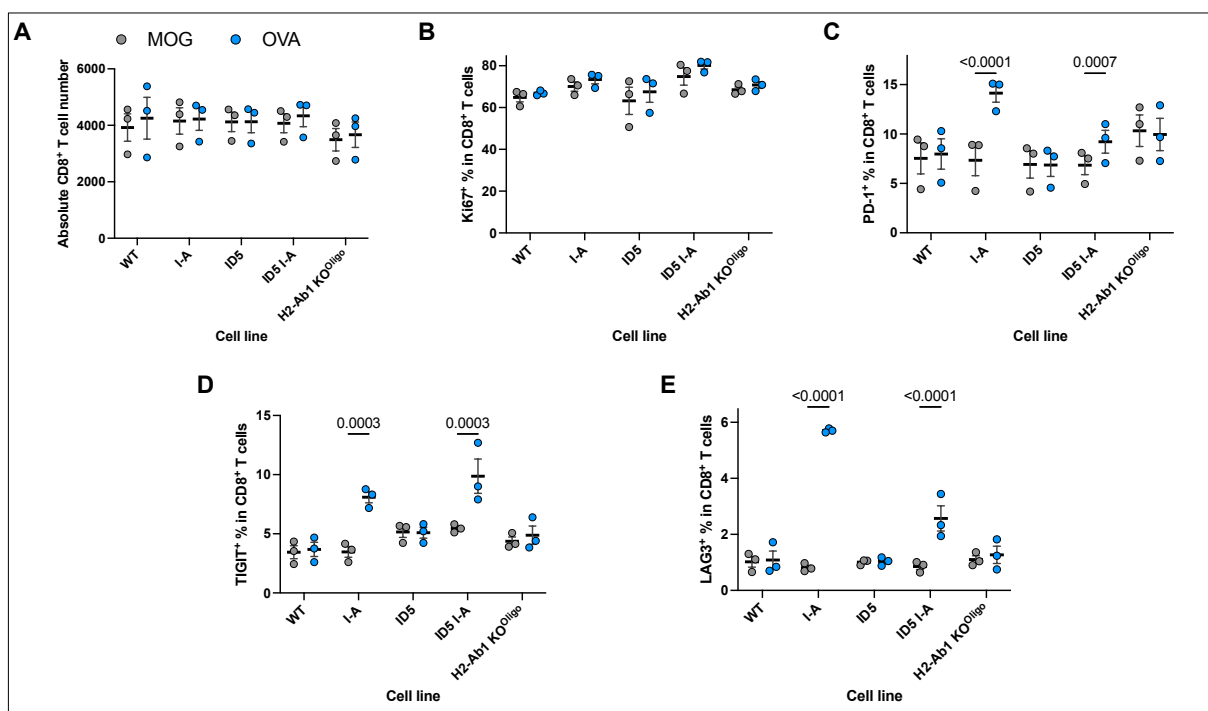


Figure 35: Glioma MHCII expression functional effects on CD8⁺ T cells

A. CD8⁺ T cell number after 3 days of coculture with peptides and established cell lines. **B.** Ki67-positive frequency of CD8⁺ T cell upon coculture. **C-E.** Exhaustion marker (PD-1, TIGIT, and LAG3)-positive CD8⁺ T cell frequencies after coculture. All were analyzed with two-way ANOVA multiple comparison corrected with Holm-Šidák method.

Results

As mentioned in **1.5 Tumoral MHCII expression and therapy efficacy**, MHCII intracellular signaling could result in cell death. Since CD4-TCR interaction with glioma MHCII did not lead to cytotoxicity, an anti-I-A antibody was employed to investigate MHCII signaling-mediated cell death in glioma cells. Nonetheless, with the antibody in culture for 24 hours, no significant cell death was observed in I-A expressing cells (**Figure. 36A**), even when further stimulated with IFN γ (**Figure. 36B**). Collectively, these data infer that glioma MHCII functions intrinsically and extrinsically to favor tumor cell by upregulating PD-L1 expression and exhausting, though proliferating, antigen-reactive T cells.

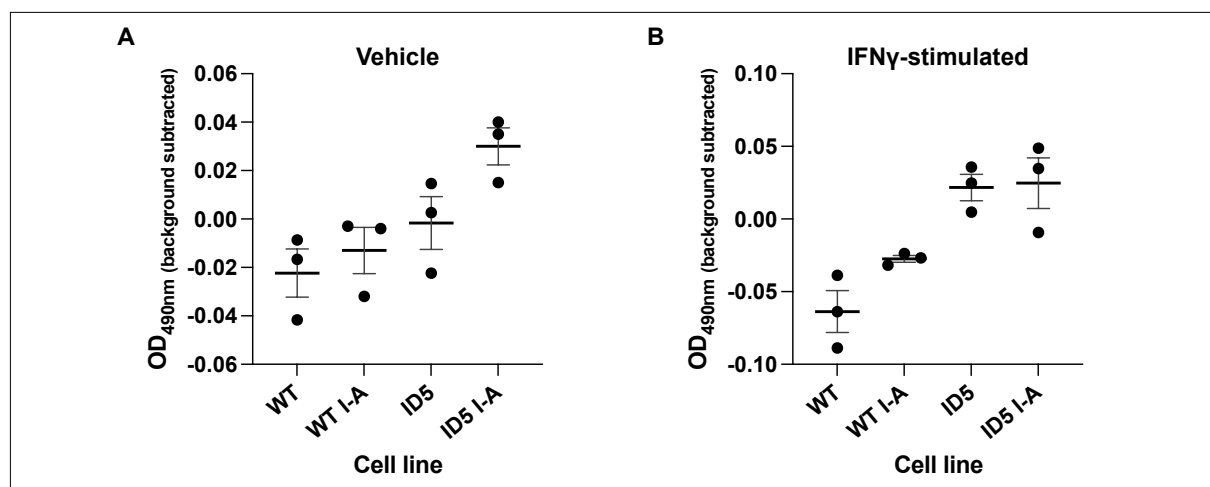


Figure 36: MHCII intracellular signaling-directed cell death

A. Unstimulated GL261 cell lines cultured with anti-I-A antibody for 24 hours. **B.** IFN γ -stimulated cell lines cultured with anti-I-A antibody for 24 hours. All were analyzed with one-way ANOVA multiple comparison corrected with Holm-Šidák method.

2.3.6 Glioma MHCII does not impact immunotherapy efficacy

In other cancer types, tumoral MHCII was found to be indicative of immunotherapy efficacy (see **1.5 Tumoral MHCII expression and therapy efficacy**), likely due to the alteration of immune microenvironment influenced by tumoral MHCII expression (**Figure. 32-35**). Since glioma MHCII led to PD-L1 upregulation, decreased CD8⁺ T cell proliferation, and T cell exhaustion (**Figure. 32C, 33D, 34 & 35**), different immunotherapy modalities were exploited. To counteract PD-L1 expression and T cell exhaustion, triple ICB (anti-PD-L1, anti-PD-1, and anti-CTLA-4) was administered; however, ICB therapeutic efficacy was so potent that all the treated mice experienced strong tumor regression except one I-A expressing tumor-bearing mouse, which experienced tumor recurrence (**Figure. 37A**). On the other hand, it was shown that MHCII⁺ glioma patients deceased earlier than those MHCII⁻, especially in IDH mutants (**Figure. 29A**); the outcome could not be recapitulated in the murine glioma model (**Figure. 37B**). The IDH1R132H mutation affects both innate and adaptive immune cells in the TME but can be targeted with vaccine therapy (Bunse et al., 2018; Friedrich et al., 2021; Platten et al., 2021; Schumacher et al., 2014). It was speculated that MHCII⁺ IDH1R132H gliomas would respond less effectively due to increased exhaustion in the milieu, yet no therapeutic efficacy was observed (**Figure. 37C&D**). Lastly, cell therapy with antigen-reactive CD4⁺ T cells was attempted, but again, no therapeutic efficacy was observed (**Figure. 37E**). In summary, the results indicate that glioma MHCII expression does not impact immunotherapy efficacy, but further explorations and validations are necessary with optimized immunotherapies in immunocompetent syngeneic murine models.

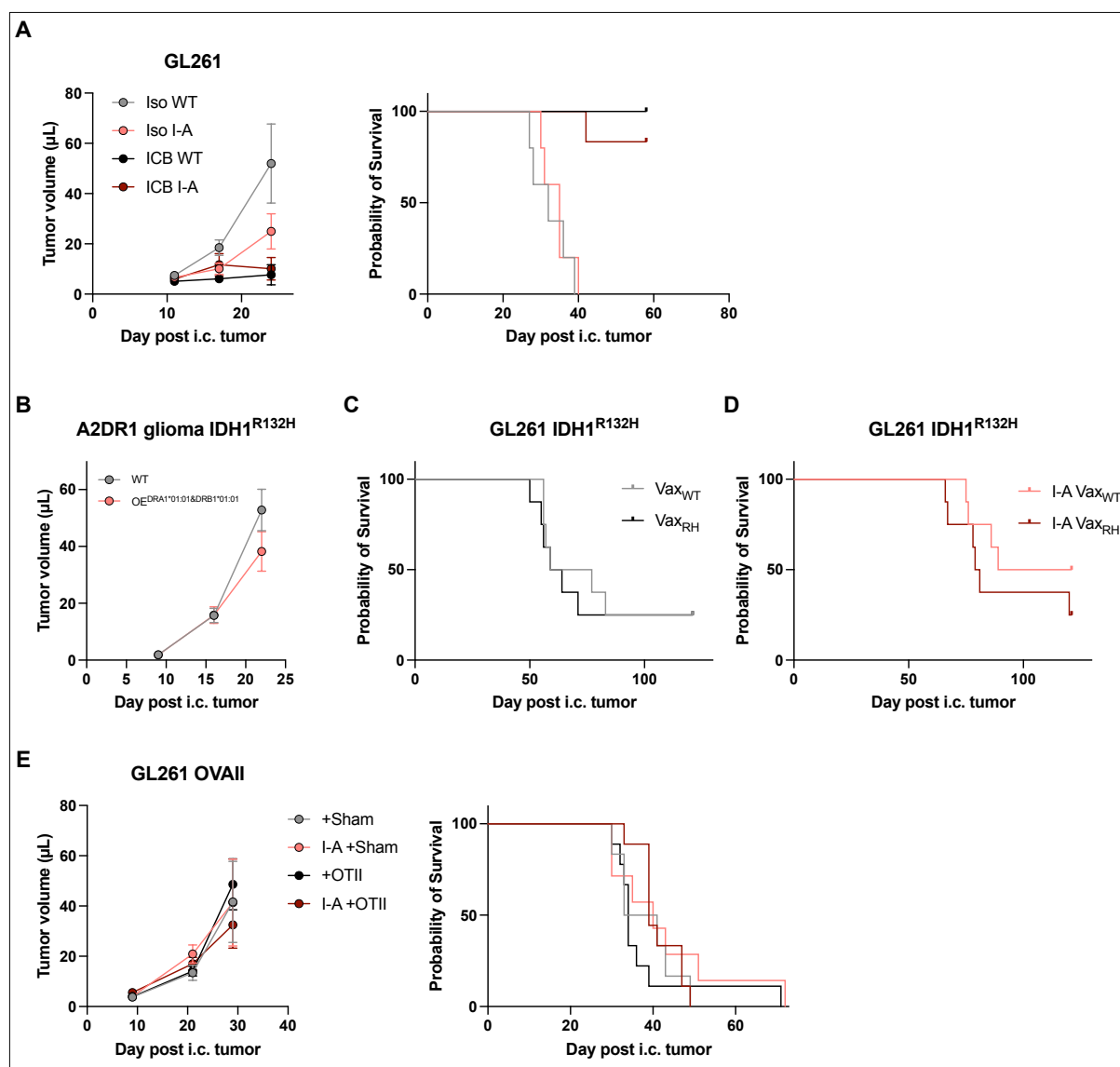


Figure 37: Glioma MHCII expression effects on immunotherapy efficacy

A. Triple ICB therapy on C57BL/6 mice i.c. orthotopically inoculated with WT GL261 and I-A-expressing GL261 cells. **B.** A2.DR1 mice i.c. orthotopically inoculated with the A2.DR1 glioma cell line with or without overexpression of human MHCII. **C.** Vaccination therapy on C57BL/6 mice i.c. orthotopically inoculated with GL261 carrying IDH1R132H. **D.** Vaccination therapy on C57BL/6 mice i.c. orthotopically inoculated with I-A-expressing GL261 carrying IDH1R132H. **E.** Cell therapy with OTII CD4⁺ T cells on C57BL/6 mice i.c. orthotopically inoculated with OVA-expressing GL261 cells. Tumor growth curves were analyzed with nonlinear regression, and survival analyses were conducted with Log-rank test.

3 Discussion

MHC-dependent therapy potential against cancers has not been fully unleashed in solid tumors, especially in brain tumors, largely due to the efforts required in antigen identification and the significant validation and safety profiling needed in TCR discovery (Bunse et al., 2022). Although MHC dependency is a restriction, it also broadens the availability of targetable antigens as long as they are processed and presented on MHC (Rosenberg and Restifo, 2015). Conventionally, researchers focused on identifying and targeting TSAs or tumor-testis antigens (TTAs) to avoid safety concerns regarding on-target, off-tumor reactivity (Baulu et al., 2023). However, this strategy is not as applicable for cancers harboring a low mutation burden, such as brain tumors (Yarchoan et al., 2017); therefore, here in this study, in order to act against brain tumors, TAAs were emphasized, and efforts were made to discover and validate their corresponding TCRs with various models and animal strains. Additional work was carried out to evidence tumoral MHCII expression in gliomas and to elucidate its effects on the TME and therapy efficacy.

To further advance MHC-dependent immunotherapy in gliomas, the following aspects should be noted:

3.1 Phase I clinical trial with the discovered PTPRZ1¹⁸¹⁴⁻¹⁸²² TCR and further discovery of PTPRZ1-reactive receptors

PTPRZ1 is essential during neurodevelopment but not in adults (Eill et al., 2020; Johnson and Vactor, 2003); intriguingly, its expression re-emerges and is required for gliomagenesis and tumor progression, but the underlying mode of action remains mysterious (Bourgonje et al., 2014; E et al., 2016; Lacore et al., 2022; Qin et al., 2017; Ulbricht et al., 2006). Targeting PTPRZ1 to combat GB is fundamentally reasonable as it contributes to tumorigenesis, and if the tumor attempts to escape therapeutic interventions by downregulating PTPRZ1 expression, the cost is losing disease malignancy. Since the identified PTPRZ1¹⁸¹⁴⁻¹⁸²² TCR shows strong potency in controlling experimental brain tumors and universal cytotoxicity to all HLA-A*02⁺ primary GB cell lines, a phase I clinical trial is in preparation, named Intraventricular T cell receptor transgenic T cell therapy to treat glioblastoma (INVENT4GB) (Bunse et al., 2023). In the trial, the feasibility and safety of TCR-T cell therapy using PTPRZ1¹⁸¹⁴⁻¹⁸²² TCR to treat recurrent GB will be assessed with i.v. and i.c.v. ACT

routes, and the maximum tolerated dosage will be evaluated. Although the TCR was only tested with cell lines established from primary GB, it is expected to react to HLA-A*02⁺ recurrent GB as no difference in PTPRZ1 expression was observed comparing primary with recurrent GB samples (**Figure. 7A&B**). The trial will mark the first-in-human TCR-T cell therapy against GB. In parallel, further interrogation and engineering of the TCR are required.

The TCR *in vitro* controls primary HLA-A*02⁺ GB cell lines, yet when applied to *in vivo* therapy with PDX models, no therapeutic efficacy is present unless additional intervention is combined (**Figure. 21**). Further experiments are necessary to quantify PTPRZ1 expression in PDX tumors and to identify if transferred T cells persist in the TME. As previously reported and shown in scRNA-seq data (see **1.3.1 GB-associated antigen and GB stem cell marker: PTPRZ1, Figure. 8E&J**), PTPRZ1 is a GB stem cell marker. Primary cells may differentiate *in vivo* in the brain microenvironment, generating differentiated malignant cells that are less PTPRZ1-upregulated, leaving a subset of PTPRZ1-prominent cancer stem cells. Combinatorial therapy with irradiation may be efficacious due to radiotherapy-induced elimination of differentiated fast-cycling cells that do not elicit PTPRZ1¹⁸¹⁴⁻¹⁸²² TCR-T cell activation, leaving radiotherapy-resistant cancer stem cells to be targeted by the PTPRZ1¹⁸¹⁴⁻¹⁸²² TCR-T cell (**Figure. 21D**). Another hypothesis is that in solid tumors, for ACT to work, reactive CD8⁺ T cell exhaustion/dysfunction must be prevented or reversed by interacting with APCs and reactive CD4⁺ T cells forming an immune triad, which licenses CD8⁺ T cells to kill (Espinosa-Carrasco et al., 2024); in the U87 TMG model, as the epitope is artificially overexpressed, CD4⁺ PTPRZ1¹⁸¹⁴⁻¹⁸²² TCR-T cells can be activated without the need for the co-receptor CD8, hijacking U87 TMG cells to form immune triads with CD8⁺ PTPRZ1¹⁸¹⁴⁻¹⁸²² TCR-T cells. On the contrary, in PDX models, the endogenously upregulated levels of PTPRZ1 can only lead to CD8⁺ PTPRZ1¹⁸¹⁴⁻¹⁸²² TCR-T cell activation but not CD4⁺ T cells. One way to force CD4⁺ PTPRZ1¹⁸¹⁴⁻¹⁸²² TCR-T cells to recognize and get activated by primary GB cells is introducing the co-receptor CD8. Another way is to identify a CD4-restricted PTPRZ1-reactive TCR; in the GAPVAC-101 trial, an MHCII epitope of PTPRZ1, PTP-010, was used and elicited immunogenicity in 50% of vaccinated patients (Hilf et al., 2018). The same workflow can be applied to isolate and identify PTP-010-MHCII reactive CD4⁺ T cells, but for

validation, an immunocompetent model with human MHC is needed so that the generated CD4⁺ TCR-T cells can function through MHCII⁺ APCs.

The identified TCR is HLA-A*0201-restricted. To expand the coverage of patients, TCRs targeting PTPRZ1 via other HLA should be developed. HLA-A*0201 is frequent in Europe, around 50% of the population carrying at least one allele while in South East Asia, only approximately 10% of the population is expected to carry at least one allele (Chang et al., 2013). Another common HLA is HLA-A*2402, which is present in roughly 50% of the population in South East Asia and East Asia but only around 20% in Europe (Chang et al., 2013; Park et al., 2016). The GAPVAC-101 trial also included a peptide of PTPRZ1, PTP-018, that is HLA-A*2402-restricted, but it only elicited immunogenicity in one out of two patients (Hilf et al., 2018). Efforts should be made to discover the T cells responsible for the vaccine-induced T cell response and examine the discovered TCR therapeutic potency.

In addition, many AI-facilitated tools are under development to reveal TCR motifs essential for reactivity against peptide-MHC (Sidhom et al., 2021). One can also optimize identified antigen-reactive TCRs with AI-selected TCR variants with, for example, TCR suite from Ardigen. Furthermore, trained with hundreds of millions of TCR sequences, AI can be generative and yield *de novo* TCRs (Leary et al., 2024), a similar concept to the currently most advanced generative AI chatbot ChatGPT. Nonetheless, these tools still lack practical laboratory validation, and extensive examination and toxicity evaluation of the engineered/generated TCRs are essential prior to further therapeutic usage.

PTPRZ1, a transmembrane receptor, can be targeted in principle with CAR instead of TCR. As studied by others, phage display library-derived PTPRZ1-reactive scFvs were identified and shown to be therapeutic in treating primary cell lines overexpressing truncated PTPRZ1 (Bedoya et al., 2023). More validation still is necessary to demonstrate its efficacy on primary GB cell lines with endogenously upregulated levels of PTPRZ1. Another crucial aspect to consider is surface protein glycosylation, which is often aberrant in cancers, including GB (Rosa-Fernandes et al., 2022; Tokumura et al., 2024). As CAR-T cell therapy is affected by protein glycosylation (Heard et al., 2022), whether the epitope of the developed PTPRZ1 CAR is masked or not needs further assessment.

3.2 Routes for adoptive cell transfer for brain tumors

Besides the cell product, the route to deliver effector cells is of importance as well. The brain is immune-privileged, specially protected by the BBB, featured by endothelial tight junctions and the additional ensheathment of astrocyte processes, which allows only small molecules crossing and not macromolecules (Daneman, 2012; Daneman and Prat, 2015), let alone cells. In disease states, for instance in Alzheimer's disease, disrupted BBB was observed and led to edema, immune cell infiltration, and imbalanced ionic homeostasis. In brain tumors, BBB leakage is heterogenous and often occurs in the core of the tumor, characterized by reduced tight junctions (Mo et al., 2021). In healthy states, some parts of the brain may allow immune cell trafficking, including the choroid plexus, which is a source for cerebral spinal fluid (CSF) and is only compartmentalized with endothelial cells and extracellular stroma but no astrocyte ensheathment (Meeker et al., 2012). Therefore, i.v. administration of therapeutic cell products still was considered to treat GB. However, few to no clinical benefits were shown with such a route to deliver effector cells despite preclinical data suggesting that i.v. route administration is applicable and beneficial (Ahmed et al., 2017; Bagley et al., 2024a; Li et al., 2024). In line with the clinical results, PTPRZ1¹⁸¹⁴⁻¹⁸²² TCR-T cells only show marginal i.c. tumor control when delivered i.v. (**Figure. 17A&B**). Further assays are necessary to reveal whether transferred cell product reaches the brain TME through BBB leakage or choroid plexus.

Recent studies have refocused on a kind of specialized endothelia, high endothelial venules (HEVs), which were first described a hundred years ago and function to facilitate lymphocyte extravasation (Blanchard and Girard, 2021; Girard and Springer, 1995). HEVs are present in lymphoid organs except for the spleen and can be found in non-lymphoid tissues too, especially in chronic inflammatory diseases. For lymphocytes to transmigrate across HEVs, briefly, L-Selectin (CD62L) binds to proteoglycan ligands on HEVs, and later, other receptors bind to ICAM-1 on HEVs to facilitate complete extravasation. During inflammatory state, molecules involved in lymphocyte recruitment and transmigration are upregulated (Veerman et al., 2019). In cancer, HEVs are associated with immune cell infiltration and favorable clinical prognosis (Martinet et al., 2011; Martinet et al., 2012). Moreover, they mediate ICB therapy efficacy as the treatment increases HEV abundance in the tumor, which facilitates more immune cell infiltration (Asrir et al., 2022). In GB, tertiary lymphoid

structures were observed in treatment-naïve and treatment-administered animals, composed of HEVs which correlated with T cell infiltration (van de Walle et al., 2021; van Hooren et al., 2021). With further targeted AAV-facilitated modification, HEVs in GB could be induced and activated to recruit immune cells and promote APC-T cell interaction locally (Ramachandran et al., 2023). Furthermore, it was identified that around the arteries and vessels in the brain, a 5-mm niche is present, termed Virchow Robin space (Reith and Haußmann, 2018). It was first reported 150 years ago and functions for the drainage of interstitial fluid into CSF, and later into lymphatic vessels ending up in cervical lymph nodes (Riba et al., 2019). It remains to be elucidated whether tumor-reactive T cells can enter brain parenchyma through lymphatic system and passing through Virchow Robin space, or directly transmigrate HEVs in the TME. On the other hand, locoregional delivery of effector cells is explored in GB, and therapeutic efficacy was demonstrated preclinically with peri-tumoral and i.cv. administration (Bedoya et al., 2023; Li et al., 2024; Wang et al., 2023), and clinically with i.cv. and intrathecal delivery (Brown et al., 2015; Brown et al., 2024; Choi et al., 2024). This allows effector cells to be in close proximity to the tumor site without the need of trafficking systemically, and to expand in the ventricular space, avoiding the immunosuppressive TME (see **1.2 Immunotherapy for brain tumors**).

3.3 Cell therapy with further equipped cell products or other effector cells

While identification of cancer-reactive receptors is important, arming and engineering cell products to traffick, function, and maintain effective in solid tumor immunosuppressive microenvironment is equally crucial. As solid tumors often make infiltrated T cells dysfunctional and exhausted (Scott et al., 2019), researchers have strived to alter the TME or further equip effector cells.

CAR-T cell development is well-advanced, and 4th generation CAR-T cells are under extensive development, in which cell products are further armed with various cytokines or chemokines for potency/persistence (IL-2, IL-7, IL-15, IL-21, and IL-23), trafficking (IL-7 and CCL19), microenvironment alteration (IL-12, IL-18, and IL-36), reprogrammed metabolism (IL-10), and antigen spreading promotion (FLT3L) (Tang et al., 2023). Additionally, non-cytokine non-chemokine 4th generation CAR-T cells are

well developed. CAR-T cells co-expressing ICB antibodies, co-stimulatory receptors, extracellular matrix remodeling enzymes, and stemness-maintaining transcription factors were explored. As mentioned, CAR-T cells secreting EGFR engager were attempted to facilitate host bystander T cells recognizing tumors and showed clinical benefits (Choi et al., 2024). The same strategy can be applied to TCR-T cells.

Besides modifying receptor-equipped conventional α/β T cells, other immune effector cells, including NK cells, macrophages and γ/δ T cells, have been engineered with tumor-reactive receptors. These effectors harbor their spontaneous programs to eradicate foreign and malignant cells: NK cells can clear out non-self and non-MHC-expressing cells and stimulate neighboring immune cells with IFN γ secretion (Chu et al., 2022), and allogenic and autologous NK cell transfer has been applied to treat cancer patients (Myers and Miller, 2020); macrophages have the ability to phagocytose target cells, remodel the microenvironment, and present antigens to T cells (Mantovani et al., 2022), and the engineered cell product of it has been used to treat GB patients, activating local immune cells with IFN α secretion in the TME (Finocchiaro et al., 2021); γ/δ T cells have, in recent years, gained more and more interest in cancer immunotherapy as their invariant TCRs recognize, instead of peptide antigen-MHC, lipid antigens on CD1 molecules and phospho-antigens through BTN proteins (Gully et al., 2021). Moreover, γ/δ T cell can be activated through innate receptors similar to those on NK cells, including NKG2D and NKp-46, while devoid of innate inhibitory receptors, KIRs (Mensurado et al., 2023). *In vitro* expansion of γ/δ T cells is thoroughly optimized (Aehnlich et al., 2020; Verkerk et al., 2024), and the expanded cells have been utilized in cell therapy (Knowles et al., 2022; Xu et al., 2020). Using their natural tumor-recognizing machinery with the addition of CAR-directed cancer killing, several preclinical models have demonstrated promising outcomes (Klichinsky et al., 2020; Liu et al., 2020; Wang et al., 2023), and several clinical trials have been conducted to evaluate CAR-engineered NK cell (Wang et al., 2024), macrophage (Reiss et al., 2022), and γ/δ T cell treatments (NCT04107142). One caveat is that these immune cells require more laborious efforts in differentiation and/or expansion, unlike α/β T cells, whose activation and expansion protocol is well-tested and streamlined with plenty of commercial kits available.

The above further modifications on T cells or receptor-equipped effector cells may be even more necessary in treating brain malignancies than other solid tumors as the

brain TME is known to be highly immunosuppressive (Bausart et al., 2022). PTPRZ1-reactive TCR should be explored with further arming of cytokines and chemokines and tested for its potency when equipped on other effector cells that are not α/β T cells.

3.4 Antigen-reactive TCR discovery platforms

As CAR development is confined to cell surface proteins, TCRs may bring cell therapy into another era in which all proteins are targetable when the tumor is not MHC-deficient and as long as the antigen processing/presentation machinery is intact. While most researchers focus on targeting neoantigens, brain tumors often harbor relatively lower mutation burden without obvious driver mutations in the majority, forcing emphasis rather on targeting CAAs. In this and previous work (Boschert et al., 2024; Krämer et al., 2024; Lindner, 2023), antigen-reactive TCRs were derived from immunized patients from vaccine therapy trials, but human materials, especially the ones vaccinated with specific antigens of interest, are not always attainable. Therefore, other means are sought.

By straightforward engraftment of human PBMCs into immunodeficient NSG mice, although the method is simple and the material is ample, most of the immune cell populations become undetectable after 2 weeks, leaving only T cells to expand and to later develop graft-versus-host disease (GvHD) (Brehm et al., 2019). A modified mouse strain was developed using NSG mice with murine MHC KO, also used in this study (**Figure. 16, 17&18**), with greatly reduced rate of GvHD upon PBMC transfer (Yarchoan et al., 2017). However, they both cannot retain APCs in the host mice and thereby cannot facilitate HLA-based T cell education *in vivo* (Chuprin et al., 2023). Subsequently, engraftment using CD34⁺ hematopoietic stem cells was established, and thymopoiesis and T cell selection could be partly recapitulated (Tang et al., 2019; Tong et al., 2020). A latest model with CD34⁺ cell engraftment combined with hormone conditioning could even draw COVID vaccine-induced B cell responses (Chupp et al., 2024). Transferring CD34⁺ cells broadens potential T cell responses as donors of various HLA types can be employed for distinct antigens of interest. Nevertheless, isolation and enrichment of hematopoietic stem cells is costly and laborious.

Transgenic human HLA mouse strains were generated to circumvent this obstacle. As used here, A2.DR1 mice carry human common HLAs, devoid of murine MHC, and are

already employed for TCR discovery for antigens of interest (Kilian et al., 2022). Nevertheless, the generated TCR is still murine, recognizing human peptide-HLA, with undefined cross-reactivity against other HLAs. Another advanced transgenic mouse strain further engineered with human TCR $\alpha\beta$ genes, CD4, and CD8 $\alpha\beta$ genes, VelociT mouse, was developed and able to generate therapeutic antigen-specific TCRs (Moore et al., 2021). With transgenic mouse strains, it is not as flexible to cover a wide breadth of HLAs.

Besides *in vivo* educating and expanding rare antigen-specific T cells, experimenters have attempted to perform it *in vitro*. Here an *in vitro* antigen-specific T cell expansion protocol was probed using PBMCs with the first day to differentiate APCs, followed by eight days of stimulation with specific peptide and maintenance with necessary cytokines (Bozkus et al., 2021), yet no apparent reactive T cell population was induced (**Figure. 27**). This might be due to too short period of expansion and too few starting materials for the rare reactive T cells. Other methods have used a large number of cells with pre-differentiated DCs, combined with tetramer sorting to identify a therapeutic TCR from healthy donors (Giannakopoulou et al., 2023), and engineered APCs expressing additional cytokines and co-stimulatory ligands to reverse and expand heavily dysfunctional and exhausted T cells in an antigen-dependent manner, and have the TCRs assayed for downstream cell therapy potency evaluation (Arnaud et al., 2021). These methods allow TCR discovery for various HLAs for antigens of interest without usage of *in vivo* hosts but lack reproducibility by others.

3.5 Models for brain tumor immunotherapy

“All models are wrong, but some are useful,” as George E.P. Box stated. It is undoubtedly challenging to recapitulate a disease covering all aspects ranging from tumor heterogeneity to the influenced microenvironment. In order to examine immunotherapy, appropriate tumor models need to be established. Several glioblastoma models have been generated with different features (Haddad et al., 2021): GL261 is commonly used in immunocompetent mice but grows bulky and is highly immunogenic relative to human GB; CT-2A cells are also frequently used and harbor a rather immunosuppressive microenvironment; SB28 cells are least employed in research but are poorly immunogenic and more closely representing human GB.

With the above models, immunotherapy can be interrogated in immunocompetent setting. As shown by others and here, ICB can be explored with the GL261 GB model (**Figure. 37A**) (Aslan et al., 2020). However, with GL261, vaccine and cell therapies cannot be applied (**Figure. 37C-E**). Further experiments are required to elucidate whether immune triads in the GB microenvironment are essential for immunotherapy efficacy (Espinosa-Carrasco et al., 2024), implicating the modification of therapies including vaccination targeting both MHC I and MHC II antigens and adoptive cell transfer of both reactive CD4⁺ and CD8⁺ T cells. Of note, TCR affinity can alter the course of T cell differentiation; therefore, choosing an appropriate-affinity TCR is crucial to avoid transferred T cells ending up playing an immunosuppressive or tumor-promoting role (Thaxton and Li, 2014). In addition, OVA model antigen interaction with OTI and OTII TCRs is high-affinity; MISTIC mice carrying a TCR targeting spontaneous Imp3 mutation serve as an alternative (Schaeffler et al., 2023). Current models used here have failed to demonstrate therapeutic efficacy on murine GB models except for ICB. Before further testing tumoral MHC II effects, GB models for single or dual ICB, vaccine therapy, and cell therapy should be established. Meanwhile, intracellular tumoral MHC II signaling should be detailed. While the exact signal transduction remains unknown, previous studies have suggested that PKC and PTK are involved (see **1.5 Tumoral MHC II expression and therapy efficacy**), and with mutations introduced into different regions of MHC II, domains required for signaling and antibody-mediated cell death were identified in B cell lymphoma (Jin et al., 2008). Nevertheless, it still awaits validation in solid tumor cancer cells.

On the other hand, currently, human materials or products are majorly tested with xenograft models on immunodeficient mice. These models often only emphasize the effector functions in cancer killing while omitting the fact that in a natural human setting, many immune and stromal cells are involved in controlling local cell recruitment, activation, and maintenance. To preserve tumor heterogeneity and cancer multicellular structures including immune and stromal cells, recent studies and here have started employing organoid systems (Wen et al., 2023). Organoid usage mitigates the consumption of animals while presenting a potent vector for drug and therapy testing with influential factors from various cells considered (Ma, 2023).

3.6 Conclusion

In summary, this thesis identified a therapeutic HLA-A*02-restricted TCR against the GB stem cell antigen PTPRZ1, derived from a patient in the GAPVAC trial with a favorable clinical course, extensively tested and demonstrated for its *in vitro* and *in vivo* potency against various GB models, and consequently, planned to be employed in a phase I first-in-human TCR-T cell therapy clinical trial, INVENT4GB, for recurrent HLA-A*02⁺ GB across Germany. Moreover, additional GAAs and their candidate immunogenic epitopes were identified, and TCRs targeting them in both MHCI and MHCII contexts were discovered using the HLA-humanized mouse strain A2.DR1 but require further therapeutic evaluation. Lastly, glioma MHCII expression was confirmed. Although its expression led to greater immune cell infiltration and an exhausted T cell phenotype, its precise role in tumor progression and effects on immunotherapy efficacy remain to be fully elucidated with further investigation.

4. Materials and Methods

4.1 Models

4.1.1 Animals

NOD-*Prkdc*^{scid}-*Il2rg*^{Tm1}/Rj (NXG) mice were purchased from Janvier labs. NOD.Cg-*Prkdc*^{scid} *H2-K1*^{tm1Bpe} *H2-Ab1*^{1em1Mvw} *H2-D1*^{tm1Bpe} *Il2rg*^{tm1Wjl}/SzJ (NSG MHC KO) mice were bred and housed at the DKFZ animal facility.

HLA-A*0201 HLA-DRA*0101 HLA-DRB1*0101 transgenic mice devoid of mouse MHC (A2.DR1 mice, B6-Tg(HLA-DRA*0101,HLA-DRB1*0101)1Dmz Tg(HLA-A/H2-D/B2M)1Bpe H2- Ab1tm1Doi B2mtm1Unc and B6-Tg(HLA-DRA*0101,HLA-DRB1*0101)1Dmz Tg(HLA-A/H2- D/B2M)1Bpe H2-Ab1tm1Doi B2mtm1Unc H2-D1tm1Bpe) were kindly provided by M. Bernard (Institute Pasteur) and bred and housed at the DKFZ animal facility (Pajot et al., 2004).

C57BL/6 mice were purchased from Janvier labs. B6-Tg(TCRaTCRb)425CBN/J Thy1a/CyJ (OTII) mice were bred and housed at the DKFZ animal facility. The TCR of OTII mice recognizes chicken ovalbumin (OVA) 323-339 peptide in the context of I-Ab (Barnden et al., 1998).

All mice were housed under Specific and Opportunistic Pathogen Free (SOPF) conditions and under 12h day/night cycle with water and chow ad libitum. All animal procedures were conducted in compliance with the institutional laboratory animal research guidelines and were approved by the governmental institutions (Regional Administrative Authority Karlsruhe, Germany, file number: G-147/18, G-263/18 and G-130/23).

4.1.2 Individual-patient tumor organoid (IPTO)

Induced pluripotent stem cells (iPSCs; AICS-0036-006, Institute for Cell Science) expressing enhanced green fluorescent protein (EGFP) were utilized to generate cerebral organoids. Organoid generation adhered to a published method (Lancaster and Knoblich, 2014), beginning with the seeding of dissociated iPSCs in 96-well round bottom ultra-low attachment plates with previously described hESC medium supplemented with 4 ng/ml basic fibroblast growth factor (bFGF; #PeproTech, 100-

18B), and 50 μ M ROCK inhibitor (#72304, Stemcell Technologies). Formed embryoid bodies were subsequently transferred to 24-well ultra-low attachment plates and 6-well ultra-low attachment plates in previously described Neural Induction Medium, followed by a transition to improved differentiation medium -A and improved differentiation medium +A (Lancaster et al., 2017), with agitation introduced from day 18. Resected tumor tissues were processed and dissected into small explants, which were subsequently inserted into incised cerebral organoids and embedded in Matrigel. Generated IPTOs were then cultured in improved differentiation medium +A on an orbital shaker in an incubator (75 rpm, 37°C). After 10 days of incubation, the IPTOs were ready for TCR-T testing.

4.2 Cell culture

4.2.1 Cell lines

U87 cells, kindly provided by Prof. Wolfgang Wick (Weiler et al., 2014), were cultured in DMEM supplemented with 10% fetal bovine serum (FBS) and 1% Penicillin/Streptomycin (P/S). U87 TMG cell line was generated by transfection with pMXs-IRES-PuroR plasmid encoding TMG as illustrated in **Figure. 10A**. Transfection was performed with Fugene HD transfection reagent (#E2312, Promega) following the manufacturer's instructions. Briefly, U87 cells were seeded at a density of 3×10^5 cells per well in a 6-well plate and rested for 24h. On the next day, the medium was replenished, and the cells were transfected with 2 μ g of the DNA plasmid and rested for another 48h. Cells stably expressing TMG were then selected with 2 μ g/ml Puromycin. T2 cells were kindly provided by Dr. Angelika Riemer, Division of Immunotherapy and Prevention, DKFZ, and cultured in RPMI-1640 supplemented with 20% FBS and 2% L-Glutamine.

HEK293 cells were cultured in IMDM supplemented with 10% FBS.

Jurkat TCR deficient cells were purchased from ATCC, and Jurkat 76-Triple parameter reporter (J76-TPR) was kindly provided by Prof. Peter Steinberger, Division for Immune Receptors and T Cell Activation, Institute of Immunology, Medical University of Vienna (Roskopf et al., 2018). Jurkat cells were cultured in RPMI-1640 supplemented with 10% FBS and 1% P/S.

Primary brain tumor samples were collected at the University hospital of Mannheim. All patients have provided written signed informed consent in accordance with the WMA Declaration of Helsinki principles. Ethical approval for the isolation of brain tumor tissue and analyses was obtained from the Mannheim Medical Faculty Ethics Committee (2017-589N-MA, 608-22, 574-23). The harvested tumors were processed with the tumor dissociation kit (#130-095-929, Miltenyi Biotec) and further enriched for tumor cells with the tumor cell isolation kit (#130-108-339, Miltenyi Biotec) following the manufacturer's instructions. The isolated tumor cells and previously established primary GB cell lines were cultured in DMEM-F12 supplemented with B27 (#17504044, Thermo Fisher), 5 µg/ml Insulin (#I9278, Sigma-Aldrich), 5 µg/ml Heparin (#H4784, Sigma-Aldrich), 20 ng/ml epidermal growth factor (EGF, #AF-100-15, Peprotech), and 20 ng/ml fibroblast growth factor (FGF, #100-18b, Peprotech) (Ratliff et al., 2022).

GL261 was cultured in DMEM supplemented with 10% FBS and 1% P/S. Transfection was conducted following the above-described workflow, and the corresponding antibiotics were added to the medium to select and expand stable cell lines (Puromycin at 2 µg/ml and Blasticidin at 9 µg/ml).

A2DR1 glioma cells were cultured in DMEM supplemented with 10% FBS and 1% P/S, and the stable cell lines were maintained with the addition of corresponding antibiotics into the medium.

All cell lines were incubated at 37°C and 5% CO₂ with saturated humidity.

4.2.2 CD4⁺ antigen-specific T cell expansion

CD4⁺ antigen-specific T cells were expanded *in vitro* as previously described (Schumacher et al., 2014). Briefly, spleen and lymph nodes from immunized A2.DR1 mice sacrificed by cervical dislocation were mashed through a 70 µm strainer. Erythrocytes were lysed using ACK lysis buffer (#A1049201, Thermo Fisher). The splenocytes and lymphocytes were then pooled and cultured in TCPM, containing 10% FBS, 1% P/S, 50 µM β-Mercaptoethanol (#M6250, Sigma), 2 mM L-Glutamine (#25030, Invitrogen), 25 mM HEPES (#15630080, Invitrogen), 1 mM Sodium Pyruvate (#11360070, Invitrogen), and 0.1 mM non-essential amino acids (#882031, Lonza) in RPMI-1640 medium, and supplemented with 10 µg/ml corresponding peptides for 7 days. From day 7 onwards, the medium was exchanged every 3-4 days with TCGM,

containing TCPM supplemented with 3% ConA supplement (kindly provided by Dr. Wolfram Osen) and 25 mM α -methylmannopyranoside (#M6882, Sigma). T cells were restimulated with 30 Gy-irradiated A2.DR1 DCs loaded with 2 μ g/ml peptide every 3-4 weeks until enough cell numbers were reached for FACS and sc sequencing.

To enrich antigen-specific CD4⁺ T cells, after weeks of expansion, T cells were subjected to IFN γ secretion assay (#130-090-516, Miltenyi) or stained for activation markers upon stimulation with A2.DR1 DCs loaded with 10 μ g/ml peptide. Up to 20 x 10³ FACS-sorted T cells were loaded for 5' single cell sequencing to retrieve single-cell TCR sequences (#1000263, 10x Genomics).

4.2.3 CD8⁺ antigen-specific T cell expansion

The protocol was adapted and modified from Wöfl and Greenberg (2014). Briefly, splenocytes and lymphocytes were isolated and processed as described in **4.2.2 CD4⁺ antigen-specific T cell expansion**. CD8⁺ T cells were then enriched with the CD8a⁺ T Cell Isolation Kit, mouse (#130-104-075, Miltenyi). Up to 1 Mio of isolated CD8⁺ T cells were seeded with 1 Mio 30 Gy-irradiated A2.DR1 DCs loaded with 2 μ g/ml peptide in TCPM supplemented with 100 ng/ml IL-21 (#210-21, Peprotech) in 0.5 ml volume in a 48-well plate. After 3 days of incubation, 0.5 ml of TCPM with 20 ng/ml IL-7 and IL-15 was directly added on top. After another 3 days, the entire well was transferred to a 24-well plate and added with another 1 ml of TCPM with 20 ng/ml IL-7 and IL-15. Every 3-4 days, half of the medium was removed and replenished with TCPM with 20 ng/ml IL-7 and IL-15.

For validation and sorting of antigen-reactive CD8⁺ T cells, expanded T cells were cocultured with 10 μ g/ml peptide-loaded DCs at an E:T=5:2 ratio overnight and stained for activation markers. Up to 20 x 10³ FACS-sorted T cells were loaded for 5' single cell sequencing to retrieve single-cell TCR sequences.

4.2.4 Dendritic cell generation

Mice were euthanized by cervical dislocation, and their femur, tibia, and fibula were removed. Both ends of the extracted bones were cut open to expose the bone marrow. After brief pulsed centrifugation, bone marrow was collected into microtubes and lysed

with ACK lysis buffer for 2 minutes. The remained cells were then counted and pelleted. Subsequently, they were resuspended in DC medium, containing 10% FBS, 1% P/S, 50 μ M β -Mercaptoethanol in DMEM supplemented with 20 ng/ml rmGM-CSF (#315-03, Peprotech) and 20 ng/ml rmlL-4 (#214-14, Peprotech), at a cell density of 1 Mio/ml in 150 mm TC-treated Cell Culture Dish with 20 mm Grid (#353025, Falcon), and incubated at 37°C and 5% CO₂ with saturated humidity for 3-4 days. To exchange the medium, half of the medium in the dish was removed into a 50 ml tube and centrifuged. The cell pellet was then resuspended in the same amount of fresh DC medium and returned to the dish. After another 3-4 days, cells in the supernatant were collected, and cells attached to the dish were dissociated with StemPro Accutase (#A1110501, Gibco), scraped with cell scraper, and washed with PBS before centrifugation. The collected cells were immature DCs and were frozen in Synth-a-Freeze Cryopreservation Medium (#A1254201, Gibco).

4.2.5 Electroporation of Jurkat cells

The Neon transfection system (Thermo Fisher) was employed to deliver TCR and reporters. For the transfection of Jurkat cells without reporters, 2 x 10⁶ Jurkat cells were resuspend in 100 μ l R buffer with 5 μ g of TCR and 5 μ g of reporter plasmids. For the transfection of J76-TPR, 2x 10⁶ cells were resuspend in 100 μ l R buffer with 5 μ g of TCR plasmid. Electroporation was then performed at 1325 V, 3 pulses, 10 ms. Reporter activity was measured by flow cytometry or a Pherastar plate reader (BMG Labtech).

4.2.6 Transduction of primary human T cells

Retroviral transduction was performed as previously described (Sauer et al., 2021). Briefly, TCRs were inserted into SFG-IRES-GFP retroviral vector (kind provision from Dr. Martin Pule, Addgene #22493; RRID:Addgene_22493) with In-Fusion Cloning (#638947, Takara). 3 x 10⁶ HEK293 cells were seeded the day before transfection in 10 ml IMDM supplemented with 10% FBS in 60.1 cm² dish. On the day of transfection, 3.75 μ g TCR-SFG along with 3.75 μ g PeqPam and 2.5 μ g RD114 packaging plasmids were resuspended in 470 ml IMDM and 30 μ l Fugene HD transfection reagent.

PeqPam and RD114 packaging plasmids were kindly gifted by Dr. Tim Sauer. After 10-minute incubation, cells were transfected with the DNA-Fugene HD mix and incubated for 48h. The viral supernatant was then collected and filtered through 0.45 µm strainers. Human T cells were obtained from healthy donors via density gradient separation followed by MACS with the Pan T cell isolation kit (#130-096-535, Miltenyi) in accordance with manufacturer's instructions. Isolated T cells were activated in CTL medium (45% RPMI-1640, 45% Click's medium, 10% FBS, 10 ng/ml IL-7 [#200-7, Peptide] and 5 ng/ml IL-15 [#200-15, Peptide]) with T Cell TransAct (#130-111-160, Miltenyi) for 48h at a concentration of 1×10^6 cells/ml. The filtered viral supernatant was plated (0.5 ml per well) in a non-tissue culture treated 24-well plate (#351147, Falcon), precoated o/n with 0.5 ml of 7 µg/ml RetroNectin (#T100B, Takara), and centrifuged at 2000g for 90 minutes at 4°C. Afterwards, the supernatant was removed and activated T cells were seeded at a concentration of 0.5×10^6 cell/ml in 1 ml CTL medium per well and centrifuged at 500g for 5 minutes. After 4 days of incubation, TCR-T cells were ready for expression analysis or coculture assays. TCR-T cells were maintained in culture with CTL medium over the course of described time, and the medium was refreshed every 3-4 days.

4.2.7 Adoptive cell transfer on IPTO

Upon the establishment of IPTOs, 150×10^3 TCR-T cells were injected in 3 µl with a 10-µl Hamilton micro-syringe. After 3-day incubation, feeder cells were first macroscopically removed with a scalpel, and the remaining tumor chunk was processed with the tumor dissociation kit (#130-095-929, Miltenyi Biotec).

4.2.8 *In vitro* vaccination with healthy donor PBMCs

Antigen-reactive T cells were expanded as previously described (Bozkus et al., 2021). Briefly, human PBMCs were isolated via density gradient separation. Some cells were used for HLA-A2-typing via flow cytometry. HLA-A2⁺ PBMCs were proceeded and resuspended in Xvivo15 medium (Lonza) at a density of 1 Mio/ml in a 96-well plate in a 200 µl volume, supplemented with 1000 unit/ml hGM-CSF (#300-03, Peptide), 500 unit/ml of hIL-4 (#200-04, Peptide), and 50 ng/ml hFlt3-L (#BT-FT3L-GMP,

Biotechne) for APC differentiation. One day later, 100 μ l supernatant was removed and replenished with 100 μ l Xvivo15 medium, supplemented with 20 μ M R848 (#tlrl-r848, InvivoGen), 200 ng/ml LPS (#L5293, Sigma-Aldrich), 20 ng/ml IL-1 β (#200-01B, Peprotech), and 20 μ g/ml peptide of interest. After another day, half of the medium was exchanged with R10 medium, containing 10 mM HEPES, 0.1 mg/ml Gentamicin, 1x GlutaMAX and 10% human serum, supplemented with 20 units/ml IL-2, 20 ng/ml IL-7, and 20 ng/ml IL-15. After 3 days of incubation, half of the medium was exchanged with R10 medium without any cytokines. Upon resting for 2 days, cells were collected and seeded in R10 medium at a density of 4 Mio/ml in a 96-well plate in a 200 μ l volume, supplemented with 10 μ g/ml peptide, 1 μ g/ml anti-CD28 (#302934, BioLegend), and 1 μ g/ml anti-CD49d (#304339, BioLegend) overnight. activation markers were then stained according to the flow cytometry protocol.

4.2.9 Knockout cell line generation

To generate KO cell lines, gRNAs were cloned into lentiCRISPR v2-Blast vector (kind gift from Alexandros Kourtesakis, Addgene #83480; RRID:Addgene_83480). Cell lines were either transfected directly with the plasmid or transduced with viruses carrying the plasmid. The virus was generated by transfecting 3×10^6 HEK cells with 6.6 μ g transfer plasmid, 3 μ g pMD2G and 5.51 μ g psPAX2 packaging plasmids with Fugene HD transfection reagent. The supernatant was collected 24h and 48h after the transfection. PEG-iT (#LV810A, System Biosciences) was added and incubated overnight at 4°C to capture and concentrate viruses. After centrifugation at 3000g for 30 minutes, the virus-bound PEG-iT at the bottom was resuspended with 300 μ l PBS and transferred into 6 ml of cell line medium containing 16 μ g/ml polybrene (#TR-1003-G, Sigma-Aldrich). The 6 ml mixture was enough to transduce 6 wells in a 6-well plate with each containing 3×10^5 cells in 1 ml. After 2 days of transduction or transfection, blasticidin was used to select stable cell lines.

4.3 Animal handling

4.3.1 Subcutaneous tumor inoculation

The U87 TMG cell line was prepared at a concentration of 4×10^6 cells/ml in a PBS-Matrigel mixture at a ratio of 1:1. Immunodeficient mice were shaved at the flank site before injecting subcutaneously 200 μ l of prepared tumor cells (8×10^5 cells) with a 27G needle slowly and steadily. Tumor-bearing mice were then monitored routinely for tumor-related symptoms and measured for tumor growth with a caliper. Upon reaching termination criteria or the experimental endpoint, mice were sacrificed with anesthesia, and organs of interest were harvested for downstream analyses.

4.3.2 Intracranial tumor inoculation

Tumor cells were resuspended at a concentration of $50\text{-}100 \times 10^6$ cells/ml in PBS, and 2 μ l of which, namely $1\text{-}2 \times 10^5$ cells, was stereotactically implanted into the right hemisphere of mice with the following coordinates: 2 mm right lateral of the bregma and 1 mm anterior to the coronal suture at a depth of 3 mm below the dural surface. A 10- μ l Hamilton micro-syringe driven by a fine-step stereotactic device (Stoelting) was employed for injection. The surgery was conducted under anesthesia (Ketamin, 100 mg/kg i.p. and Xylazin, 10 mg/kg i.p.) and analgesia (Carprofen, 5 mg/kg s.c.). Mice continued to receive analgesia for 3 days post-surgery and were checked daily for tumor-related symptoms. Upon termination criteria or the experimental endpoint, mice were sacrificed with anesthesia, and organs of interest were harvested for downstream analyses.

4.3.3 Intravenous adoptive cell transfer

T cells generated or isolated from transgenic mice were resuspended at a concentration of $10\text{-}25 \times 10^6$ cells/ml in PBS. Mice were shortly warmed with red-light lamp before intravenously receiving ACT of $2\text{-}5 \times 10^6$ cells in 200 μ l PBS with a 27G needle. On the day of and the day after ACT, mice were given 5×10^4 units of IL-2 i.p. in 100 μ l PBS.

4.3.4 Intracerebroventricular adoptive cell transfer

2-5 x 10⁶ T cells were resuspended in 4 µl PBS and stereotactically injected into the cerebroventricular space of the mice with the following coordinates: 0.5 mm left lateral to the bregma at a depth of 1.8 mm below the dural surface. A 10-µl Hamilton microsyringe driven by a nine step stereotactic device (Stoelting) was employed for injection. The surgery was conducted under anesthesia (Ketamin, 100 mg/kg i.p. and Xylazin, 10 mg/kg i.p.) and analgesia (Carprofen, 5 mg/kg s.c.). Mice continued to receive analgesia for 3 days post-surgery.

4.3.5 Organ harvest and murine brain tumor processing

To isolate OTII T cells, OTII mice were euthanized by cervical dislocation. Cervical lymph nodes and spleens were harvested and strained through a 70 µm strainer. Spleenocytes were further lysed with ACK lysis buffer for 2 minutes. Afterwards, lymphocytes and spleenocytes were pooled and stimulated with OVA peptide at 2 µg/ml at a cell density of 5 Mio/ml in TCPM supplemented with 50 unit/ml IL-2 for 4 days. T cells were then enriched with the Pan T Cell Isolation Kit II, mouse (#130-095-130, Miltenyi) or CD4⁺ T Cell Isolation Kit, mouse (#130-104-454, Miltenyi).

To profile immune cells in the TME, tumor-bearing mice were euthanized by anesthesia overdose, followed by perfusion with PBS. Tumor-bearing hemispheres were then extracted, minced, transferred to 1 ml HBSS containing freshly diluted Liberase (Sigma-Aldrich) at 50 µg/ml, and incubated at 37°C for 30 minutes with shaking. Afterwards, the mixture was vortexed and strained through 100 µm and 70 µm strainers. Following centrifugation at 500g for 5 minutes, the pellet was resuspended in 10 ml PBS and 4.5 ml Percoll (#17089101, Cytiva), vigorously mixed, and centrifuged at 2700 rpm for 30 minutes at room temperature without brake. Myeline was then removed, and the remaining cells were isolated following PBS washing and centrifugation. The collected cells were then stained for markers according to the flow cytometry protocol.

4.3.6 Immune checkpoint blockade treatment (ICB)

Triple ICB was applied here, including 200 µg anti-PD-L1 (#P363, Leinco), 250 µg anti-PD-1 (#P362, Leinco), and 100 µg anti-CTLA-4 (#C2855, Leinco). The antibodies were prepared in 100 µl PBS and injected i.p. into tumor-bearing mice on day 11, 14, and 17 after tumor inoculation.

4.3.7 Vaccination and vaccine therapy

For immunization of A2.DR1 mice to generate antigen-reactive T cells, 100 µg of each peptide was prepared separately or pooled together with another 100 µg of another peptide for combined vaccination in 100 µl of emulsion, generated by mixing with Montanide. The peptide emulsion was s.c. injected with 50 µl into both lateral pectoral regions. Additionally, 600 ng rmGM-CSF in 100 µl PBS was s.c. injected between the two peptide injection sites on the chest. Aldara cream containing 5% imiquimod (Meda Pharma) was applied topically to the injection sites. A booster vaccine with peptide only was performed on day 10, including Aldara cream application. On day 21, immunized mice were euthanized by cervical dislocation, and their lymph nodes and spleens were harvested for downstream procedures.

For vaccine therapy on tumor-bearing mice, on day 7 after tumor inoculation, 200 µg peptide in 200 µl PBS was i.v. injected along with i.p. administration of 5×10^4 units of IL-2 on the day of vaccination and the day after. The same amount and volume of peptide was used as a booster on day 15.

4.3.8 Magnetic resonance imaging

MRI was conducted by the small animal imaging core facility at DKFZ with a Bruker BioSpec 3Tesla (Ettlingen, Germany) with Para Vision software 360 V1.1. Mice were anesthetized with 3.5% sevoflurane in air, and the imaging was performed with a T2 TurboRARE sequence: TE = 48 ms, TR = 3350 ms, FOV 20 x 20 mm, slice thickness 1 mm, averages = 3, Scan Time = 3m21s, echo spacing 12 ms, rare factor 8, slices 20, image size 192 x 192. Tumor volume was assessed by manual segmentation using Bruker Para Vision software 6.0.1.

4.4 Antibody-based assays

4.4.1 Immunofluorescence

Human FFPE GB samples were collected at the Pathology Department of Heidelberg University hospital. Sectioned samples on slides were prewarmed at 60°C for 1h, followed by immediate immersion in histoclear/Xylool for 10 minutes and another 10-minute immersion in fresh histoclear/Xylool. The slides then underwent 2 sequential submersions in 100% EtOH for 5 minutes each, followed by serial hydration with 96%, 70%, and 50% EtOH, and lastly VE-water for 3 minutes each. Heat-mediated antigen retrieval was then performed with cell conditioning solution (CC1, #950-124, Ventana) for 30 minutes in a steamer. After cooling down, the slides were quickly rinsed twice with PBS and permeabilized with 0.1% Tween 20 in PBS (T-PBS) for 10 minutes at RT. Blocking was done with 1:10 diluted donkey serum in T-PBS for 1h at RT. After a quick wash with T-PBS, the slides were stained with primary antibodies diluted in T-PBS o/n at 4°C. On the next day, slides were washed 3 times with T-PBS for 5 minutes each. Secondary antibodies with fluorophores were 1:200 diluted in T-PBS at incubated with the slides for 1h at RT. Subsequently, slides were washed 3 times with T-PBS for 5 minutes each, and quickly rinsed with PBS. To quench the autofluorescence, 0.1% Sudan Black B (#199664, Sigma-Aldrich) in 70% EtOH was applied for 10 minutes at RT. Lastly, the slides were washed 3 times with 0.02% Tween20 in PBS for 5 minutes each time before mounted (#00-4959-52, Invitrogen).

Murine brains were harvested and embedded in OCT Compound (Sakura) before freezing at -80°C. Later, they were sectioned at 7 µm thickness, placed on slides and stored at -80°C. Before staining, slides were thawed at RT for at least 15 minutes, followed by 20-minute fixation with pre-chilled -20°C methanol. After removal from methanol, they were air-dried at RT for 5 minutes. A hydrophobic pen was used to circle sample sections on slides. Slides were then quickly rinsed with PBS and incubated with T-PBS for 30 minutes. After another PBS quick wash, blocking was done with 1:10 diluted donkey serum in T-PBS for 1h at RT. Upon a quick wash with T-PBS, slides were stained with primary antibodies (see **4.4.5 Antibodies and fluorescence labeling kits**) diluted in T-PBS o/n at 4°C. On the next day, slides were washed 3 times with T-PBS for 5 minutes each. Secondary antibodies with fluorophores were 1:200 diluted in T-PBS and incubated with the slides for 1h at RT.

Lastly, the slides were washed 3 times with T-PBS for 5 minutes each time before mounted. The stained slides were kept at 4°C for up to a week and imaged with VS200 Research Slide Scanner (Olympus Lifescience).

4.4.2 Flow cytometry and fluorescence-activated cell sorting (FACS)

Lineage, surface activation, and subset markers were stained with the antibodies listed in **4.4.5 Antibodies and fluorescence labeling kits** in PBS. eFluor 780 fixable viability dye (#65-0865-14, Invitrogen) was used following the instructions to exclude dead cells. For intracellular staining of cytokines and effector proteins, cells were incubated with 1:1000 diluted GolgiPlug and GolgiStop (#555029 and #554724, BD Biosciences) for 5h. After extracellular and viability staining, cells were fixed and permeabilized with Fixation/Permeabilization solution (#554714, BD Biosciences) for 30 minutes on ice, followed by 2 washes with 1x BD Perm/Wash buffer. Intracellular staining antibodies were diluted in 1x BD Perm/Wash buffer and incubated with cells for 30 minutes on ice. After another 2 washes with 1x BD Perm/Wash buffer, cells were ready for acquisition. For cell counting, 123count eBeads (#01-1234-42, Invitrogen) were diluted and loaded to the well just before acquisition. Cell counts were then calculated based on the bead dilution and volume used. Stained cells were acquired using BD Canto or LSRFortessa and Bio Rad ZE5 or sorted using BD Aria.

4.4.3 Enzyme-linked immunosorbent spot (ELISpot)

ELISpot was performed as previously described (Schumacher et al., 2014). Briefly, ELISpot plates (#MAIPSWU10, Millipore) were wetted with a short incubation with 35% EtOH and extensive PBS wash, followed by incubation with 100 µl of 15 µg/ml IFN γ coating antibody (#AN-18, Mabtech) over night at 4°C. After several washes with PBS and blocking with TCPM at room temperature, splenocytes collected from immunized mice were resuspended and seeded in 200 µl TCPM at a cell density of 2 Mio/ml supplemented with 10 µg/ml peptides. For the positive control, 20 ng/ml PMA and 1 µg/ml ionomycin were used. After 36h of incubation, cells were removed from the plate. PBS was used to wash the plate, and 100 µl of 1 µg/ml biotinylated IFN γ detection antibody (#R4-6A2, Mabtech) in PBS with 0.5% FBS was incubated on the

plate for 2h at room temperature. Afterwards, 100 μ l of 1 μ g/ml streptavidin-ALP (Mabtech) in PBS with 0.5% FBS was applied for 1h at room temperature. Lastly, streptavidin-ALP was removed, and the plate was incubated with APL development buffer (Bio Rad) until distinct spots emerged. The ELISpot was then quantified with ImmunoSpot Analyzer (Cellular Technology Ltd).

4.4.4 T2 presentation assay

T2 cells are deficient in TAP, making surface HLA-A2 expression unstable without a processed peptide loaded. The assay determines if the exogenous peptide can bind to HLA-A2 on T2 cells and stabilize the surface expression. Briefly, 2×10^5 T2 cells were seeded in a 96-well plate in 200 μ l AIM-V medium and incubated with 10 μ g/ml peptides with 5 μ g/ml β 2-M (#551089, BD Pharmingen) for 3h at 37°C. After the incubation, cells were stained and analyzed for HLA-A2 expression according to the flow cytometry protocol.

4.4.5 Antibodies and fluorescence labeling kits

Target species	Target	Fluorophore	Provider	Catalog
Human	GFAP	-	Dako	GA524
Human/Mouse	PTPRZ1	-	BD Biosciences	610179
Human	CD3	-	Dako	A0452
Human	HLA-ABC	-	BioLegend	311402
-	Fixable viability dye	eFluor 780	Invitrogen	65-0865-14
-	CellTrace Proliferation kit	Far Red	Invitrogen	C34572
Human	CD3	BV510	BioLegend	300448
Human	CD45	PerCP	BioLegend	368506
Human	CD45	Spark UV387	BioLegend	304086
Human	CD8	PerCP-Cy5.5	BioLegend	344710
		PE Cy7	BioLegend	344712
Human	CD4	PE Dazzle 594	BioLegend	300548
Human	CD62L	BV711	BioLegend	304860
Human	CD45RA	BV785	BioLegend	304140
Human	CD137	PE	BioLegend	309804
Human	IFN γ	BV421	BioLegend	502532
Human	TNF α	BV605	BioLegend	502936
Human	Granzyme B	PerCP-Cy5.5	BioLegend	372212
Human	Perforin	AF 700	BioLegend	353324

Materials and Methods

Human	HLA-A2	PE APC	BioLegend BioLegend	343306 343308
Human	HLA-DR	BV711 FITC	BioLegend BioLegend	307644 307632
Mouse	TCR β	PE	BioLegend	109207
Mouse	TCR β	APC	BioLegend	109212
Mouse	CD45	AF 700 BV510	BioLegend BioLegend	103128 103138
Mouse	CD3	BV711 BV421 BUV395	BioLegend BioLegend BD Biosciences	100241 100228 740268
Mouse	CD4	BV510 APC	BioLegend BioLegend	100559 100516
Mouse	CD8	PerCP-Cy5.5 AF 700	BioLegend BioLegend	100734 100730
Mouse	CD69	APC	BioLegend	104514
Mouse	IFN γ	PE Cy7	BioLegend	505826
Mouse	TNF α	FITC	BioLegend	506304
Mouse	CD11c	BV711	BioLegend	117349
Mouse	CD40	PerCP-eFluor710	Invitrogen	46-0401- 82
Mouse	CD80	PE Cy7	BioLegend	104734
Mouse	CD86	BV605	BioLegend	105037
Mouse	CD107a	APC	BioLegend	121614
Mouse	CD137	PE	BioLegend	106106
Mouse	CD39	PE Dazzle 594	BioLegend	143812
Mouse	Ki69	FITC	BioLegend	151212
Mouse	LAG3	BV785	BioLegend	125219
Mouse	PD-1	PerCP-eFluor710	Invitrogen	46-9985- 82
Mouse	CTLA-4	PE	BioLegend	106306
Mouse	TIGIT	PE Cy7	BioLegend	142108
Mouse	TIM-3	BV605	BioLegend	119721
Mouse/Human	TCF1	BV421	BD Biosciences	566692
Mouse/Human	TOX	APC	Miltenyi	130-118- 335
Mouse	CXCR3	BV421	BioLegend	126522
Mouse/Human	T-BET	PE Cy7	BioLegend	644824
Mouse	CCR4	PE	BioLegend	131204
Mouse/Human	GATA3	PerCP-Cy5.5	BioLegend	653812
Mouse	CD25	AF 700	BioLegend	102024
Mouse	CD44	BV605	BioLegend	103047
Mouse	CD127	FITC	BioLegend	135008
Mouse	FOXP3	APC	Invitrogen	17-5773- 82
Mouse	CD11b	BV711	BioLegend	101242
Mouse	I-A/I-E	FITC PerCP-Cy5.5	BioLegend BioLegend	107606 107626

Mouse	H-2Kb	APC	Invitrogen	17-5958-82
Mouse	IgG	AF 647	Invitrogen	A31571
Rabbit	IgG	AF 488	Invitrogen	A21206

4.5 Molecular assays

4.5.1 Untargeted ligandomics

Immunoprecipitation of HLA class I:peptide complexes was performed as previously described with additional steps for the forced oxidation of methionine using H₂O₂ and the reduction and alkylation of cysteine using tris(2-carboxyethyl)phosphine and iodoacetamide (Chong et al., 2018). Lyophilized peptides were dissolved in 12 μ l of 5% ACN in 0.1% TFA and spiked with 0.5 μ l of 100 fmol/ μ l Peptide Retention Time Calibration Mixture and 10 fmol/ μ l JPTRT 11, a subset of peptides from the Retention Time Standardization Kit (JPT), and transferred to QuanRecovery Vials with MaxPeak HPS (Waters, Milford, MA, USA). All samples were analyzed using an UltiMate 3000 RSLCnano system coupled to an Orbitrap Exploris 480 equipped with a FAIMS Pro Interface (Thermo Fisher). For chromatographic separation, peptides were first loaded onto a trapping cartridge (Acclaim PepMap 100 C18 μ -Precolumn, 5 μ m, 300 μ m i.d. x 5 mm, 100 \AA ; Thermo Fisher) and then eluted and separated using a nanoEase M/Z Peptide BEH C18 130A 1.7 μ m, 75 μ m x 200mm (Waters). Total analysis time was 120 min, and separation was performed using a flow rate of 0.3 μ l/min with a gradient starting from 1% solvent B (100% ACN, 0.1% TFA) and 99% solvent A (0.1% FA in H₂O) for 0.5 min. The concentration of solvent B was increased to 2.5% in 12.5 min, to 28.6% in 87 min, and then to 38.7% in 1.4 min. Subsequently, the concentration of solvent B was increased to 80% in 2.6 min and kept at 80% solvent B for 5 min for washing. Finally, the column was re-equilibrated at 1% solvent B for 11 min. The LC system was coupled on-line to the mass spectrometer using a Nanospray-Flex ion source (Thermo Fisher), a SimpleLink Uno liquid junction (FossilonTech), and a CoAnn ESI Emitter (Fused Silica 20 μ m ID, 365 μ m OD with orifice ID 10 μ m; CoAnn Technologies). The mass spectrometer was operated in positive mode, and a spray voltage of 2400 V was applied for ionization with an ion transfer tube temperature of 275°C. For ion mobility separation, the FAIMS module was operated with standard resolution and a total carrier gas flow of 4.0 l/min. Each sample was injected twice

using either a compensation voltage of -50 V or -65 V for maximal orthogonality and thus increased immunopeptidome coverage. Full Scan MS spectra were acquired for a range of 300 – 1650 m/z with a resolution of 120.000 (RF Lens 50%, AGC Target 300%). MS/MS spectra were acquired in data-independent mode using 44 previously determined dynamic mass windows optimized for HLA class I peptides with an overlap of 0.5 m/z. HCD collision energy was set to 28%, and MS/MS spectra were recorded with a resolution of 30.000 (normalized AGC target 3000%). MS raw data was analyzed using Spectronaut software (version 17.6, Biognosys) (Bruderer et al., 2015) and searched against the UniProtKB/Swiss-Prot database (retrieved: 21.10.2021, 20387 entries). Search parameters were set to non-specific digestion and a peptide length of 7-15 amino acids. Carbamidomethylation of cysteine and oxidation of methionine were included as variable modifications. Results were reported with 1% FDR at the peptide level. Peptides identified by Spectronaut were further analyzed using NetMHCpan 4.1 (Reynisson et al., 2020a) . Predicted non-binders were excluded from the analysis.

4.5.2 LDH release

To detect LDH from killed cells, the CytoTox 96 Non-Radioactive Cytotoxicity Assay kit (#G1780, Promega) was used following the manufacturer's protocol. Briefly, 150×10^3 TCR-T cells and 75×10^3 tumor cells were cocultured for 24h unless stated otherwise. 100 μ L supernatant was collected after centrifugation at 500g for 5 minutes. 50 μ L of the collected supernatant was then mixed with 50 μ L of CytoTox 96 Reagent and incubated at RT for 30 minutes in the dark. After incubation, 50 μ L of Stop Solution was pipetted into the wells, and the absorbance at 490 nm was then recorded. Background from the medium and spontaneous cell leaking were subtracted.

4.5.3 RNAscope™

Target RNA transcripts on slides were detected with the RNAscope 2.5 HD Duplex Kit (#322435, Advanced Cell Diagnostics) following manufacturer's instructions. Briefly, slides with sectioned frozen murine brains were removed from -80°C and immediately fixed with pre-chilled 10% neutral buffered formalin at 4°C. To dehydrate the slides,

they were then serially immersed in 50%, 70%, and 100% EtOH at RT. After another immersion in fresh 100% EtOH, slides were either immediately used or stored in 100% EtOH at -20°C for up to a week. To stain the slides, they were first air-dried and pre-treated with RNAscope Hydrogen Peroxide. After a quick wash with PBS, they were then pre-treated with RNAscope Protease IV. Slides were subsequently quickly rinsed with PBS. For target detection, custom probes were manufactured, and the probe mix was applied to slides and incubated in the HybEZ Oven for 2h at 40°C. Next, the slides were washed with 1X Wash Buffer and kept in 5X SSC at RT o/n. The next day, slides were washed with 1X Wash Buffer and underwent a series of amplification steps with Amp 1-6 following the manual. The first probe was then detected with FastRed. After more washes with 1X Wash Buffer, slides underwent another series of amplification steps with Amp 7-10 following the instructions. The second probe was then detected with FastGreen. After more washes with 1X Wash Buffer, slides were counterstained with 50% Hematoxylin staining solution. Next, slides were immediately rinsed with tap water, followed by drying in the HybEZ Oven at 60°C. Once the slides cooled down, they were briefly dipped in fresh Xylene and mounted with VectaMount Mounting Medium (#H-5000, Vector Labs). The samples were then imaged with VS200 Research Slide Scanner.

4.5.4 RNA isolation

Cells were harvested and pelleted, and their RNA was isolated with the PicoPure RNA Isolation kit (#KIT0204, Applied Biosystems) following manufacturer's instructions. The eluted RNA was used directly for reverse transcription or stored at -80°C.

4.5.5 Reverse transcription

cDNA of the isolated RNA was generated with SuperScript II Reverse Transcriptase (#18064014, Invitrogen) following manufacturer's manual. The generated cDNA was 1:100 diluted in Nuclease-free water and stored at -20°C.

4.5.6 qPCR

2x qPCR SYBR Green master mix (#SL-9902R, Steinbrenner) was used for cDNA quantification. 5 μ L of diluted cDNA was mixed with 1 μ l of 10 μ M forward and 1 μ l of 10 μ M reverse primers, and 10 μ l of 2x qPCR SYBR Green master mix with sterile water added to make up a total 20 μ l volume. The mixture was first denatured at 95°C for 1 minute, followed by 40 cycles of: 95°C for 5 seconds, 56°C for 5 seconds, and 72°C for 10 seconds with melting curve on Quantstudio 3. Gene expression was calculated using the $\Delta\Delta$ CT method with GAPDH gene as an internal control.

Target Species	Target	Provider	Sequence
Human	GAPDH	Sigma	Fwd: TCTCTGCTCCTCCTGTTTCGAC Rev: TGAGCGATGTGGCTCGGCT
Synthetic	TMG	Sigma	Fwd: ACCTCCAGCTGGAGTCCATG Rev: TGGTGGTGGACCTGTGTAAGAAT
Synthetic	Control TMG	Sigma	Fwd: GCCTACACCACCGCCGA Rev: GCGATAGGGATCAGCATGCTG

4.6 Computational analysis

4.6.1 TCGA and publicly available dataset analysis

TCGA data were downloaded using the package TCGAbiolinks (2.28.4) (Colaprico et al., 2016). Sc GB and glioma datasets were downloaded according to the provided instructions (Neftel et al., 2019; Venteicher et al., 2017). The data were handled with Seurat (5.0.3) (Hao et al., 2023). Cell state scores were directly used if specified in the dataset; otherwise, they were calculated based on the defined gene sets with the AddModuleScore function (Neftel et al., 2019). GSC scores were calculated with the published gene set (Patel et al., 2014). Tumoral MHCII score was calculated with singscore (1.20.0) using all MHCII gene expression as UpSet genes and PTPRC and ITGAM as DownSet genes (Bhuva et al., 2020). Gene set enrichment analysis was conducted with fgsea (1.30.0) (Korotkevich et al., 2021).

4.6.2 Single-cell RNA-seq and analysis

Isolated primary tumor cells and non-tumor cells from brain tumor samples and IPTO cells were resuspended in 0.04% BSA in PBS; up to 20 x 10³ cells were loaded for 5'

single cell sequencing (#1000263, 10x Genomics), and the libraries were prepared according to the manufacturer's protocol. Single-cell data were aligned with cellranger (7.0.0) and handled with Seurat (5.0.3). Cells expressing few transcripts or genes were excluded before normalization. Doublets were identified and excluded with scDblFinder (1.14.0) (Germain et al., 2022). Harmony (1.0.3) was subsequently used to integrate datasets (Korsunsky et al., 2019). Canonical markers were employed to identify and annotate cell types. Module gene sets were derived from previous studies and their scores were calculated using the AddModuleScore function in Seurat. Plots were made with ggplot2 (3.5.0) and SCpubr (2.0.2) (Blanco-Carmona, 2022; Wickham, 2016).

4.6.3 ARDitox off-target prediction

Off-targets were predicted as described previously (Pienkowski et al., 2023). Briefly, 9-mer peptides of the human proteome that share at least 5 amino acids with the target epitope were shortlisted. Next, epitopes derived from frequent single nucleotide polymorphisms with a frequency more than 1% were included. High-affinity presented epitopes predicted with ARDisplay were selected (Mazzocco et al., 2021). The safety score compared the physico-chemical properties of probable TCR-facing amino acids.

4.6.4 Immunogenic epitope prediction

MHCI epitopes were predicted with NetMHCpan-4.1 (Reynisson et al., 2020a), and MHCII epitopes with NetMHCIIpan-4.0 (Reynisson et al., 2020b). To shortlist candidate epitopes for vaccination, they were ranked based on their EL scores. Furthermore, the epitope sequences were blasted with blast.ncbi.nlm.nih.gov, and those with similar sequences to other proteins than the selected GAAs were excluded.

4.6.5 Statistical analysis and figures

Data are presented as individual values or as mean \pm SEM unless stated otherwise. Applied statistical tests are indicated in the figure legends. GraphPad Prism 9.0 was used for statistical tests and plots. Some figures were created with BioRender.com.

5. References

Aehnlich, P., Carnaz Simões, A.M., Skadborg, S.K., Holmen Olofsson, G., and Straten, P. (2020). Expansion With IL-15 Increases Cytotoxicity of V γ 9V δ 2 T Cells and Is Associated With Higher Levels of Cytotoxic Molecules and T-bet. *Frontiers in Immunology* 11.

Ah-Pine, F., Khettab, M., Bedoui, Y., Slama, Y., Daniel, M., Doray, B., and Gasque, P. (2023). On the origin and development of glioblastoma: multifaceted role of perivascular mesenchymal stromal cells. *Acta Neuropathologica Communications* 2023 11:1 11.

Ahmed, N., Brawley, V., Hegde, M., Bielałowicz, K., Kalra, M., Landi, D., Robertson, C., Gray, T.L., Diouf, O., Wakefield, A., *et al.* (2017). HER2-Specific CAR-Modified Virus-Specific T Cells for Progressive Glioblastoma. *JAMA Oncology* 3.

Al-Daccak, R., Mooney, N., and Charron, D. (2004). MHC class II signaling in antigen-presenting cells. *Current Opinion in Immunology* 16.

Arnaud, M., Chiffelle, J., Genolet, R., Navarro Rodrigo, B., Perez, M.A.S., Huber, F., Magnin, M., Nguyen-Ngoc, T., Guillaume, P., Baumgaertner, P., *et al.* (2021). Sensitive identification of neoantigens and cognate TCRs in human solid tumors. *Nature Biotechnology* 2021 40:5 40.

Aslan, K., Turco, V., Blobner, J., Sonner, J.K., Liuzzi, A.R., Núñez, N.G., De Feo, D., Kickingreder, P., Fischer, M., Green, E., *et al.* (2020). Heterogeneity of response to immune checkpoint blockade in hypermutated experimental gliomas. *Nature Communications* 2020 11:1 11.

Asrir, A., Tardiveau, C., Coudert, J., Laffont, R., Blanchard, L., Bellard, E., Veerman, K., Bettini, S., Lafouresse, F., Vina, E., *et al.* (2022). Tumor-associated high endothelial venules mediate lymphocyte entry into tumors and predict response to PD-1 plus CTLA-4 combination immunotherapy. *Cancer Cell* 40.

- Axelrod, M.L., Cook, R.S., Johnson, D.B., and Balko, J.M. (2019). Biological Consequences of MHC-II Expression by Tumor Cells in Cancer. *Clinical Cancer Research* 25.
- Bagley, S.J., Binder, Z.A., Lamrani, L., Marinari, E., Desai, A.S., Nasrallah, M.P., Maloney, E., Brem, S., Lustig, R.A., Kurtz, G., *et al.* (2024a). Repeated peripheral infusions of anti-EGFRvIII CAR T cells in combination with pembrolizumab show no efficacy in glioblastoma: a phase 1 trial. *Nature Cancer* 2024 5:3 5.
- Bagley, S.J., Logun, M., Fraietta, J.A., Wang, X., Desai, A.S., Bagley, L.J., Nabavizadeh, A., Jarocha, D., Martins, R., Maloney, E., *et al.* (2024b). Intrathecal bivalent CAR T cells targeting EGFR and IL13R α 2 in recurrent glioblastoma: phase 1 trial interim results. *Nature Medicine* 2024 30:5 30.
- Barnden, M.J., Allison, J., Heath, W.R., and Carbone, F.R. (1998). Defective TCR expression in transgenic mice constructed using cDNA-based α - and β -chain genes under the control of heterologous regulatory elements. *Immunology and Cell Biology* 76.
- Baulu, E., Gardet, C., Chuvin, N., and Depil, S. (2023). TCR-engineered T cell therapy in solid tumors: State of the art and perspectives. *Science Advances* 9.
- Bausart, M., Pr eat, V., and Malfanti, A. (2022). Immunotherapy for glioblastoma: the promise of combination strategies. *Journal of Experimental & Clinical Cancer Research* 2022 41:1 41.
- Bawden, E., and Gebhardt, T. (2023). The multifaceted roles of CD4+ T cells and MHC class II in cancer surveillance. *Current Opinion in Immunology* 83.
- Bedoya, D.M., Marinari, E., Davanture, S., Castillo, L.C., Erraiss, S., Dockerill, M., Badiola, S.B., Winssinger, N., Schaller, K., Bijlenga, P., *et al.* (2023). PTPRZ1-targeting RNA CAR-T cells exert antigen-specific and bystander antitumor activity in glioblastoma. *bioRxiv*.

References

Berger, C., Jensen, M.C., Lansdorp, P.M., Gough, M., Elliott, C., and Riddell, S.R. (2008). Adoptive transfer of effector CD8⁺ T cells derived from central memory cells establishes persistent T cell memory in primates. *The Journal of Clinical Investigation* 118.

Bhuva, D.D., Cursons, J., and Davis, M.J. (2020). Stable gene expression for normalisation and single-sample scoring. *Nucleic Acids Research* 48.

Blanchard, L., and Girard, J.-P. (2021). High endothelial venules (HEVs) in immunity, inflammation and cancer. *Angiogenesis* 2021 24:4 24.

Blanco-Carmona, E. (2022). Generating publication ready visualizations for Single Cell transcriptomics using SCpubr. *bioRxiv*, 2022.2002.2028.482303.

Boschert, T., Kromer, K., Lerner, T., Lindner, K., Haltenhof, G., Tan, C.L., Jähne, K., Poschke, I., Bunse, L., Eisele, P., *et al.* (2024). H3K27M neoepitope vaccination in diffuse midline glioma induces B and T cell responses across diverse HLA loci of a recovered patient. *Science Advances* 10.

Bourgonje, A.M., Navis, A.C., Schepens, J.T.G., Verrijp, K., Hovestad, L., Hilhorst, R., Harroch, S., Wesseling, P., Leenders, W.P.J., and Hendriks, W.J.A.J. (2014). Intracellular and extracellular domains of protein tyrosine phosphatase PTPRZ-B differentially regulate glioma cell growth and motility. *Oncotarget* 5.

Bozkus, C.C., Blazquez, A.B., Enokida, T., and Bhardwaj, N. (2021). A T-cell-based immunogenicity protocol for evaluating human antigen-specific responses. *STAR Protocols* 2.

Bozza, M., Roia, A.D., Correia, M.P., Berger, A., Tuch, A., Schmidt, A., Zörnig, I., Jäger, D., Schmidt, P., and Harbottle, R.P. (2021). A nonviral, nonintegrating DNA nanovector platform for the safe, rapid, and persistent manufacture of recombinant T cells. *Science Advances* 7.

Brehm, M.A., Kenney, L.L., Wiles, M.V., Low, B.E., Tisch, R.M., Burzenski, L., Mueller, C., Greiner, D.L., and Shultz, L.D. (2019). Lack of acute xenogeneic graft-

versus-host disease, but retention of T-cell function following engraftment of human peripheral blood mononuclear cells in NSG mice deficient in MHC class I and II expression. *The FASEB Journal* 33.

Brison, N., Debeer, P., and Tylzanowski, P. (2014). Joining the fingers: A HOXD13 story. *Developmental Dynamics* 243.

Brown, C.E., Badie, B., Barish, M.E., Weng, L., Ostberg, J.R., Chang, W.-C., Naranjo, A., Starr, R., Wagner, J., Wright, C., *et al.* (2015). Bioactivity and Safety of IL13R α 2-Redirected Chimeric Antigen Receptor CD8⁺ T Cells in Patients with Recurrent Glioblastoma. *Clinical Cancer Research* 21.

Brown, C.E., Hibbard, J.C., Alizadeh, D., Blanchard, M.S., Natri, H.M., Wang, D., Ostberg, J.R., Aguilar, B., Wagner, J.R., Paul, J.A., *et al.* (2024). Locoregional delivery of IL-13R α 2-targeting CAR-T cells in recurrent high-grade glioma: a phase 1 trial. *Nature Medicine* 2024 30:4 30.

Bruderer, R., Bernhardt, O.M., Gandhi, T., Miladinović, S.M., Cheng, L.-Y., Messner, S., Ehrenberger, T., Zanotelli, V., Butscheid, Y., Escher, C., *et al.* (2015). Extending the Limits of Quantitative Proteome Profiling with Data-Independent Acquisition and Application to Acetaminophen-Treated Three-Dimensional Liver Microtissues *[S]. *Molecular & Cellular Proteomics* 14.

Bunse, L., Bunse, T., Krämer, C., Chih, Y.-C., and Platten, M. (2022). Clinical and Translational Advances in Glioma Immunotherapy. *Neurotherapeutics* 19.

Bunse, L., Kratzmann, M., Chih, Y., Sanghvi, K., de Roia, A., Harbottle, R., Eichmüller, S., Benner, A., Green, E., Poschke, I., *et al.* (2023). P06.05.A INTRACEREBROVENTRICULAR TCR-TRANSGENIC T CELL THERAPY TO TREAT GLIOBLASTOMA (INVENT4GB). *Neuro-Oncology* 25.

Bunse, L., Pusch, S., Bunse, T., Sahm, F., Sanghvi, K., Friedrich, M., Alansary, D., Sonner, J.K., Green, E., Deumelandt, K., *et al.* (2018). Suppression of antitumor T

References

cell immunity by the oncometabolite (R)-2-hydroxyglutarate. *Nature Medicine* 2018 24:8 24.

Bunse, L., Schumacher, T., Sahm, F., Pusch, S., Oezen, I., Rauschenbach, K., Gonzalez, M., Solecki, G., Osswald, M., Capper, D., *et al.* (2015). Proximity ligation assay evaluates IDH1R132H presentation in gliomas. *Journal of Clinical Investigation*.

Cantile, M., Franco, R., Tschan, A., Baumhoer, D., Zlobec, I., Schiavo, G., Forte, I., Bihl, M., Liguori, G., Botti, G., *et al.* (2009). HOX D13 expression across 79 tumor tissue types. *International Journal of Cancer* 125.

Cappell, K.M., and Kochenderfer, J.N. (2023). Long-term outcomes following CAR T cell therapy: what we know so far. *Nature Reviews Clinical Oncology* 2023 20:6 20.

Carter, S.L., Cibulskis, K., Helman, E., McKenna, A., Shen, H., Zack, T., Laird, P.W., Onofrio, R.C., Winckler, W., Weir, B.A., *et al.* (2012). Absolute quantification of somatic DNA alterations in human cancer. *Nature Biotechnology* 2012 30:5 30.

Chang, C.X.L., Tan, A.T., Or, M.Y., Toh, K.Y., Lim, P.Y., Chia, A.S.E., Froesig, T.M., Nadua, K.D., Oh, H.-L.J., Leong, H.N., *et al.* (2013). Conditional ligands for Asian HLA variants facilitate the definition of CD8+ T-cell responses in acute and chronic viral diseases. *European Journal of Immunology* 43.

Chen, W., Zhang, W., Wu, R., Cai, Y., Xue, X., and Cheng, J. (2019). Identification of biomarkers associated with histological grade and prognosis of gastric cancer by co-expression network analysis. *Oncology Letters* 18.

Cho, H.-J., Lee, S., Ji, Y.G., and Lee, D.H. (2018). Association of specific gene mutations derived from machine learning with survival in lung adenocarcinoma. *PLOS ONE* 13.

Choi, B.D., Gerstner, E.R., Frigault, M.J., Leick, M.B., Mount, C.W., Balaj, L., Nikiforow, S., Carter, B.S., Curry, W.T., Gallagher, K., *et al.* (2024). Intraventricular

CARv3-TEAM-E T Cells in Recurrent Glioblastoma. *New England Journal of Medicine* 390.

Chong, C., Marino, F., Pak, H., Racle, J., Daniel, R.T., Müller, M., Gfeller, D., Coukos, G., and Bassani-Sternberg, M. (2018). High-throughput and Sensitive Immunopeptidomics Platform Reveals Profound Interferon- γ -Mediated Remodeling of the Human Leukocyte Antigen (HLA) Ligandome *. *Molecular & Cellular Proteomics* 17.

Chu, J., Gao, F., Yan, M., Zhao, S., Yan, Z., Shi, B., and Liu, Y. (2022). Natural killer cells: a promising immunotherapy for cancer. *J Transl Med* 20, 240.

Chupp, D.P., Rivera, C.E., Zhou, Y., Xu, Y., Ramsey, P.S., Xu, Z., Zan, H., and Casali, P. (2024). A humanized mouse that mounts mature class-switched, hypermutated and neutralizing antibody responses. *Nature Immunology* 2024 25:8 25.

Chuprin, J., Buettner, H., Seedhom, M.O., Greiner, D.L., Keck, J.G., Ishikawa, F., Shultz, L.D., and Brehm, M.A. (2023). Humanized mouse models for immunology research. *Nature Reviews Clinical Oncology* 2023 20:3 20.

Cohen, C.J., Zhao, Y., Zheng, Z., Rosenberg, S.A., and Morgan, R.A. (2006). Enhanced Antitumor Activity of Murine-Human Hybrid T-Cell Receptor (TCR) in Human Lymphocytes Is Associated with Improved Pairing and TCR/CD3 Stability. *Cancer Research* 66.

Colaprico, A., Silva, T.C., Olsen, C., Garofano, L., Cava, C., Garolini, D., Sabedot, T.S., Malta, T.M., Pagnotta, S.M., Castiglioni, I., *et al.* (2016). TCGAAbiolinks: an R/Bioconductor package for integrative analysis of TCGA data. *Nucleic Acids Research* 44.

Creelan, B.C., Wang, C., Teer, J.K., Toloza, E.M., Yao, J., Kim, S., Landin, A.M., Mullinax, J.E., Saller, J.J., Saltos, A.N., *et al.* (2021). Tumor-infiltrating lymphocyte

References

treatment for anti-PD-1-resistant metastatic lung cancer: a phase 1 trial. *Nature Medicine* 2021 27:8 27.

Daneman, R. (2012). The blood–brain barrier in health and disease. *Annals of Neurology* 72.

Daneman, R., and Prat, A. (2015). *The Blood–Brain Barrier*. Cold Spring Harbor Perspectives in Biology 7.

Deleyrolle, L.P., Harding, A., Cato, K., Siebzehnruhl, F.A., Rahman, M., Azari, H., Olson, S., Gabrielli, B., Osborne, G., Vescovi, A., *et al.* (2011). Evidence for label-retaining tumour-initiating cells in human glioblastoma. *Brain* 134.

Dhatchinamoorthy, K., Colbert, J.D., and Rock, K.L. (2021). Cancer Immune Evasion Through Loss of MHC Class I Antigen Presentation. *Frontiers in Immunology* 12.

Drougkas, K., Karampinos, K., Karavolias, I., Koumprentziotis, I.-A., Ploumaki, I., Triantafyllou, E., Trontzas, I., and Kotteas, E. (2022). Comprehensive clinical evaluation of CAR-T cell immunotherapy for solid tumors: a path moving forward or a dead end? *Journal of Cancer Research and Clinical Oncology* 2022 149:6 149.

Dutoit, V., Herold-Mende, C., Hilf, N., Schoor, O., Beckhove, P., Bucher, J., Dorsch, K., Flohr, S., Fritsche, J., Lewandrowski, P., *et al.* (2012). Exploiting the glioblastoma peptidome to discover novel tumour-associated antigens for immunotherapy. *Brain* 135.

Dutoit, V.e., Migliorini, D., Ranzanici, G., Marinari, E., Widmer, V.e., Lobrinus, J.A., Momjian, S., Costello, J., Walker, P.R., Okada, H., *et al.* (2018). Antigenic expression and spontaneous immune responses support the use of a selected peptide set from the IMA950 glioblastoma vaccine for immunotherapy of grade II and III glioma. *OncolImmunology* 7.

E, P., E, P., P, C., T, T., A, P., and D, B. (2016). Pleiotrophin and its receptor protein tyrosine phosphatase beta/zeta as regulators of angiogenesis and cancer. *Biochimica et Biophysica Acta* 1866.

- Eill, G.J., Sinha, A., Morawski, M., Viapiano, M.S., and Matthews, R.T. (2020). The protein tyrosine phosphatase RPTP ζ /phosphacan is critical for perineuronal net structure. *Journal of Biological Chemistry* 295.
- Espinosa-Carrasco, G., Chiu, E., Scrivo, A., Zumbo, P., Dave, A., Betel, D., Kang, S.W., Jang, H.-J., Hellmann, M.D., Burt, B.M., *et al.* (2024). Intratumoral immune triads are required for immunotherapy-mediated elimination of solid tumors. *Cancer Cell* 42.
- Finocchiaro, G., Gentner, B., Farina, F., Capotondo, A., Eoli, M., Anghileri, E., Carabba, M.G., Cuccarini, V., Meco, F.D., Legnani, F., *et al.* (2021). A phase I-IIa study of genetically modified Tie-2 expressing monocytes in patients with glioblastoma multiforme (TEM-GBM Study). *Journal of Clinical Oncology* 39.
- Foroutan, M., Bhuvu, D.D., Lyu, R., Horan, K., Cursons, J., and Davis, M.J. (2018). Single sample scoring of molecular phenotypes. *BMC Bioinformatics* 2018 19:1 19.
- Friedrich, M., Sankowski, R., Bunse, L., Kilian, M., Green, E., Ramallo Guevara, C., Pusch, S., Poschet, G., Sanghvi, K., Hahn, M., *et al.* (2021). Tryptophan metabolism drives dynamic immunosuppressive myeloid states in IDH-mutant gliomas. *Nature Cancer* 2021 2:7 2.
- Fujikawa, A., Sugawara, H., Tanaka, T., Matsumoto, M., Kuboyama, K., Suzuki, R., Tanga, N., Ogata, A., Masumura, M., and Noda, M. (2017). Targeting PTPRZ inhibits stem cell-like properties and tumorigenicity in glioblastoma cells. *Scientific Reports* 2017 7:1 7.
- Garmany, A., Yamada, S., and Terzic, A. (2021). Longevity leap: mind the healthspan gap. *npj Regenerative Medicine* 2021 6:1 6.
- Germain, P.-L., Lun, A., Garcia Meixide, C., Macnair, W., Robinson, M.D., Germain, P.-L., Lun, A., Meixide, C.G., Macnair, W., and Robinson, M.D. (2022). Doublet identification in single-cell sequencing data using scDbIFinder. *F1000Research* 2022 10:979 10.

References

Giannakopoulou, E., Lehander, M., Viriding Culleton, S., Yang, W., Li, Y., Karpanen, T., Yoshizato, T., Rustad, E.H., Nielsen, M.M., Bollineni, R.C., *et al.* (2023). A T cell receptor targeting a recurrent driver mutation in FLT3 mediates elimination of primary human acute myeloid leukemia in vivo. *Nature Cancer* 2023 4:10 4.

Girard, J.-P., and Springer, T.A. (1995). High endothelial venules (HEVs): specialized endothelium for lymphocyte migration. *Immunology Today* 16.

Gully, B.S., Rossjohn, J., and Davey, M.S. (2021). Our evolving understanding of the role of the $\gamma\delta$ T cell receptor in $\gamma\delta$ T cell mediated immunity. *Biochemical Society Transactions* 49.

Guo, M., Liu, M.Y.R., and Brooks, D.G. (2024). Regulation and impact of tumor-specific CD4⁺ T cells in cancer and immunotherapy. *Trends in Immunology* 45.

Guzman, G., Pellet, K., Reed, M.R., and Rodriguez, A. (2023). CAR T-cells to treat brain tumors. *Brain Research Bulletin* 196.

Haddad, A.F., Young, J.S., Amara, D., Berger, M.S., Raleigh, D.R., Aghi, M.K., and Butowski, N.A. (2021). Mouse models of glioblastoma for the evaluation of novel therapeutic strategies. *Neuro-Oncology Advances* 3.

Hanahan, D. (2022). Hallmarks of Cancer: New Dimensions. *Cancer Discovery* 12.

Hao, Y., Stuart, T., Kowalski, M.H., Choudhary, S., Hoffman, P., Hartman, A., Srivastava, A., Molla, G., Madad, S., Fernandez-Granda, C., *et al.* (2023). Dictionary learning for integrative, multimodal and scalable single-cell analysis. *Nature Biotechnology* 2023 42:2 42.

Harrison, C. (2024). TCR cell therapies vanquish solid tumors — finally. *Nature Biotechnology* 2024.

Heard, A., Landmann, J.H., Hansen, A.R., Papadopolou, A., Hsu, Y.-S., Selli, M.E., Warrington, J.M., Lattin, J., Chang, J., Ha, H., *et al.* (2022). Antigen glycosylation

regulates efficacy of CAR T cells targeting CD19. *Nature Communications* 2022 13:1 13.

Hilf, N., Kuttruff-Coqui, S., Frenzel, K., Bukur, V., Stevanović, S., Gouttefangeas, C., Platten, M., Tabatabai, G., Dutoit, V., van der Burg, S.H., *et al.* (2018). Actively personalized vaccination trial for newly diagnosed glioblastoma. *Nature* 2018 565:7738 565.

Hinrichs, C.S., Borman, Z.A., Gattinoni, L., Yu, Z., Burns, W.R., Huang, J., Klebanoff, C.A., Johnson, L.A., Kerkar, S.P., Yang, S., *et al.* (2011). Human effector CD8+ T cells derived from naive rather than memory subsets possess superior traits for adoptive immunotherapy. *Blood* 117.

Hoang-Minh, L.B., Siebzehnrubl, F.A., Yang, C., Suzuki-Hatano, S., Dajac, K., Loche, T., Andrews, N., Massari, M.S., Patel, J., Amin, K., *et al.* (2018). Infiltrative and drug-resistant slow-cycling cells support metabolic heterogeneity in glioblastoma. *The EMBO Journal*.

Hu, H.-f., Ye, Z., Qin, Y., Xu, X.-w., Yu, X.-j., Zhuo, Q.-f., and Ji, S.-r. (2021). Mutations in key driver genes of pancreatic cancer: molecularly targeted therapies and other clinical implications. *Acta Pharmacologica Sinica* 2021 42:11 42.

Hubert, K.A., and Wellik, D.M. (2023). Hox genes in development and beyond. *Development* 150.

Jarboe, J.S., Johnson, K.R., Choi, Y., Lonser, R.R., and Park, J.K. (2007). Expression of Interleukin-13 Receptor $\alpha 2$ in Glioblastoma Multiforme: Implications for Targeted Therapies. *Cancer Research* 67.

Jhunjunwala, S., Hammer, C., and Delamarre, L. (2021). Antigen presentation in cancer: insights into tumour immunogenicity and immune evasion. *Nature Reviews Cancer* 2021 21:5 21.

References

Jin, L., Stolpa, J.C., Young, R.M., Pugh-Bernard, A.E., Refaeli, Y., and Cambier, J.C. (2008). MHC class II structural requirements for the association with Ig α/β , and signaling of calcium mobilization and cell death. *Immunology Letters* 116.

Johnson, D.B., Estrada, M.V., Salgado, R., Sanchez, V., Doxie, D.B., Opalenik, S.R., Vilgelm, A.E., Feld, E., Johnson, A.S., Greenplate, A.R., *et al.* (2016). Melanoma-specific MHC-II expression represents a tumour-autonomous phenotype and predicts response to anti-PD-1/PD-L1 therapy. *Nature Communications* 2016 7:1 7.

Johnson, K.G., and Vactor, D.V. (2003). Receptor Protein Tyrosine Phosphatases in Nervous System Development. *Physiological Reviews* 83.

Katikaneni, D.S., and Jin, L. (2019). B cell MHC class II signaling: A story of life and death. *Human Immunology* 80.

Kaur, R., Bhardwaj, A., and Gupta, S. (2023). Cancer treatment therapies: traditional to modern approaches to combat cancers. *Molecular Biology Reports* 2023 50:11 50.

Keridani, D., Aerakis, E., Verrou, K.-M., Angelidis, I., Douka, K., Maniou, M.-A., Stamoulis, P., Goudevenou, K., Prados, A., Tzaferis, C., *et al.* (2022). Lung tumor MHCII immunity depends on in situ antigen presentation by fibroblasts. *Journal of Experimental Medicine* 219.

Khelil, M.B., Godet, Y., Abdeljaoued, S., Borg, C., Adotévi, O., Loyon, R., Ben Khelil, M., Godet, Y., Abdeljaoued, S., Borg, C., *et al.* (2022). Harnessing Antitumor CD4+ T Cells for Cancer Immunotherapy. *Cancers* 2022, Vol 14, Page 260 14.

Kilian, M., Friedrich, M., Sanghvi, K., Green, E., Pusch, S., Kawauchi, D., Löwer, M., Sonner, J.K., Krämer, C., Zaman, J., *et al.* (2022). T-cell Receptor Therapy Targeting Mutant Capicua Transcriptional Repressor in Experimental Gliomas. *Clinical Cancer Research* 28.

Kilian, M., Sheinin, R., Tan, C.L., Friedrich, M., Krämer, C., Kaminitz, A., Sanghvi, K., Lindner, K., Chih, Y.-C., Cichon, F., *et al.* (2023). MHC class II-restricted antigen

presentation is required to prevent dysfunction of cytotoxic T cells by blood-borne myeloids in brain tumors. *Cancer Cell* 41.

Kim, G.B., Aragon-Sanabria, V., Randolph, L., Jiang, H., Reynolds, J.A., Webb, B.S., Madhankumar, A., Lian, X., Connor, J.R., Yang, J., *et al.* (2020). High-affinity mutant Interleukin-13 targeted CAR T cells enhance delivery of clickable biodegradable fluorescent nanoparticles to glioblastoma. *Bioactive Materials* 5.

Klichinsky, M., Ruella, M., Shestova, O., Lu, X.M., Best, A., Zeeman, M., Schmierer, M., Gabrusiewicz, K., Anderson, N.R., Petty, N.E., *et al.* (2020). Human chimeric antigen receptor macrophages for cancer immunotherapy. *Nature Biotechnology* 2020 38:8 38.

Knowles, L.J., Malik, M., Nussebaumer, O., Brown, A., van Wetering, S., and Koslowski, M. (2022). Abstract CT525: GDX012U-001 A phase 1, open-label, dose escalation, and dose expansion study to assess the safety, tolerability, and preliminary antileukemic activity of GDX012 in patients with MRD positive AML. *Cancer Research* 82.

Kohlgruber, A.C., Dezfulian, M.H., Sie, B.M., Wang, C.I., Kula, T., Laserson, U., Larman, H.B., and Elledge, S.J. (2024). High-throughput discovery of MHC class I- and II-restricted T cell epitopes using synthetic cellular circuits. *Nature Biotechnology* 2024.

Korotkevich, G., Sukhov, V., Budin, N., Shpak, B., Artyomov, M.N., and Sergushichev, A. (2021). Fast gene set enrichment analysis. *bioRxiv*.

Korsunsky, I., Millard, N., Fan, J., Slowikowski, K., Zhang, F., Wei, K., Baglaenko, Y., Brenner, M., Loh, P.-r., and Raychaudhuri, S. (2019). Fast, sensitive and accurate integration of single-cell data with Harmony. *Nature Methods* 2019 16:12 16.

Krämer, C., Kilian, M., Chih, Y.-C., Kourtesakis, A., Hoffmann, D.C., Boschert, T., Koopmann, P., Sanghvi, K., De Roia, A., Jung, S., *et al.* (2024). NLGN4X TCR transgenic T cells to treat gliomas. *Neuro-Oncology* 26.

References

- Kuboyama, K., Fujikawa, A., Masumura, M., Suzuki, R., Matsumoto, M., and Noda, M. (2012). Protein Tyrosine Phosphatase Receptor Type Z Negatively Regulates Oligodendrocyte Differentiation and Myelination. *PLOS ONE* 7.
- Lacore, M.G., Delmas, C., Nicaise, Y., Kowalski-Chauvel, A., Cohen-Jonathan-Moyal, E., and Seva, C. (2022). The Glycoprotein M6a Is Associated with Invasiveness and Radioresistance of Glioblastoma Stem Cells. *Cells* 2022, Vol 11, Page 2128 11.
- Lancaster, M.A., Corsini, N.S., Wolfinger, S., Gustafson, E.H., Phillips, A.W., Burkard, T.R., Otani, T., Livesey, F.J., and Knoblich, J.A. (2017). Guided self-organization and cortical plate formation in human brain organoids. *Nature Biotechnology* 2017 35:7 35.
- Lancaster, M.A., and Knoblich, J.A. (2014). Generation of cerebral organoids from human pluripotent stem cells. *Nature Protocols* 2014 9:10 9.
- Leary, A.Y., Scott, D., Gupta, N.T., Waite, J.C., Skokos, D., Atwal, G.S., and Hawkins, P.G. (2024). Designing meaningful continuous representations of T cell receptor sequences with deep generative models. *Nature Communications* 2024 15:1 15.
- Li, X., Zhao, L., Li, W., Gao, P., and Zhang, N. (2024). HER2-targeting CAR-T cells show highly efficient anti-tumor activity against glioblastoma both in vitro and in vivo. *Genes & Immunity* 2024 25:3 25.
- Lindner, K. (2023). Identification and validation of neoepitope-specific T cell receptors for glioma immunotherapy. Heidelberg University Library.
- Liu, G., Ying, H., Zeng, G., Wheeler, C.J., Black, K.L., and Yu, J.S. (2004). HER-2, gp100, and MAGE-1 Are Expressed in Human Glioblastoma and Recognized by Cytotoxic T Cells. *Cancer Research* 64.
- Liu, Y., Zhou, Y., Huang, K.-H., Fang, X., Li, Y., Wang, F., An, L., Chen, Q., Zhang, Y., Shi, A., *et al.* (2020). Targeting epidermal growth factor-overexpressing triple-

negative breast cancer by natural killer cells expressing a specific chimeric antigen receptor. *Cell Proliferation* 53.

Ma, X. (2023). Individualized patient-derived tumor organoids model brain tumor ecosystem. Heidelberg University Library.

Maeda, N., Nishiwaki, T., Shintani, T., Hamanaka, H., and Noda, M. (1996). 6B4 Proteoglycan/Phosphacan, an Extracellular Variant of Receptor-like Protein-tyrosine Phosphatase ζ /RPTP β , Binds Pleiotrophin/Heparin-binding Growth-associated Molecule (HB-GAM). *Journal of Biological Chemistry* 271.

Mantovani, A., Allavena, P., Marchesi, F., and Garlanda, C. (2022). Macrophages as tools and targets in cancer therapy. *Nature Reviews Drug Discovery* 2022 21:11 21.

Marco, R.C.D., Monzo, H.J., and Ojala, P.M. (2023). CAR T Cell Therapy: A Versatile Living Drug. *International Journal of Molecular Sciences* 2023, Vol 24, Page 6300 24.

Martinet, L., Garrido, I., Filleron, T., Le Guellec, S., Bellard, E., Fournie, J.-J., Rochaix, P., and Girard, J.-P. (2011). Human Solid Tumors Contain High Endothelial Venules: Association with T- and B-Lymphocyte Infiltration and Favorable Prognosis in Breast Cancer. *Cancer Research* 71.

Martinet, L., Guellec, S.L., Filleron, T., Lamant, L., Meyer, N., Rochaix, P., Garrido, I., and Girard, J.-P. (2012). High endothelial venules (HEVs) in human melanoma lesions. *Oncolmmunology* 1.

Mazzocco, G., Niemiec, I., Myronov, A., Skoczylas, P., Kaczmarczyk, J., Sanecka-Duin, A., Gruba, K., Król, P., Drwal, M., Szczepanik, M., *et al.* (2021). AI Aided Design of Epitope-Based Vaccine for the Induction of Cellular Immune Responses Against SARS-CoV-2. *Frontiers in Genetics* 12.

McLellan, A.D., and Ali Hosseini Rad, S.M. (2019). Chimeric antigen receptor T cell persistence and memory cell formation. *Immunology and Cell Biology* 97.

References

Meeker, R.B., Williams, K., Killebrew, D.A., and Hudson, L.C. (2012). Cell trafficking through the choroid plexus. *Cell Adhesion & Migration* 6.

Melenhorst, J.J., Chen, G.M., Wang, M., Porter, D.L., Chen, C., Collins, M.A., Gao, P., Bandyopadhyay, S., Sun, H., Zhao, Z., *et al.* (2022). Decade-long leukaemia remissions with persistence of CD4⁺ CAR T cells. *Nature* 2022 602:7897 602.

Mendiratta, G., Ke, E., Aziz, M., Liarakos, D., Tong, M., and Stites, E.C. (2021). Cancer gene mutation frequencies for the U.S. population. *Nature Communications* 2021 12:1 12.

Mensurado, S., Blanco-Domínguez, R., and Silva-Santos, B. (2023). The emerging roles of $\gamma\delta$ T cells in cancer immunotherapy. *Nature Reviews Clinical Oncology* 2023 20:3 20.

Meyran, D., Zhu, J.J., Butler, J., Tantaló, D., MacDonald, S., Nguyen, T.N., Wang, M., Thio, N., D'Souza, C., Qin, V.M., *et al.* (2023). TSTEM-like CAR-T cells exhibit improved persistence and tumor control compared with conventional CAR-T cells in preclinical models. *Science Translational Medicine* 15.

Michel, S., Linnebacher, M., Alcaniz, J., Voss, M., Wagner, R., Dippold, W., Becker, C., Doeberitz, M.v.K., Ferrone, S., and Kloor, M. (2010). Lack of HLA class II antigen expression in microsatellite unstable colorectal carcinomas is caused by mutations in HLA class II regulatory genes. *International Journal of Cancer* 127.

Migliorini, D., Dutoit, V., Allard, M., Grandjean Hallez, N., Marinari, E., Widmer, V., Philippin, G., Corlazzoli, F., Gustave, R., Kreutzfeldt, M., *et al.* (2019). Phase I/II trial testing safety and immunogenicity of the multipeptide IMA950/poly-ICLC vaccine in newly diagnosed adult malignant astrocytoma patients. *Neuro-Oncology* 21.

Min, H.-Y., and Lee, H.-Y. (2023). Cellular Dormancy in Cancer: Mechanisms and Potential Targeting Strategies. *Cancer Research and Treatment* 55.

- Mitra, A., Barua, A., Huang, L., Ganguly, S., Feng, Q., and He, B. (2023). From bench to bedside: the history and progress of CAR T cell therapy. *Frontiers in Immunology* 14.
- Mo, F., Pellerino, A., Soffietti, R., Rudà, R., Mo, F., Pellerino, A., Soffietti, R., and Rudà, R. (2021). Blood–Brain Barrier in Brain Tumors: Biology and Clinical Relevance. *International Journal of Molecular Sciences* 2021, Vol 22, Page 12654 22.
- Monberg, T.J., Borch, T.H., Svane, I.M., and Donia, M. (2023). TIL Therapy: Facts and Hopes. *Clinical Cancer Research* 29.
- Moore, M.J., Zhong, M., Hansen, J., Gartner, H., Grant, C., Huang, M., Harris, F.M., Tu, N., Bowerman, N.A., Edelmann, K.H., *et al.* (2021). Humanization of T cell–mediated immunity in mice. *Science Immunology* 6.
- Mullard, A. (2022). FDA approval of Immunocore’s first-in-class TCR therapeutic broadens depth of the T cell engager platform. *Nature Reviews Drug Discovery* 2022 21:3 21.
- Myers, J.A., and Miller, J.S. (2020). Exploring the NK cell platform for cancer immunotherapy. *Nature Reviews Clinical Oncology* 2020 18:2 18.
- Nagai, K., Fujii, M., and Kitazume, S. (2022). Protein Tyrosine Phosphatase Receptor Type Z in Central Nervous System Disease. *International Journal of Molecular Sciences* 2022, Vol 23, Page 4414 23.
- Nagy, Z.A., Hubner, B., Löhning, C., Rauchenberger, R., Reiffert, S., Thomassen-Wolf, E., Zahn, S., Leyer, S., Schier, E.M., Zahradnik, A., *et al.* (2002). Fully human, HLA-DR-specific monoclonal antibodies efficiently induce programmed death of malignant lymphoid cells. *Nature Medicine* 2002 8:8 8.
- NatBiotech (2024). World’s first TIL therapy approved. *Nature Biotechnology* 2024 42:3 42.

References

- Nathan, P., Hassel, J.C., Rutkowski, P., Baurain, J.-F., Butler, M.O., Schlaak, M., Sullivan, R.J., Ochsenreither, S., Dummer, R., Kirkwood, J.M., *et al.* (2021). Overall Survival Benefit with Tebentafusp in Metastatic Uveal Melanoma. *New England Journal of Medicine* 385.
- Neftel, C., Laffy, J., Filbin, M.G., Hara, T., Shore, M.E., Rahme, G.J., Richman, A.R., Silverbush, D., Shaw, M.L., Hebert, C.M., *et al.* (2019). An Integrative Model of Cellular States, Plasticity, and Genetics for Glioblastoma. *Cell* 178.
- Nehama, D., Ianni, N.D., Musio, S., Du, H., Patané, M., Pollo, B., Finocchiaro, G., Park, J.J.H., Dunn, D.E., Edwards, D.S., *et al.* (2019). B7-H3-redirected chimeric antigen receptor T cells target glioblastoma and neurospheres. *EBioMedicine* 47.
- O'Rourke, D.M., Nasrallah, M.P., Desai, A., Melenhorst, J.J., Mansfield, K., Morrisette, J.J.D., Martinez-Lage, M., Brem, S., Maloney, E., Shen, A., *et al.* (2017). A single dose of peripherally infused EGFRvIII-directed CAR T cells mediates antigen loss and induces adaptive resistance in patients with recurrent glioblastoma. *Science Translational Medicine* 9.
- Oldford, S.A., Robb, J.D., Codner, D., Gadag, V., Watson, P.H., and Drover, S. (2006). Tumor cell expression of HLA-DM associates with a Th1 profile and predicts improved survival in breast carcinoma patients. *International Immunology* 18.
- Pajot, A., Michel, M.-L., Fazilleau, N., Pancré, V., Auriault, C., Ojcius, D.M., Lemonnier, F.A., and Lone, Y.-C. (2004). A mouse model of human adaptive immune functions: HLA-A2.1-/HLA-DR1-transgenic H-2 class I-/class II-knockout mice. *European Journal of Immunology* 34.
- Park, H.J., Kim, Y.J., Kim, D.H., Kim, J., Park, K.H., Park, J.-W., and Lee, J.-H. (2016). HLA Allele Frequencies in 5802 Koreans: Varied Allele Types Associated with SJS/TEN According to Culprit Drugs. *Yonsei Medical Journal* 57.
- Park, I.A., Hwang, S.-H., Song, I.H., Heo, S.-H., Kim, Y.-A., Bang, W.S., Park, H.S., Lee, M., Gong, G., and Lee, H.J. (2017). Expression of the MHC class II in triple-

- negative breast cancer is associated with tumor-infiltrating lymphocytes and interferon signaling. *PLOS ONE* 12.
- Patel, A.P., Tirosh, I., Trombetta, J.J., Shalek, A.K., Gillespie, S.M., Wakimoto, H., Cahill, D.P., Nahed, B.V., Curry, W.T., Martuza, R.L., *et al.* (2014). Single-cell RNA-seq highlights intratumoral heterogeneity in primary glioblastoma. *Science* 344.
- Pei, Z., Wang, B., Chen, G., Nagao, M., Nakafuku, M., and Campbell, K. (2011). Homeobox genes *Gsx1* and *Gsx2* differentially regulate telencephalic progenitor maturation. *Proceedings of the National Academy of Sciences* 108.
- Perez-Pinera, P., Zhang, W., Chang, Y., Vega, J.A., and Deuel, T.F. (2007). Anaplastic Lymphoma Kinase Is Activated Through the Pleiotrophin/Receptor Protein-tyrosine Phosphatase β/ζ Signaling Pathway: AN ALTERNATIVE MECHANISM OF RECEPTOR TYROSINE KINASE ACTIVATION. *Journal of Biological Chemistry* 282.
- Phan, T.G., and Croucher, P.I. (2020). The dormant cancer cell life cycle. *Nature Reviews Cancer* 20:7 20.
- Pienkowski, V.M., Boschert, T., Skoczylas, P., Sanecka-Duin, A., Jasiński, M., Król-Józaga, B., Mazzocco, G., Stachura, S., Bunse, L., Kaczmarczyk, J., *et al.* (2023). ARDitox: platform for the prediction of TCRs potential off-target binding. *bioRxiv*.
- Platten, M., Bunse, L., Wick, A., Bunse, T., Le Cornet, L., Harting, I., Sahm, F., Sanghvi, K., Tan, C.L., Poschke, I., *et al.* (2021). A vaccine targeting mutant IDH1 in newly diagnosed glioma. *Nature* 2021 592:7854 592.
- Poorolajal, J. (2020). Neglected Major Causes of Death Much Deadlier Than COVID-19. *Journal of Research in Health Sciences* 20.
- Poschke, I.C., Hassel, J.C., Rodriguez-Ehrenfried, A., Lindner, K.A.M., Heras-Murillo, I., Appel, L.M., Lehmann, J., Lövgren, T., Wickström, S.L., Lauenstein, C., *et al.* (2020). The Outcome of Ex Vivo TIL Expansion Is Highly Influenced by Spatial

References

Heterogeneity of the Tumor T-Cell Repertoire and Differences in Intrinsic In Vitro Growth Capacity between T-Cell Clones. *Clinical Cancer Research* 26.

Punnanitinont, A., Kannisto, E.D., Matsuzaki, J., Odunsi, K., Yendamuri, S., Singh, A.K., Patnaik, S.K., Punnanitinont, A., Kannisto, E.D., Matsuzaki, J., *et al.* (2020). Sublethal Radiation Affects Antigen Processing and Presentation Genes to Enhance Immunogenicity of Cancer Cells. *International Journal of Molecular Sciences* 2020, Vol 21, Page 2573 21.

Qin, E.Y., Cooper, D.D., Abbott, K.L., Lennon, J., Nagaraja, S., Mackay, A., Jones, C., Vogel, H., Jackson, P.K., and Monje, M. (2017). Neural Precursor-Derived Pleiotrophin Mediates Subventricular Zone Invasion by Glioma. *Cell* 170.

Ramachandran, M., Vaccaro, A., Walle, T.v.d., Georganaki, M., Lugano, R., Vemuri, K., Kourougkiaouri, D., Vazaios, K., Hedlund, M., Tsaridou, G., *et al.* (2023). Tailoring vascular phenotype through AAV therapy promotes anti-tumor immunity in glioma. *Cancer Cell* 41.

Ratliff, M., Kim, H., Qi, H., Kim, M., Ku, B., Azorin, D.D., Hausmann, D., Khajuria, R.K., Patel, A., Maier, E., *et al.* (2022). Patient-Derived Tumor Organoids for Guidance of Personalized Drug Therapies in Recurrent Glioblastoma. *International Journal of Molecular Sciences* 2022, Vol 23, Page 6572 23.

Reiss, K.A., Yuan, Y., Ueno, N.T., Johnson, M.L., Gill, S., Dees, E.C., Chao, J., Angelos, M., Shestova, O., Serody, J.S., *et al.* (2022). A phase 1, first-in-human (FIH) study of the anti-HER2 CAR macrophage CT-0508 in subjects with HER2 overexpressing solid tumors. *Journal of Clinical Oncology* 40.

Reith, W., and Haußmann, A. (2018). Bedeutung der Virchow-Robin-Räume. *Der Radiologe* 2018 58:2 58.

Reynisson, B., Alvarez, B., Paul, S., Peters, B., and Nielsen, M. (2020a). NetMHCpan-4.1 and NetMHCIIpan-4.0: improved predictions of MHC antigen

presentation by concurrent motif deconvolution and integration of MS MHC eluted ligand data. *Nucleic Acids Research* 48.

Reynisson, B., Barra, C., Kaabinejadian, S., Hildebrand, W.H., Peters, B., and Nielsen, M. (2020b). Improved Prediction of MHC II Antigen Presentation through Integration and Motif Deconvolution of Mass Spectrometry MHC Eluted Ligand Data. *Journal of Proteome Research* 19.

Riba, M., Augé, E., Campo-Sabariz, J., Moral-Anter, D., Molina-Porcel, L., Ximelis, T., Ferrer, R., Martín-Venegas, R., Pelegrí, C., Vilaplana, J., *et al.* (2019). Corpora amylacea act as containers that remove waste products from the brain. *Proceedings of the National Academy of Sciences* 116.

Rosa-Fernandes, L., Oba-Shinjo, S.M., Macedo-da-Silva, J., Marie, S.K.N., and Palmisano, G. (2022). Aberrant Protein Glycosylation in Brain Cancers, with Emphasis on Glioblastoma. *Advances in Experimental Medicine and Biology*.

Rosenberg, S.A., and Restifo, N.P. (2015). Adoptive cell transfer as personalized immunotherapy for human cancer. *Science* 348.

Roskopf, S., Leitner, J., Paster, W., Morton, L.T., Hagedoorn, R.S., Steinberger, P., and Heemskerk, M.H.M. (2018). A Jurkat 76 based triple parameter reporter system to evaluate TCR functions and adoptive T cell strategies. *Oncotarget* 9.

Roudko, V., Bozkus, C.C., Orfanelli, T., McClain, C.B., Carr, C., O'Donnell, T., Chakraborty, L., Samstein, R., Huang, K.-I., Blank, S.V., *et al.* (2020). Shared Immunogenic Poly-Epitope Frameshift Mutations in Microsatellite Unstable Tumors. *Cell* 183.

Sauer, T., Parikh, K., Sharma, S., Omer, B., Sedloev, D., Chen, Q., Angenendt, L., Schliemann, C., Schmitt, M., Müller-Tidow, C., *et al.* (2021). CD70-specific CAR T cells have potent activity against acute myeloid leukemia without HSC toxicity. *Blood* 138.

References

Schaettler, M.O., Desai, R., Wang, A.Z., Livingstone, A.J., Kobayashi, D.K., Coxon, A.T., Bowman-Kirigin, J.A., Liu, C.J., Li, M., Bender, D.E., *et al.* (2023). TCR-engineered adoptive cell therapy effectively treats intracranial murine glioblastoma. *Journal for ImmunoTherapy of Cancer* 11.

Schumacher, T., Bunse, L., Pusch, S., Sahm, F., Wiestler, B., Quandt, J., Menn, O., Osswald, M., Oezen, I., Ott, M., *et al.* (2014). A vaccine targeting mutant IDH1 induces antitumour immunity. *Nature* 2014 512:7514 512.

Schweighofer, C.D., Tuchscherer, A., Sperka, S., Meyer, T., Rattel, B., Stein, S., Ismail, S., Elter, T., Staib, P., Reiser, M., *et al.* (2012). Clinical safety and pharmacological profile of the HLA-DR antibody 1D09C3 in patients with B cell chronic lymphocytic leukemia and lymphoma: results from a phase I study. *Cancer Immunology, Immunotherapy* 2012 61:12 61.

Scott, A.C., DüNDAR, F., Zumbo, P., Chandran, S.S., Klebanoff, C.A., Shakiba, M., Trivedi, P., Menocal, L., Appleby, H., Camara, S., *et al.* (2019). TOX is a critical regulator of tumour-specific T cell differentiation. *Nature* 2019 571:7764 571.

Shelton, J., Zotow, E., Smith, L., Johnson, S.A., Thomson, C.S., Ahmad, A., Murdock, L., Nagarwalla, D., and Forman, D. (2024). 25 year trends in cancer incidence and mortality among adults aged 35-69 years in the UK, 1993-2018: retrospective secondary analysis. *BMJ* 384.

Shi, Y., Ping, Y.-F., Zhou, W., He, Z.-C., Chen, C., Bian, B.-S.-J., Zhang, L., Chen, L., Lan, X., Zhang, X.-C., *et al.* (2017). Tumour-associated macrophages secrete pleiotrophin to promote PTPRZ1 signalling in glioblastoma stem cells for tumour growth. *Nature Communications* 2017 8:1 8.

Sidhom, J.-W., Larman, H.B., Pardoll, D.M., and Baras, A.S. (2021). DeepTCR is a deep learning framework for revealing sequence concepts within T-cell repertoires. *Nature Communications* 2021 12:1 12.

Soos, J.M., Krieger, J.I., Stüve, O., King, C.L., Patarroyo, J.C., Aldape, K., Wosik, K., Slavin, A.J., Nelson, P.A., Antel, J.P., *et al.* (2001). Malignant glioma cells use MHC class II transactivator (CIITA) promoters III and IV to direct IFN- γ -inducible CIITA expression and can function as nonprofessional antigen presenting cells in endocytic processing and CD4⁺ T-cell activation. *Glia* 36.

Stevanović, S., Helman, S.R., Wunderlich, J.R., Langhan, M.M., Doran, S.L., Kwong, M.L.M., Somerville, R.P.T., Klebanoff, C.A., Kammula, U.S., Sherry, R.M., *et al.* (2019). A Phase II Study of Tumor-infiltrating Lymphocyte Therapy for Human Papillomavirus–associated Epithelial Cancers. *Clinical Cancer Research* 25.

Suzuki, A., Sekiya, S., Gunshima, E., Fujii, S., and Taniguchi, H. (2010). EGF signaling activates proliferation and blocks apoptosis of mouse and human intestinal stem/progenitor cells in long-term monolayer cell culture. *Laboratory Investigation* 2010 90:10 90.

Tan, C.L., Lindner, K., Boschert, T., Meng, Z., Rodriguez Ehrenfried, A., De Roia, A., Haltenhof, G., Faenza, A., Imperatore, F., Bunse, L., *et al.* (2024). Prediction of tumor-reactive T cell receptors from scRNA-seq data for personalized T cell therapy. *Nature Biotechnology* 2024.

Tang, L., Pan, S., Wei, X., Xu, X., and Wei, Q. (2023). Arming CAR-T cells with cytokines and more: Innovations in the fourth-generation CAR-T development. *Molecular Therapy* 31.

Tang, Y., Yang, Y.-G., Bai, O., Xia, J., and Hu, Z. (2019). Long-Term Survival and Differentiation of Human Thymocytes in Human Thymus-Grafted Immunodeficient Mice. *Immunotherapy* 11.

Thaxton, J.E., and Li, Z. (2014). To affinity and beyond: Harnessing the T Cell receptor for cancer immunotherapy. *Human Vaccines & Immunotherapeutics* 10.

TheHumanProteinAtlas (2024). Protein expression summary across tissues. www.proteinatlas.org.

References

Tian, R., Basu, M.K., and Capriotti, E. (2015). Computational methods and resources for the interpretation of genomic variants in cancer. *BMC Genomics* 2015 16:8 16.

Tokumura, K., Sadamori, K., Yoshimoto, M., Tomizawa, A., Tanaka, Y., Fukasawa, K., and Hinoi, E. (2024). The Bioinformatics Identification of Potential Protein Glycosylation Genes Associated with a Glioma Stem Cell Signature. *BioMedInformatics* 2024, Vol 4, Pages 75-88 4.

Tong, Q.-Y., Zhang, J.-C., Guo, J.-L., Li, Y., Yao, L.-Y., Wang, X., Yang, Y.-G., and Sun, L.-G. (2020). Human Thymic Involution and Aging in Humanized Mice. *Frontiers in Immunology* 11.

Ulapane, K.R., Kopec, B.M., Siahaan, T.J., Ulapane, K.R., Kopec, B.M., and Siahaan, T.J. (2019). Improving In Vivo Brain Delivery of Monoclonal Antibody Using Novel Cyclic Peptides. *Pharmaceutics* 2019, Vol 11, Page 568 11.

Ulbricht, U., Eckerich, C., Fillbrandt, R., Westphal, M., and Lamszus, K. (2006). RNA interference targeting protein tyrosine phosphatase ζ /receptor-type protein tyrosine phosphatase β suppresses glioblastoma growth in vitro and in vivo. *Journal of Neurochemistry* 98.

van de Walle, T., Vaccaro, A., Ramachandran, M., Pietilä, I., Essand, M., and Dimberg, A. (2021). Tertiary Lymphoid Structures in the Central Nervous System: Implications for Glioblastoma. *Frontiers in Immunology* 12.

van Hooren, L., Vaccaro, A., Ramachandran, M., Vazaios, K., Libard, S., van de Walle, T., Georganaki, M., Huang, H., Pietilä, I., Lau, J., *et al.* (2021). Agonistic CD40 therapy induces tertiary lymphoid structures but impairs responses to checkpoint blockade in glioma. *Nature Communications* 2021 12:1 12.

Veerman, K., Tardiveau, C., Martins, F., Coudert, J., and Girard, J.-P. (2019). Single-Cell Analysis Reveals Heterogeneity of High Endothelial Venules and Different Regulation of Genes Controlling Lymphocyte Entry to Lymph Nodes. *Cell Reports* 26.

Venteicher, A.S., Tirosh, I., Hebert, C., Yizhak, K., Neftel, C., Filbin, M.G., Hovestadt, V., Escalante, L.E., Shaw, M.L., Rodman, C., *et al.* (2017). Decoupling genetics, lineages, and microenvironment in IDH-mutant gliomas by single-cell RNA-seq. *Science* 355.

Verkerk, T., Pappot, A.T., Jorritsma, T., King, L.A., Duurland, M.C., Spaapen, R.M., and van Ham, S.M. (2024). Isolation and expansion of pure and functional $\gamma\delta$ T cells. *Frontiers in Immunology* 15.

Viardot, A., and Bargou, R. (2018). Bispecific antibodies in haematological malignancies. *Cancer Treatment Reviews* 65.

Viner, N.J., Nelson, C.A., Deck, B., and Unanue, E.R. (1996). Complexes generated by the binding of free peptides to class II MHC molecules are antigenically diverse compared with those generated by intracellular processing. *The Journal of Immunology* 156.

Wang, G., and Wang, W. (2022). Advanced Cell Therapies for Glioblastoma. *Frontiers in Immunology* 13.

Wang, J., Zhuo, Z., Wang, Y., Yang, S., Chen, J., Wang, Y., Geng, S., Li, M., Du, X., Lai, P., *et al.* (2022). Identification and Validation of a Prognostic Risk-Scoring Model Based on Ferroptosis-Associated Cluster in Acute Myeloid Leukemia. *Frontiers in Cell and Developmental Biology* 9.

Wang, J.-Y., and Wang, L. (2023). CAR-T cell therapy: Where are we now, and where are we heading? *Blood Science* 5.

Wang, W., Liu, Y., He, Z., Li, L., Liu, S., Jiang, M., Zhao, B., Deng, M., Wang, W., Mi, X., *et al.* (2024). Breakthrough of solid tumor treatment: CAR-NK immunotherapy. *Cell Death Discovery* 2024 10:1 10.

Wang, Y., Ji, N., Zhang, Y., Chu, J., Pan, C., Zhang, P., Ma, W., Zhang, X., Xi, J.J., Chen, M., *et al.* (2023). B7H3-targeting chimeric antigen receptor modification

References

enhances antitumor effect of V γ 9V δ 2 T cells in glioblastoma. *Journal of Translational Medicine* 2023 21:1 21.

Weiler, M., Blaes, J., Pusch, S., Sahm, F., Czabanka, M., Luger, S., Bunse, L., Solecki, G., Eichwald, V., Jugold, M., *et al.* (2014). mTOR target NDRG1 confers MGMT-dependent resistance to alkylating chemotherapy. *Proceedings of the National Academy of Sciences* 111.

Wen, J., Liu, F., Cheng, Q., Weygant, N., Liang, X., Fan, F., Li, C., Zhang, L., and Liu, Z. (2023). Applications of organoid technology to brain tumors. *CNS Neuroscience & Therapeutics* 29.

Wickham, H. (2016). *ggplot2: Elegant Graphics for Data Analysis* (Springer-Verlag New York).

Wölfel, M., and Greenberg, P.D. (2014). Antigen-specific activation and cytokine-facilitated expansion of naive, human CD8⁺ T cells. *Nature Protocols* 2014 9:4 9.

Xiao, Q., Nobre, A., Piñeiro, P., Berciano-Guerrero, M.-Á., Alba, E., Cobo, M., Lauschke, V.M., Barragán, I., Xiao, Q., Nobre, A., *et al.* (2020). Genetic and Epigenetic Biomarkers of Immune Checkpoint Blockade Response. *Journal of Clinical Medicine* 2020, Vol 9, Page 286 9.

Xu, F., Shanguan, X., Pan, J., Yue, Z., Shen, K., Ji, Y., Zhang, W., Zhu, Y., Sha, J., Wang, Y., *et al.* (2021). HOXD13 suppresses prostate cancer metastasis and BMP4-induced epithelial-mesenchymal transition by inhibiting SMAD1. *International Journal of Cancer* 148.

Xu, Y., Xiang, Z., Alnaggar, M., Kouakanou, L., Li, J., He, J., Yang, J., Hu, Y., Chen, Y., Lin, L., *et al.* (2020). Allogeneic V γ 9V δ 2 T-cell immunotherapy exhibits promising clinical safety and prolongs the survival of patients with late-stage lung or liver cancer. *Cellular & Molecular Immunology* 2020 18:2 18.

Yadav, C., Yadav, R., Nanda, S., Ranga, S., Ahuja, P., and Tanwar, M. (2024). Role of HOX genes in cancer progression and their therapeutical aspects. *Gene* 919.

Yadav, D., Kwak, M., Chauhan, P.S., Puranik, N., Lee, P.C.W., and Jin, J.-O. (2022). Cancer immunotherapy by immune checkpoint blockade and its advanced application using bio-nanomaterials. *Seminars in Cancer Biology* 86.

Yan, H., Parsons, D.W., Jin, G., McLendon, R., Rasheed, B.A., Yuan, W., Kos, I., Batinic-Haberle, I., Jones, S., Riggins, G.J., *et al.* (2009). IDH1 and IDH2 Mutations in Gliomas. *New England Journal of Medicine* 360.

Yang, C., Tian, G., Dajac, M., Doty, A., Wang, S., Lee, J.-H., Rahman, M., Huang, J., Reynolds, B.A., Sarkisian, M.R., *et al.* (2022). Slow-Cycling Cells in Glioblastoma: A Specific Population in the Cellular Mosaic of Cancer Stem Cells. *Cancers* 2022, Vol 14, Page 1126 14.

Yang, H., Liang, S.-Q., Schmid, R.A., and Peng, R.-W. (2019). New Horizons in KRAS-Mutant Lung Cancer: Dawn After Darkness. *Frontiers in Oncology* 9.

Yarchoan, M., Hopkins, A., and Jaffee, E.M. (2017). Tumor Mutational Burden and Response Rate to PD-1 Inhibition. *New England Journal of Medicine* 377.

Yazawa, T., Kamma, H., Fujiwara, M., Matsui, M., Horiguchi, H., Satoh, H., Fujimoto, M., Yokoyama, K., and Ogata, T. (1999). Lack of class II transactivator causes severe deficiency of HLA-DR expression in small cell lung cancer. *The Journal of Pathology* 187.

Yin, J., and Guo, Y. (2021). HOXD13 promotes the malignant progression of colon cancer by upregulating PTPRN2. *Cancer Medicine* 10.

Younger, A.R., Amria, S., Jeffrey, W.A., Mahdy, A.E.M., Goldstein, O.G., Norris, J.S., and Haque, A. (2007). HLA class II antigen presentation by prostate cancer cells. *Prostate Cancer and Prostatic Diseases* 2008 11:4 11.

Zhang, Y., and Zhang, Z. (2020). The history and advances in cancer immunotherapy: understanding the characteristics of tumor-infiltrating immune cells and their therapeutic implications. *Cellular & Molecular Immunology* 2020 17:8 17.

References

Zhao, X., Sun, M., Zhao, J., Leyva, J.A., Zhu, H., Yang, W., Zeng, X., Ao, Y., Liu, Q., Liu, G., *et al.* (2007). Mutations in HOXD13 Underlie Syndactyly Type V and a Novel Brachydactyly-Syndactyly Syndrome. *The American Journal of Human Genetics* 80.

Zhong, Z.B., Shan, M., Qian, C., Liu, T., Shi, Q.Y., Wang, J., Liu, Y., Liu, Y., Huang, Y.X., and Pang, D. (2015). Prognostic significance of HOXD13 expression in human breast cancer. *Int J Clin Exp Pathol* 8, 11407-11413.

Zhuang, L., Yao, Y., Peng, L., Cui, F., Chen, C., Zhang, Y., Sun, L., Yu, Q., and Lin, K. (2021). Silencing GS Homeobox 2 Alleviates Gemcitabine Resistance in Pancreatic Cancer Cells by Activating SHH/GLI1 Signaling Pathway. *Digestive Diseases and Sciences* 2021 67:8 67.